PROCEDURE AND ANALYSIS OF MINERAL SAMPLES USING HIGH RESOLUTION X-RAY MICRO TOMOGRAPHY

by

Ching Hao Hsieh

A thesis submitted to the faculty of
The University of Utah
in partial fulfillment of the requirements for the degree of

Master of Science

Department of Metallurgical Engineering

The University of Utah

May 2012

The University of Utah Graduate School

STATEMENT OF THESIS APPROVAL

The thesis of **Ching Hao Hsieh**

has been approved by the following supervisory committee members:

Jan D. Miller	, Chair	**Dec. 5, 2011** Date Approved
Raj K. Rajamani	, Member	**Dec. 5, 2011** Date Approved
Chen-Luh Lin	, Member	**Dec. 5, 2011** Date Approved

and by **Jan D. Miller** , Chair of

the Department of **Metallurgical Engineering**

and by Charles A. Wight, Dean of The Graduate School.

ABSTRACT

This thesis deals with the procedures and considerations of High Resolution X-ray Micro Tomography (HRXMT) to describe the internal structure and composition of multiphase mineral particles using XRadia's Micro XCT 400. Issues such as sampling statistics, sample preparation, scan conditions adjustment, image evaluation, and data analysis are considered. Mineral characterization using Computed Tomography (CT) standards is also discussed with the procedure of making a CT standard and comparison of HRXMT results and automated analysis of polished sections (QEMSCAN) results. In order to record and establish scan conditions, a database is provided.

The use of XMuDat is discussed step by step for the user to easily evaluate the mass attenuation coefficient relationship of a mineral sample. The operating procedures of the XRadia Micro XCT 400 system are also set for a new user to be able to understand and operate the system for a sample scan.

Several applications using HRXMT are also discussed. First, a few oil shale samples have been investigated to acquire high resolution internal structure images. Second, the methodology for rapid radiographic scans to identify heavy metal mineral rich regions in low grade ores is developed as an initial attempt to effectively link mine to mill. Finally, scans and analysis of teeth are presented to define internal structures in three dimensional images using CT Standards.

TABLE OF CONTENTS

LIST OF TABLES

LIST OF FIGURES

ACKNOWLEDGEMENTS

I would like to thank my super advisor, Professor Jan D. Miller, for his guidance, encouragement, and patience during my time pursuing a master's degree. Thanks to Professor Chen-Luh, Lin for his advice, time and support. Thanks are also given to Professor Raj Rajamani for suggestions on my research. I want to show my appreciation to the Institute for Clean and Secure Energy, University of Utah, who funded me for my research; Professor Erich Petersen for the QEMSCAN courses and experiments; PhD candidate Francisco Medina for the sample preparation and countless help; and PhD candidate Kevin Uno for the teeth sample and references. Finally, I want to thank Hui-Chun, Chi, who has supported me for many years as a best friend and listener.

CHAPTER 1

INTRODUCTION

New mineral processing technology for improved productivity and efficiency is an important factor in today's highly competitive market place. This is especially true in the case of particle separation processes used in the mineral industries. In general, the separation efficiency for multiphase particulate systems depends on the statistical characteristics of particle microstructures, such as composition distribution, surface exposure of mineral grains, etc. For continued technological progress in multiphase particulate separation processes, quantitative spatial analysis of multiphase particles in three-dimensions needs to be developed. Such quantitative information must be accurate enough so that the measured values can be used as parameters for simulation models, process design procedures and plant control strategies.

1.1 Analysis of Mineral Samples

At present, the traditional examination methods for multiphase mineral particles using 2D polished section images are recognized to have several disadvantages, including long sample preparation time, biased sampling and limited information. In addition, or consequently, the extent of liberation is always overestimated. Hence, a nondestructive method called x-ray computed tomography (XCT) has been developed for mineral particle examination in 3D with advantages of simple sample preparation and shorter analysis time. X-ray images (projections) of the sample are taken at different angles, and

used to reconstruct the sample providing internal structure and spatial variation in composition for multiphase particles based on differences of x-ray attenuation. However, conventional XCT medical scanners have limitations. They are designed for low density material and not suitable for high density and high atomic number minerals and metals. Applications in the medical field use low energy radiation body scans for patients' safety. The focal x-ray source, fan beam geometry, and detector are also limited by resolution and machine design. In the first generation of Micro XCT scanners, resolution is limited by the geometry of source, sample, and detector (Miller and Lin, 2009). Now XRadia's Micro XCT 400 has redesigned the micro scanner with improved resolution using advanced x-ray optics. The new High Resolution X-ray Micro Tomography (HRXMT) can reach a voxel resolution of 1 μm, while the latest nanoCT offered by XRadia can achieve a voxel resolution to 50 nm. Utilization of these developments to describe the complex structures of multiphase mineral particles is now receiving considerable attention.

1.2 Research Objectives

Using the state-of-the-art XCT machine from XRadia, the Micro XCT 400, operating and analysis procedures for mineral systems will be developed. Although many of the operating procedures for the Micro XCT 400 have been developed by XRadia, details for the analysis of mineral samples have not been established. The Micro XCT 400 provides a higher energy source and better resolution than any other commercially available machine. Using the XRadia Micro XCT 400, two objectives have been established for this thesis research: the primary objective is to establish standard operating procedures for detailed 3D analysis of multiphase mineral particles to acquire

internal structure and composition information for particle populations. This operating procedure (hardware) includes consideration of operating conditions and variables such as sample composition, energy level, noise correction, etc.; the secondary objective is to develop standard data analysis procedures (software) for applications in mineral characterization, particle segmentation, and quantitative analysis. Several case studies will be presented by way of examples.

In this thesis, the history and theory of X-ray tomography is reviewed in Chapter 2. Procedures for conventional cone beam scans and the new High Resolution X-ray Micro Tomography design are presented in Chapter 3. General operating procedures of multiphase mineral particles will be discussed starting with sample evaluation and estimation of attenuation coefficients, followed by sample preparation and operating conditions. Scan procedures are discussed from a practical point of view, including conditions for tomographic analysis and reconstruction. Analytical applications also are discussed with respect to specific operating procedures. Several copper ores are scanned to set up a CT standard. A QEMSCAN (Quantitative Evaluation of Minerals by SCANning electron microscopy) for mineral composition analysis is set compared to the HRXMT result for a corresponding polished section plane with the help of the CT Standard. A database with record and query functions is set for the scan conditions.

Next in Chapter 4, applications are considered by way of case studies. An oil shale scan for internal structure is discussed with the evaluation of scan conditions and results. Rapid radiographic scan for precious metal searching is developed for a silver-copper mix compound ore case study, including methodology and discussion. A teeth scan for mineral structure characterization is operated and analyzed.

Finally, the findings of this thesis research will be summarized and conclusions presented in Chapter 5. The use of XMuDat and operating procedures of using XRadia Micro XCT 400 for sample scanning are presented in the Appendices step by step for users to have a general idea of how to perform a full scan.

CHAPTER 2

X-RAY TOMOGRAPHY – HISTORY AND THEORY

2.1. Review of X-ray Tomography

X-ray micro computed tomography (micro XCT) systems were introduced commercially a decade ago for the 3D visualization, characterization and analysis of multiphase systems at the micron level of voxel resolution. The foundation of x-ray computed tomography is to measure the x-ray attenuation of the sample with an appropriate detector. X-ray photons are generated from a point source, penetrate the sample, are absorbed and then the attenuated beams are collected on the detector (see Figure 2.1). The sample absorbs a certain amount of x-ray photons as determined by sample density, atomic number, thickness and linear attenuation coefficient. The x-ray photons which escape from the sample are captured by the detector and the intensity measure creating a radiograph, or "projection". The projection of x-ray photons is defined for a specific angular position. A collection of projections at different angles in a full rotation can be processed for a three-dimensional reconstruction known as a "backprojection" (Herman, 1980). The backprojected image is a 3D matrix composed of linear attenuation coefficients for the sample, volumetric picture elements (voxels). The variation in voxel intensity distinguishes the structure and material characteristics. Importantly, the reconstruction is directly into a 3D image, as shown in Figure 2.1. Of course, any 2D section of the 3D image can be created from the 3D tomographic data set.

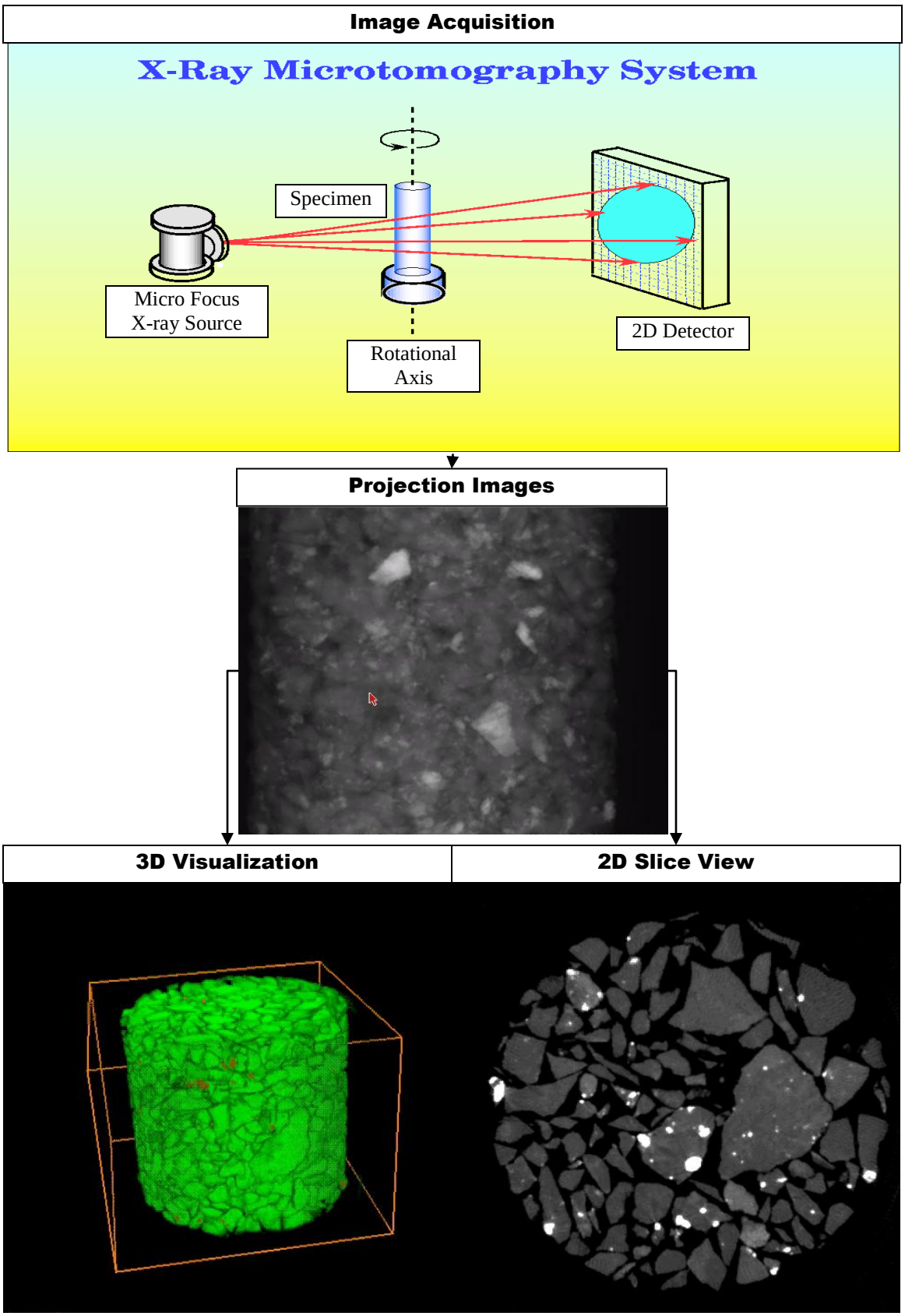

Figure 2.1 – Process of X-ray Computed Tomography.

The first XCT technique was developed with millimeter resolution in Great Britain in 1972 by Hounsfield for medical use (Wellington and Vinegar, 1987). This technique has been improved by using multiple detectors in the second generation scanners. In the third generation system, a great improvement in speed was obtained by using a fan-beam geometry source and correlated motion control detectors. The fourth generation scanners were based on fan-beam geometry with the source rotating within a fixed ring of high-efficiency detectors (Wellington and Vinegar, 1987).

The development and application of micro XCT for mineral and other multiphase systems includes a design for rotating the sample instead of rotating the source/detector (see Figure 2.2). These conventional cone beam systems are based on the principle of point projection of an x-ray source through the sample onto a detector. Resolution and field of view are controlled by moving the source and detector forward or backward in a certain range. In this design, the achievable resolution is a function of the x-ray source size, the distance between source and example, and the detector resolution.

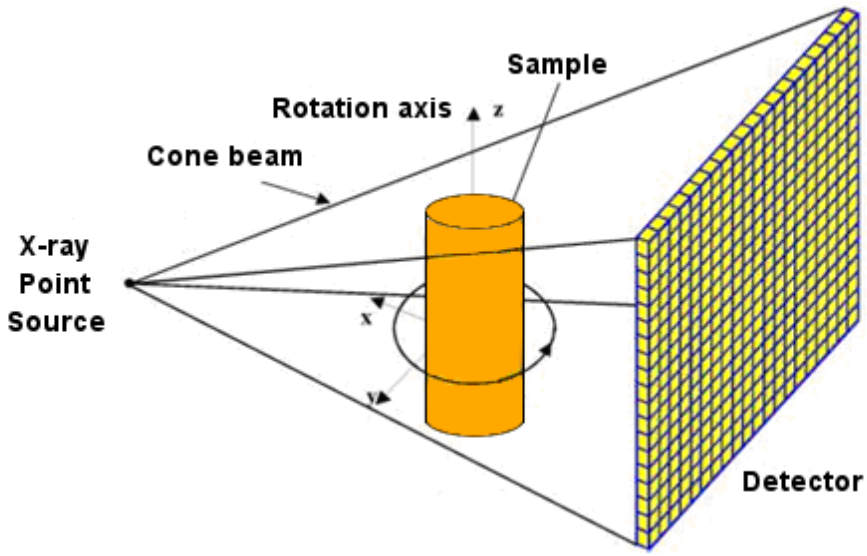

Figure 2.2 – Cone beam X-ray Computerized Tomography.

The resolution is thought to be driven by the x-ray source spot size. In this design, the voxel resolution can be expected to be ten microns corresponding to the ability to describe mineral structures and composition of multiphase particles having a particle size on the order of 100 microns.

More recently in 2007, High-Resolution X-ray Micro Tomography (HRXMT) became available from XRadia, which employs an x-ray detector having sub-micron resolution combined with a microfocus x-ray source. In this way, the voxel resolution was extended to one micron and, consequently, the structure and composition of multiphase particles having a size on the order of 10 microns can be imaged in 3D. In this system, working distances between source, sample and detector are typically around 100 mm, so that full tomography even for larger samples can be achieved. The basic layout of the system is shown in Figure 2.3.

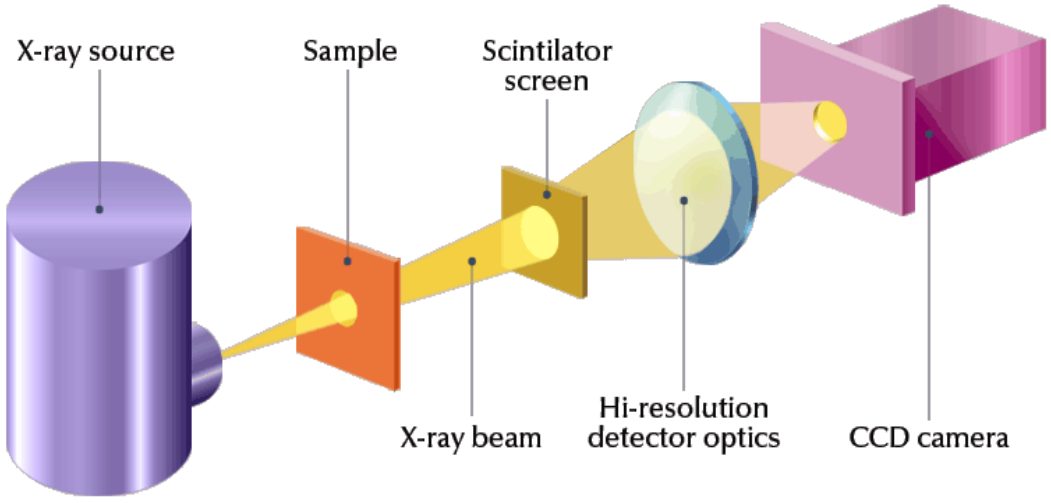

Figure 2.3 – The XRadia's High-Resolution Micro XCT 400.

The HRXMT redesigned source system changes the beam projection geometry. Unlike the conventional cone beam system, the HRXMT microfocus x-ray source emits x-ray photons in parallel beam geometry, increasing cover volume and sampling rate at the top and bottom section of the sample, as shown in Figure 2.4. In the detector part, a high resolution detector has been used for transforming x-ray into optical light by different lens using x-ray detectors, which increased the image resolution by magnification. The resolution is enhanced from 50 microns per voxel to 1 micron per voxel, theoretically. The image quality is dramatically increased, with the advantage of being able to distinguish mineral phases in greater detail.

In Figure 2.5, a 1.70x0.85 mm copper ore sample is shown in a three-dimensional view, and the tomography image has been taken in two generation machines with different resolutions. The left image is reconstructed at a voxel resolution of 20 microns using a conventional cone beam point projection instrument. The image on the right was reconstructed at a voxel resolution of 2 microns using the HRXMT parallel beam system designed by XRadia. It is obvious that the multiphase image taken at a voxel resolution of 2 micron shows finer internal structure detail than the image taken at 20 micron voxel resolution.

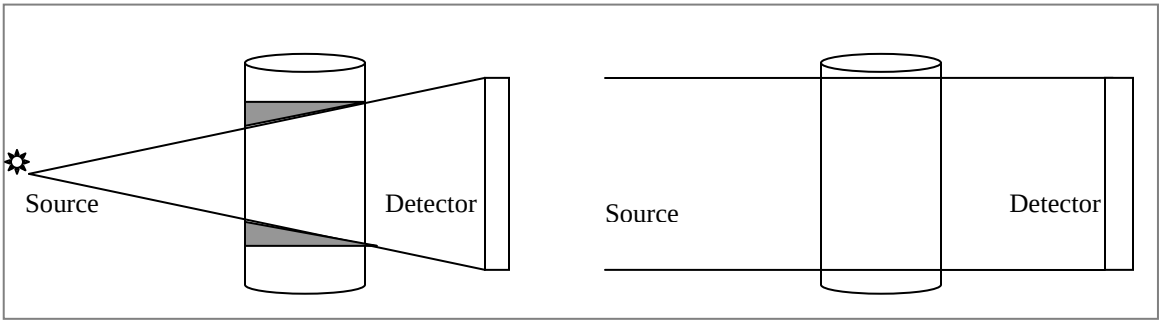

Figure 2.4 – Comparison of conventional cone beam projection and parallel beam projection.

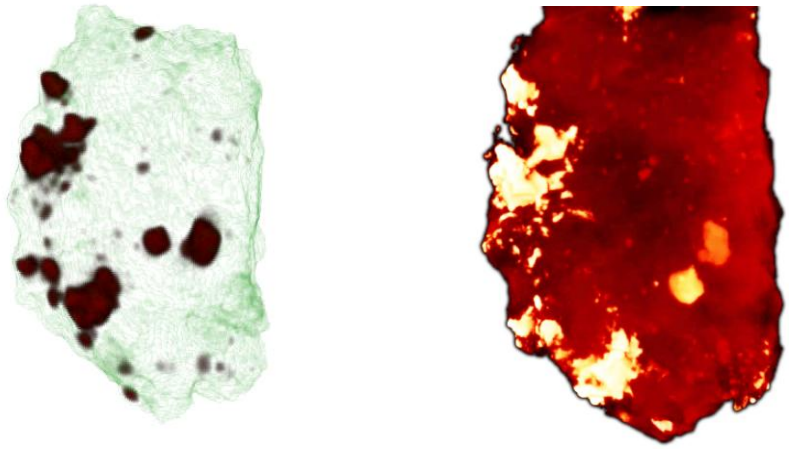

Figure 2.5 – Copper ore sample in different resolution.

2.2 Linear Attenuation Coefficient

The measured intensity by the detector can be expressed by certain formulas. According to Beer's Law (McCullough, 1975), a monochromatic beam with energy E and incident photon flux density or intensity (number of photons/unit time and area), ϕ_0, on passing through different materials that absorb x-ray photons having thickness *x*, will have an emerging photon intensity ϕ given by

$$\phi = \phi_0 * \exp\left(-\mu(\rho, Z, E) * x\right) \tag{2.1}$$

where μ is the linear attenuation coefficient, depending on density ρ, and atomic number Z in the form

$$\mu = \rho\left(a + \frac{bZ^{3.8}}{E^{3.2}}\right) \tag{2.2}$$

where *a* is a nearly energy-independent coefficient called the Klen-Nishina coefficient and b is a constant (McCullough, 1975). The dominant x-ray interaction for the HRXMT energy range (40kV to 150kV) is photoelectric absorption, which is accounted by the second term with 3.8 power dependence in equation 2.2 (Wellington and Vinegar, 1987).

In a sample consisting of a mixture of atomic species, the photoelectric absorption is proportional to the effective atomic number $Z_{eff,}$

$$Z_{eff} = \left(\sum f_i Z_i^{3.8} \right)^{\frac{1}{3.8}} \tag{2.3}$$

where f_i is the fraction of electrons on the *i*-th atomic number species.

When the x-ray photons travel across a heterogeneous object which contains materials of different attenuation coefficients, the linear attenuation coefficient is a space variant function dependent on the distribution of material in the sample being interrogated. The intensity can be derived from equation 2.1 (Videla, 2006).

$$\phi = \phi_0(x) * \exp\left(- \int_0^x \mu(\rho, Z, E) dx \right) \tag{2.4}$$

The attenuation coefficient can be acquired from equation 2.4 if the energy level of the scan is determined. However, for a complicated compound or heterogeneous material, it is difficult to calculate the effective linear attenuation coefficient. Software that facilitates the calculation is discussed in this thesis to solve such problems.

2.3 Estimation of Mineral Attenuation Coefficients

It is very important to estimate the linear attenuation coefficient before the scan has been taken. An evaluation of sample composition is necessary. The mass attenuation coefficient has a linear relationship with energy according to Beer's law (equation 2.4). If the energy is fixed, it is expected that the material can be identified by giving density, atomic number, distance and measured linear attenuation coefficient. On the other hand, scans for heavy materials with high density and high atomic number require a high level x-ray energy source to get enough x-ray photons to the detector. Appropriate energy levels for the x-ray source are required to acquire images of high quality. In the mining and mineral processing industry, sample materials are composed of many different minerals and many different elements. Beer's Law still works, but it is very difficult to calculate the linear attenuation coefficient. In such cases, a software application called XMuDat (International Atomic Energy Agency, 1998) can be used to select the required energy level for the scan.

XMuDat provides a preview of the linear relationship of x-ray mass attenuation coefficient and energy which is based on a monochromatic energy source. Data for mass attenuation-, mass energy transfer- and mass energy absorption coefficients in a photon energy range of 1 keV to 50 MeV can be determined. Six absorbing materials can be set up individually. Each material can be composed of components chosen from the elements (Z=1 to 92) and further from 200 compounds and mixtures of dosimetric interest. By consideration of expected elements and compound densities, the software will plot a graph of the linear attenuation coefficient for different energy levels, including the K edge effect, which creates a peak in the linear curve.

Although the x-ray source in the HRXMT is using a polychromatic beam which is different from the monochromatic beam for which XMuDat was created, the functional relationship with the linear attenuation coefficient is the same. The polychromatic source generates x-ray beams of various energy levels having a normal distribution. Using selected filter(s) which will be discussed in Chapter 3, x-rays below a certain energy level can be removed. Consequently, the linear attenuation coefficient produced from XMuDat provides a good estimate of that needed for HRXMT measurements. XMuDat is a good reference and can be used to help evaluate the sample before scanning in order to establish appropriate operating conditions. Usage of XMuDat is discussed in Appendix A.

Minerals listed in Figure 2.6 are the elements of an ore sample from an Au/Ag mine in Central America. The sample contains a number of sulfide minerals of interest including chalcopyrite, bornite, covellite and pyrite. This graph provides a general idea of the required energy level for a particular mineral being scanned. However, a few issues are revealed that must be considered under certain conditions. First, the required energy level can be decided according to the graph. Conventional CT scans with a medical scanner would use a low voltage to obtain better contrast and less harm to the patient. In the mineral scan, a higher energy level is required due to higher density and high atomic number in order to obtain images having good contrast and sufficient x-ray transmission. In a mixed compound, the effective atomic number dominates the attenuation coefficient rather than density according to equation 2.2. For instance, pyrite (FeS_2) has a density about 5 g/cm³, which is higher than the density of chalcopyrite ($CuFeS_2$, 4.25g/cm³). However chalcopyrite has a higher attenuation coefficient than pyrite due to the presence of copper, which absorbs more x-ray photons than iron.

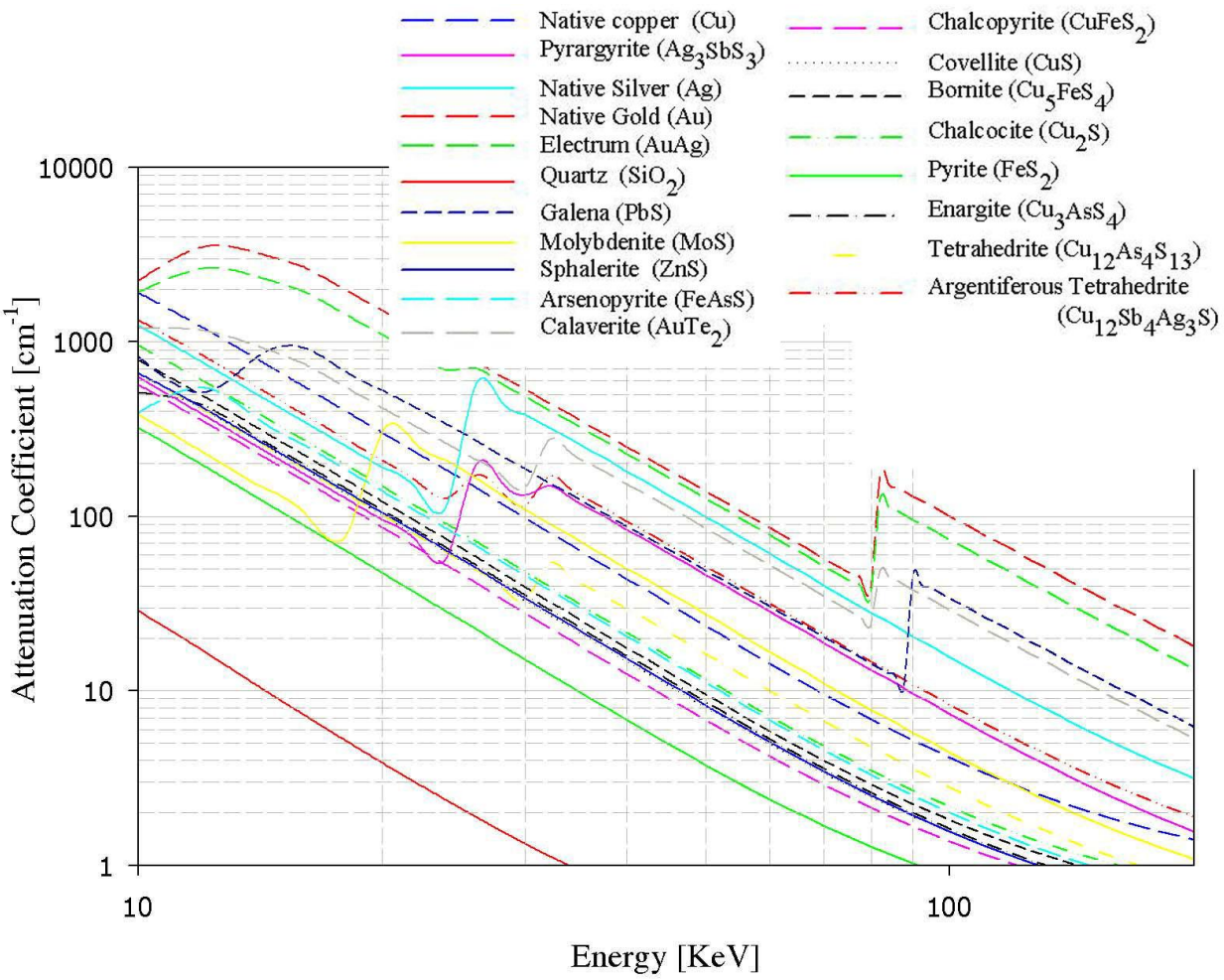

Figure 2.6 – Mineral attenuation coefficients using XMuDat

Followed by curve changes, the significant K edge effect of specific minerals is in the plot persecuted in Figure 2.6. Molybdenite, silver and pyrargyrite have the K edge effect at a lower voltage (around 40KeV), while gold, electrum and galena have the effect at a higher voltage (around 80-90 KeV). This effect helps us to distinguish different mineral phases at a specific voltage. For instance, Galena (PbS) and Gold (Au) are difficult to differentiate at a low voltage. A scan to distinguish these materials should hold energy at more than 100 KeV.

CHAPTER 3

PROCEDURES FOR OPERATING MICRO XCT 400

3.1 XRadia's Micro XCT 400

The commercial design of the HRMXT, Micro XCT 400, shown in Figure 3.1 (XRadia; Product, 2010) features the x-ray chamber (A), which is made of solid lead to protect from any radiation leakage; the terminal panel (B), where the operatior can monitor and manipulate samples through a surveillance camera and screen; the mainframe (C), for data acquisition; and the power adapter (D). An additional Uninterruptible Power Supply (UPS) has been installed in case of power suspension or fluctuation (E).

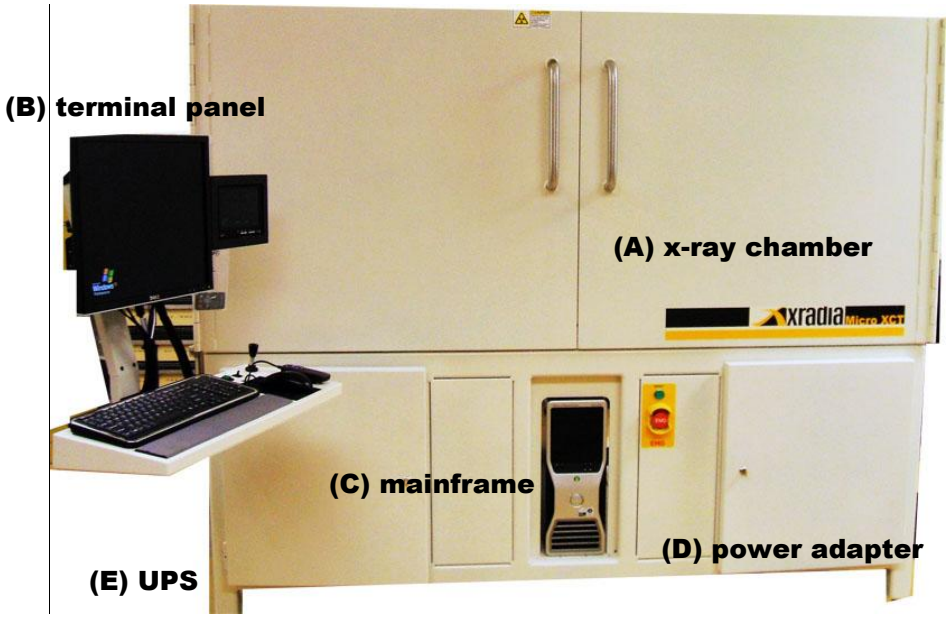

Figure 3.1 – The XRadia Micro XCT 400 system.

Figure 3.2 shows the x-ray source (A), detector (B), sample stage (C) and a granite rock foundation (D). The HRXMT equipment, including parts (A), (B) and (C), are set on a foundation of a heavy granite rock (D) in order to avoid any tilt, motion or vibration during the scan. The x-ray source generates x-rays which pass through a filter penetrating the sample on the stage and then the intensity of the transmitted radiation is measured on the detector. The sample stage is able to rotate through a full 360º, and raise or lower the sample in a certain range. The source and the detector can also be moved forward or backward to adjust the distance, or the axial position adjusted as needed, to obtain a better field of view and x-ray intensity.

The sample itself can move on the x axis (direction from source to detector), y axis (sample raises or descent) and z axis (from door side to inner side) in a micron precision. The orientation of 3 axes is shown in Figure 3.3.

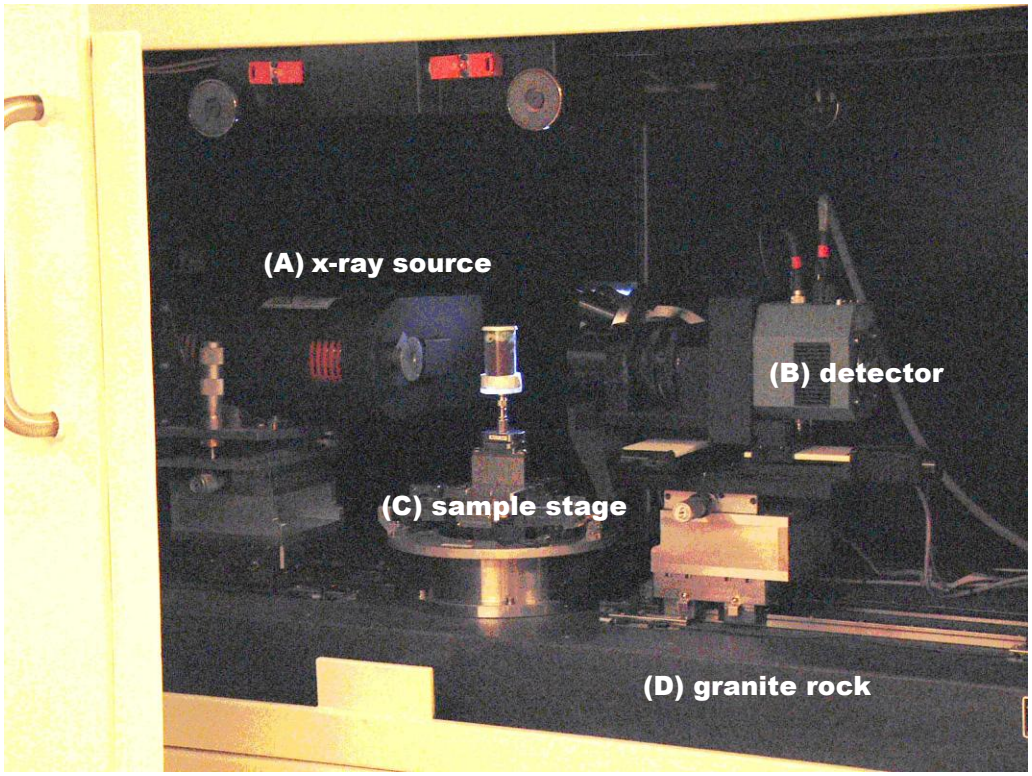

Figure 3.2 – Internal features of of XRadia Micro XCT-400.

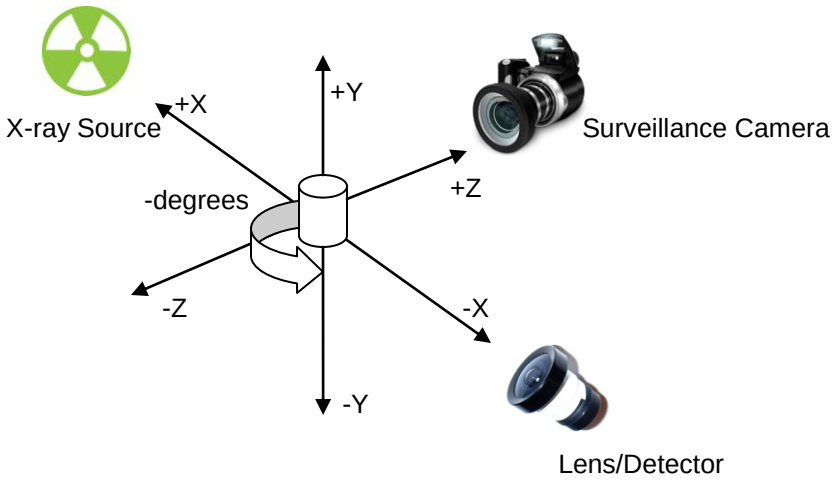

Figure 3.3 – Orientation in X, Y and Z axes for HRXMT measurements.

Source, sample stage and detector movement can be done using XMController, the operating software for Micro XCT 400. The spatial relationship of each unit can be adjusted at the micron level. While the machine turns on the x-ray source, the chamber is sealed to prevent radiation released from the chamber. Sample status and movement can be observed through the surveillance camera and displayed on a terminal monitor. A consecutive scan with a short exposure time (typically 1 second) can also help catch the sample position with the XMController. This automated system keeps the user safe and allows for higher resolution of images.

3.2 Sample Preparation

To obtain a high quality image from HRXMT for subsequent data analysis, sample preparation is very important to achieve designed scan results. The preparation procedures must satisfy particle sampling statistics and not affect the mass linear attenuation coefficient of the sample itself. With this consideration, the sampling technique and sample holder/container will be discussed in the following paragraphs.

The particle samples are must frequently considered for HRXMT analysis. Particle size and range are the two main issues for consideration in the preparation of the sample. The minimum particle size is required to be at least five to ten times of the voxel resolution in order to obtain enough voxels to distinguish the particle. A narrow size range is also helpful to get an unambiguous result. In this regard, a uniform particle size is preferred, especially for subsequent data analysis such as particle segmentation and mineral grain characterization.

The main purpose of the sample holder/container is to hold the sample on the stage in a fixed, steady position during scanning of the sample. The first consideration for the container is to stabilize the sample during the scan while rotating through different angles; the second consideration is the mass attenuation coefficient of the container which has to be as low as possible, yet still providing sufficient support and stability for the sample.

3.2.1 Sampling Particulate Materials

In mineral processing, there are many methods used for sampling particulate materials, including the splitter and the spinning riffle (Herbst and Sepulveda, 1985). The simplest method of obtaining a sample consists of random grabbing amounts of a well-mixed particle population. This method is known as grab sampling with two advantages: simplicity and speed. However, the sampling accuracy varies with each grab, and is influenced by the particle size range, distribution and grade. Other techniques provide better representation and consistency.

Coning and quartering methods are applied for particulate sampling when no sampling tools are available. A conical heap is formed with particles to be sampled and is

split into four “equal” parts by dividing it with a spatula or shovel in a cross-shaped pattern. Two opposite quarters are removed and the other two are remixed. The procedure is repeat for a few iterations until the sample mass is reduced to the required amount. Sampling accuracy is dependent on the operator’s skill such as mixing, heap forming, volume dividing and particle segregation. Despite these disadvantages, this method is still a very simple and fast way to sample particulate materials.

A similar method to coning and quartering is splitting using a sample splitter instead of hand dividing. The material sample is randomly separated into two approximately equal portions on passing through the device. In this way, half of the sample material will be discarded and the amount reduced accordingly.

Another method called the spinning riffle method provides more reliable sampling by using a rotating table and a vibrating sample feeder to separate material to subsamples evenly. The feeder vibrates at a certain frequency to control the feed rate. The speed of table rotation is also controlled in order to fill every container evenly without loss of particles.

A more precise sampling device has been developed using the riffle method with automatic control on vibration and rotation speed, which is called a Rotary Micro Riffler. Figure 3.4 shows the Rotary Micro Riffler and testing tubes. Eight testing tubes are able to be loaded at once. Sample materials are divided into eight parts in each procedure. The mineral particles are poured into the funnel on the top of the spinning splitters after establishing the slope and feeding rate. Particles are divided into rotating tubes evenly. After a few iterations, the mineral sample is ready to be collected and put into containers for the HRXMT scanning.

Figure 3.4 – Rotary Micro Riffler and testing tubes.

To meet the statistical requirement of raw material amount for sampling, a simple estimation of raw material weight equation using Gy's equation (Gy, P.M., 1963) is given by equation 3.1.

The basic Gy's equation is:

$$M = \frac{Cd^3}{s^2} \tag{3.1}$$

where M is the minimum weight of sample required (gram),

C is the sampling constant (g/cm^3),

d is the diameter of the largest particle in the sample material (cm),

s is the statistical error that can be tolerated in the analysis of sample.

The sample constant, C, is specific to the material being sampled, taking into account the mineral content, and its degree of liberation

$$C = fglm \tag{3.2}$$

where *f* is the shape factor (~0.5) for typical ores; (~0.2) for precious metal,

g is the particle distribution factor (0.25) for normal size distribution; for closely sized particles (0.5),

l is liberation factor (0 ~ 1), which can be derived in equation 3.3 and shown in Table 3.1.

$$l = \frac{Top\,Size}{Liberation\,Size} = \frac{d}{L} \tag{3.3}$$

m is the mineralogical composition factor which can be calculated as,

$$m = \frac{1-a}{a}\left[\left(-a\right)\bar{r} + at\right] \tag{3.4}$$

where *r* is the valuable mineral mean density,

t is the gangue minerals mean density,

a is the fractional average mineral content of the material being sampled.

For example, a minimum sampling weight for mineral exposure/liberation is to be acquired by the following conditions: particle top size is 1.8 cm with an overall Cu content of 0.85%, the confidence level is 95% (95 times out of 100). Densities for copper mineral and gangue minerals are 4.1 g/cm^3 and 2.65 g/cm^3, respectively. The liberation size is assumed at 200 microns.

Table 3.1 – Liberation factors.

d/L	<1	1 to 4	4 to 10	10 to 40	40 to 100	100 to 400	>400
L	1	0.8	0.4	0.2	0.1	0.05	0.02

When the top size of the material is 1.8 cm, then

d = 1.8 cm,

$$2s = \frac{0.05}{0.85} = 0.0588 \Rightarrow s = 0.0294$$

$$\frac{d}{L} = \frac{1.8}{0.02} = 90.0 \Rightarrow \ l = 0.1 \text{ from Table 3.1.}$$

For $0.85 \pm 0.05\%$ Cu content, then

a = 0.0085 , r = 4.1, and t = 2.65.

Therefore, from equation 3.4,

m = 476.815 g/cm^3, and

$C = fglm$ = 0.5x0.25x0.1x476.815 = 5.96 g/cm^3.

The minimum weight of sample required can be calculated as,

$$M = \frac{Cd^3}{s^2} = \frac{5.96x1.8^3}{0.0294^2} = 40213.2445g = 40.2132\ kg$$

Table 3.2 provides a brief list of different particle size and corresponding minimum sample weight calculated by Gy's equation. In the HRXMT, the sample amount of each scan is relatively low compared to the raw material. For a very small particle size less than 270 mesh (< 53 microns), the calculated sample amount in Table 3.2 is 0.86 grams, which is not sufficient for HRXMT sample preparation. Hence, Table 3.3 provides recommended sample amounts by weight of different particle sizes.

Table 3.2 – Minimum required sample weight for different size fraction.

D (cm)	1.8	1.0	0.5	0.2	0.1	0.05
Min. weight (kg)	40.2132	6.8952	0.8619	0.0552	0.006	0.00086

Table 3.3 – Suggested sample weight for practical purposes in HRXMT applications.

Size	> ½”	1/2-3/8”	3/8 – 1/4"	1/4 – 1/8”	1/8 – 10 mesh	10 – 100 mesh	100 – 200 mesh	< 200 mesh
W (kg)	100	100	100	10	10	10	10	10

Considering the chance of contamination during sample preparation, disposal of the tubes is the choice for sample preparation. A nondisposable testing tube must be cleaned before reuse. Cleaning of vibratory funnel, conveyance channel, brush, and tube junction parts is also necessary. All samples examined in this thesis are well sieved to constrain the particles in a specific size range, and these particle size fractions are sampled using the Rotary Micro Riffler.

3.2.2 Particle Packing

Distinct from the medical CT scan where patients are stationary in the chamber, in the case of HRXMT scan, the sample is fixed and rotates on the stage. The particle sample is well-confined and held by frictional forces in a cylindrical aligned container. Any small movement will cause reconstruction failure and error. Hence, careful preparation of the packed particle bed is necessary to simultaneously scan a large number of particles. Figure 3.5 shows some common cylindrical tubes as sample containers.

Particle samples are poured into the tube sample holder, the particles being well-confined and well packed. In some experiments, the scan objective is to observe the internal structure and inside fractures such as porosity and crack damage. Styrofoam is used for the cotton swab tube (2mm diameter) while a plunger is used for the syringe tube (5mm diameter) to confine the particles. In Figure 3.6, Styrofoam is again introduced to seal both ends of the tube and stabilize particle positions in the tube.

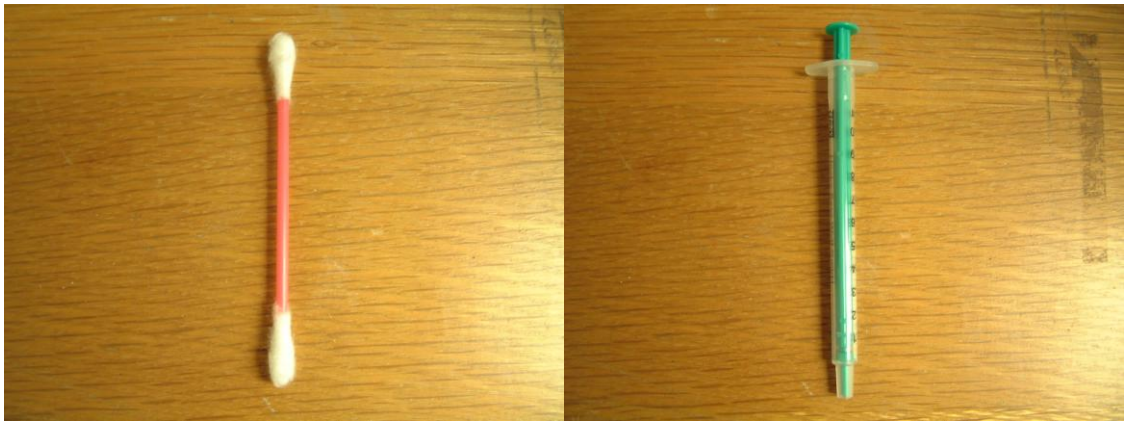

Figure 3.5 – A cotton swabs tube (2mm diameter) and a syringe tube (5mm diameter).

Figure 3.6 – Mineral particles are confined by Styrofoam layers in a syringe tube.

The particles in Figure 3.6 are confined between Styrofoam layers. Other sample holders can be used, of course. For a big chunk of sample or large amount of particles, an aluminum-copper alloy is contained in a Styrofoam bowl in the left image, and the nickel mineral particle is confined in a plastic container on the sample holder in the right image in Figure 3.7. For brittle rock or soft tissue samples, sample holders clip or grab the sample as shown in Figure 3.8 for different sample holders. These sample holders are necessary in order to hold the tube or sample pieces on the sample stage, and keep the sample perpendicular during the scan process.

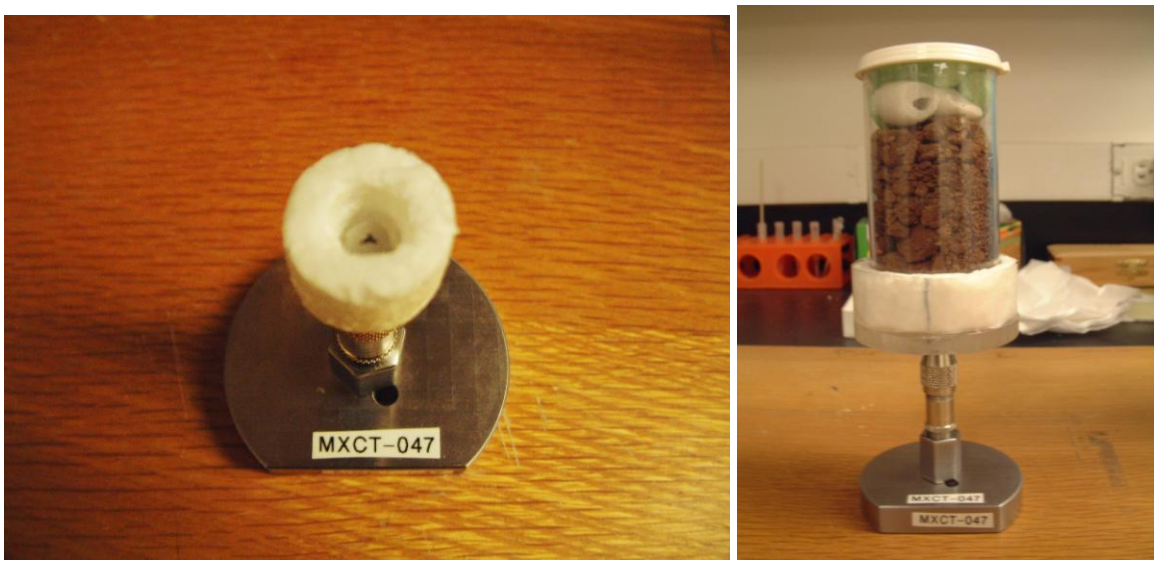

Figure 3.7 – The aluminum-copper alloy sample and the nickel ore particles sample.

Figure 3.8 – Sample holders.

Although the plastic tube wall and Styrofoam absorbs almost no x-ray photons during the scan, use of a thick tube as the container is not encouraged, especially epoxy. Epoxy has an attenuation coefficient similar to silica mineral such as quartz. Figure 3.9 shows a cross-sectional, one slice view of the reconstructed image. The sample was being sealed by epoxy. Note that the particles are visualized in gray scaled color and the difference can be identified, while the attenuation contrast is too close to discriminate particle and epoxy. The heavy mineral phase can be seen by the naked eye with experience, while the computing algorithm can not identify the attenuation coefficient differences at a 5% level of difference; such is the case for the silica/epoxy boundaries.

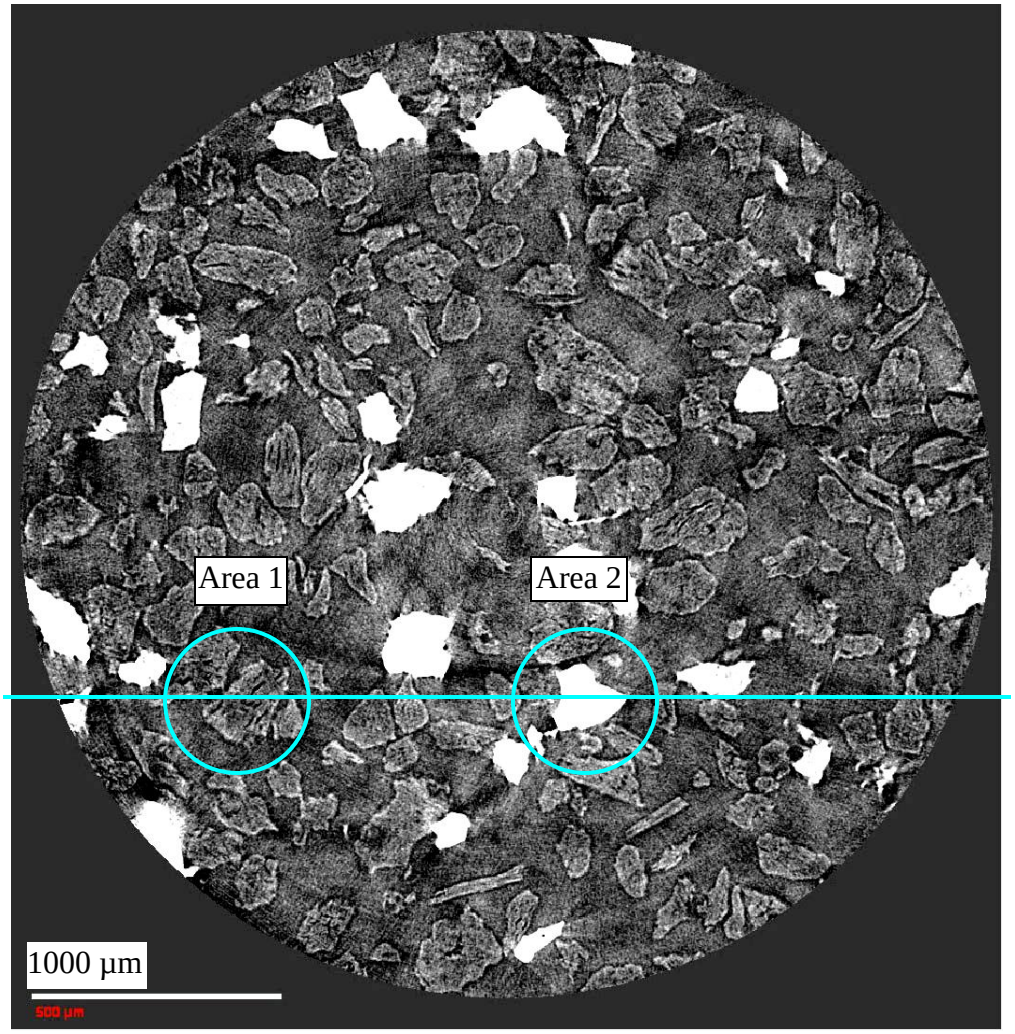

Figure 3.9 – Cross section image from a siliceous copper ore.

Two circled areas have been marked in Figure 3.9. Circle 1 contains both silicate materials and epoxy resin, and circle 2 contains high density materials/copper and resin. Figure 3.10 shows the attenuation coefficient distribution of a line across the epoxy-filled particle bed. The corresponding line scans are shown in Figure 3.10. Attenuation at each pixel on the line scan across the mineral areas and epoxy area has been measured and plotted. As we know, epoxy resin has a lower attenuation coefficient than the heavy mineral phase; however, it also has a similar attenuation with the silica mineral phase in many cases.

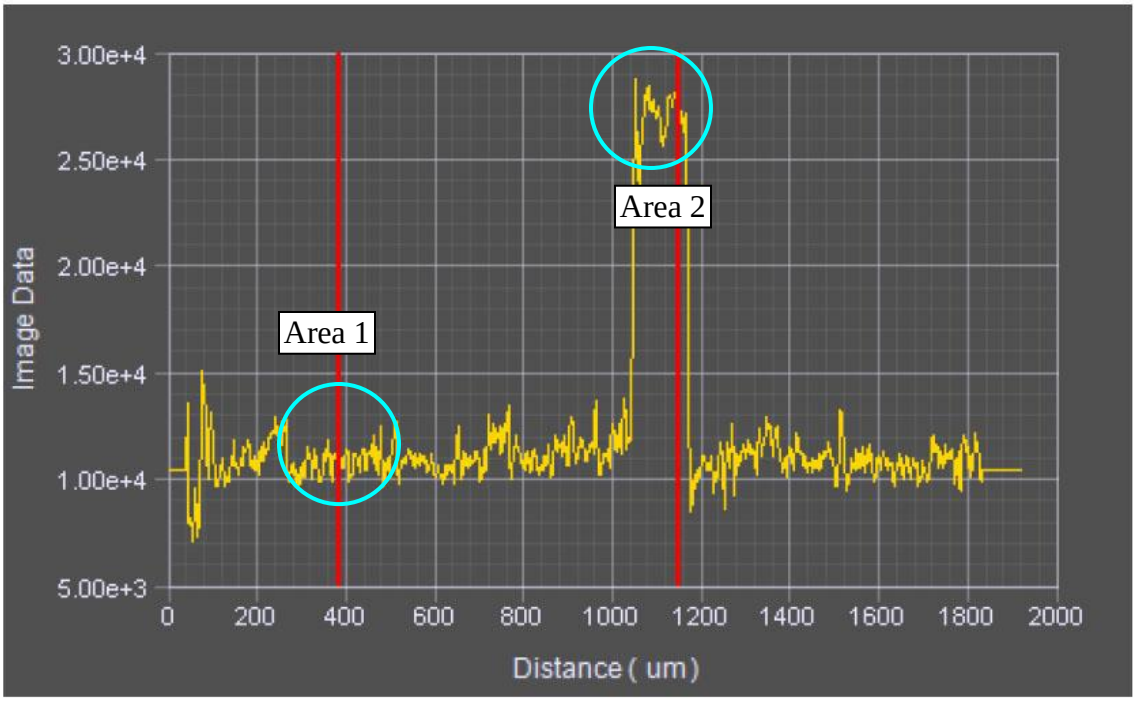

Figure 3.10 – Pixel/attenuation distribution at the cross line in Figure 3.9.

The two vertical lines in Figure 3.10 are the locations of two corresponding circles in Figure 3.9. The line in Figure 3.9 across materials contains both void and silicate particle boundaries. In the 2nd area, high density material/copper has a significant difference of attenuation coefficient with epoxy resin; however, in the 1st area, the void is filled by epoxy and the readings of attenuation coefficient are similar to those of the silicate minerals. Readings of Area 1 in Figure 3.10 are almost the same. Two phases are not well distinguished with these small differences using existing computer algorithms.

Using the packed bed method and containers without resin can simply avoid such misinterpretation caused by very close densities of silicate minerals and resin. For samples that have to be sealed in resin for other examinations, it is recommended the HRXMT scan should be taken first and be able to obtain a high quality result before the samples are being mounted in resin.

3.3 Scan Conditions

Image creation for CT analysis is based on material properties such as density, mineral composition and atomic number. The image quality for the CT scan depends on the difference in attenuation coefficients and the scan conditions are determined by this difference. In addition, the purpose of the scan such as observation of internal structure, analysis of mineral composition and description of structure geometry, also determines the scan conditions as well as dominant minerals, sample size and expected resolution. In Section 3.3.1 and following sections, scan conditions will be discussed with respect to scan purposes and sample characteristics.

3.3.1 Source Voltage

The generation of x-rays using an x-ray tube or radioactive materials releases photons and generates heat. To stabilize the operating environment of the x-ray source, the XRadia Micro XCT 400 machine needs a "warm up" time to cool the x-ray source down to minus 60ºC (XRadia, pp. 175, 2010). It is necessary to reach the temperature in order for the x-ray power source and output to obtain a stable and consistent level for each scan. The cooling process usually takes about 15 minutes and maintains this temperature at -60 ºC.

X-ray source voltage determines the attenuation coefficient. According to Beer's law (equation 2.4), the linear attenuation coefficient is mainly determined by energy and atomic number because of equation 2.2 and the 3.8 power dependence on those variables. Of course, the material property of the sample must be considered; hence, a higher x-ray energy level is required for material with a higher atomic number. A scan of a mixture of materials having both high and low atomic numbers raises the question of the appropriate

energy level for the source. High density and high atomic number materials are not able to be identified at low voltages. On the other hand, at higher voltages, low density and low atomic number materials may transmit too many photons and saturate the detector. The difference between high and low attenuation coefficient materials on image quality is known as “contrast”.

In order to decide an appropriate x-ray energy level, the software XMuDat is introduced to provide a general view for a complicated sample in advance of the scan. The software XMuDat can simulate different minerals and elemental components in a sample, and then plot the relationship between attenuation coefficient and energy. This simulation is accurate for monochromatic x-ray sources and the value is a theoretical prediction. Thus, for heterogeneous particles of irregular shape, the attenuation coefficients may not be as predicted from XMuDat. However, the XMuDat is able to provide an estimate of operating conditions for the analysis. It should be noted that the x-ray source for the XRadia Micro XCT 400 system is polychromatic, having an energy level from 40KV to 150KV. The energy unit used in XMuDat is keV. Figure 3.11 shows a linear regression of keV with voltage which can be used as an estimate for the voltage setting.

This linear regression presented in Figure 3.11 was obtained by a series of micro CT scans at different energy levels (Metscher, 2009). According to the list of kev-KV readings, equation 3.5 describes the relationship for kev to KV, which is used for the XMuDat estimation and for the Micro XCT 400 operation.

$$kev = 11.348 + 0.3693 \times KV \tag{3.5}$$

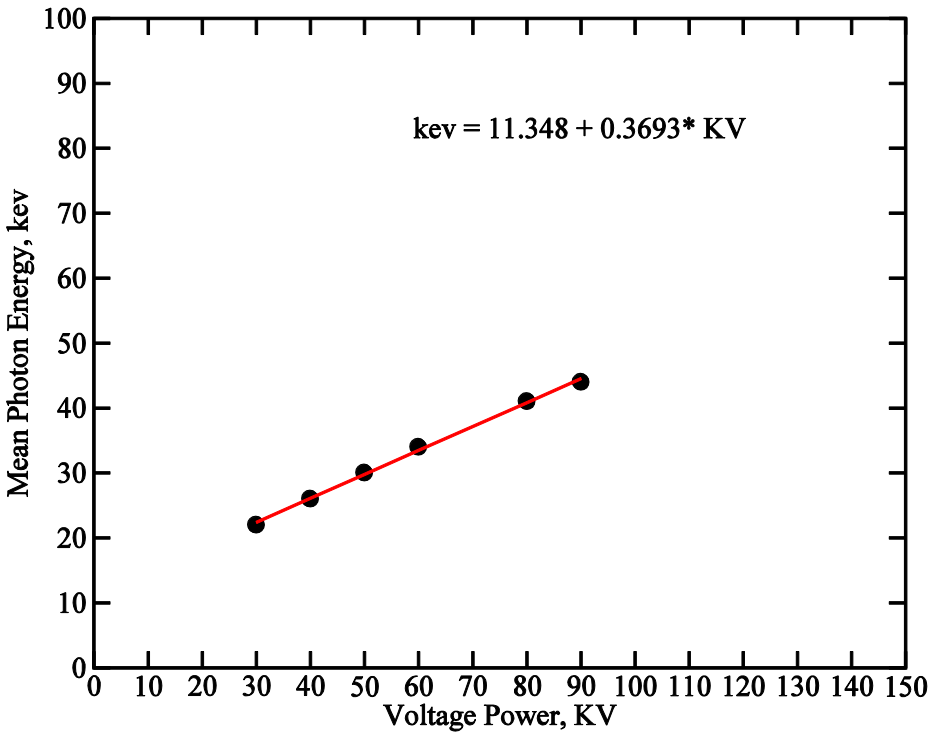

Figure 3.11 –Linear regression of keV – KV relationship between photon energy and voltage.

Using XMuDat, the voltage can be defined by the most prominent or dense material in the sample which means a specific mineral phase having higher density and higher atomic number requires higher voltage to establish the necessary transmission. A minimum attenuation coefficient reading of material has to be greater than 3,000 in order to obtain enough x-ray photons for image contrast and characterization.

For the very high atomic number material scans, it is not possible to elevate the source voltage to more than 150KV. In this case, exposure time has to be extended to have enough photon flux at the detector. However, the exposure time is also limited due to an artifact called overexposure of the reference and will be discussed in Section 3.3.2 regarding the detector. This artifact will cause the reference malfunction and lose contrast of low-attenuation materials. In addition to making sure that the reading will not pass the

limitation due to power fluctuations, the cap of the x-ray intensity reading is set at 60000. Table 3.4 shows a list of voltages corresponding to maximum exposure time of the reference before over-exposure under different conditions. In Table 3.4, the distance between source and detector is fixed at -44mm/12mm; physical filter is 150µm glass; the distance at 0.5X magnification is fixed at -75mm/60mm due to the lens size. The distance of scanning source to detector is set at a minimum range to obtain maximum x-ray intensity. In other words, a longer distance allows for longer exposure time than those specified in Table 3.4.

A general idea of commonly used energies for different minerals is given in Figure 3.12 using XMuDat: Gypsum and low density materials are sufficient in 40KV, while copper minerals require a higher energy level around 80KV as does molybdenite. For some very dense and high atomic number material, like mercury, the voltage can be set to 150KV, the maximum voltage of the machine. Specific voltage and energy level for different mineral scans can be estimated and the expected attenuation coefficients determined using XMuDat. To raise or lower the voltage is simple. The XMcontroller, an XRadia developed software for Micro XCT 400 system operation and maintenance, provides an easy access control window to change source voltage and power which can be done in a few seconds after the system is fully warmed up.

Table 3.4 – Maximum exposure time at different source voltage.

Magnification	40KV	60KV	80KV	100KV	150KV
0.5X	3 secs	1 sec	< 1sec	< 1sec	<1 sec
4X	16 secs	10 secs	8 secs	6 secs	5 secs
10X	80 secs	55 secs	43 secs	37 secs	31 secs
20X	66 secs	51 secs	44 secs	40 secs	37 secs

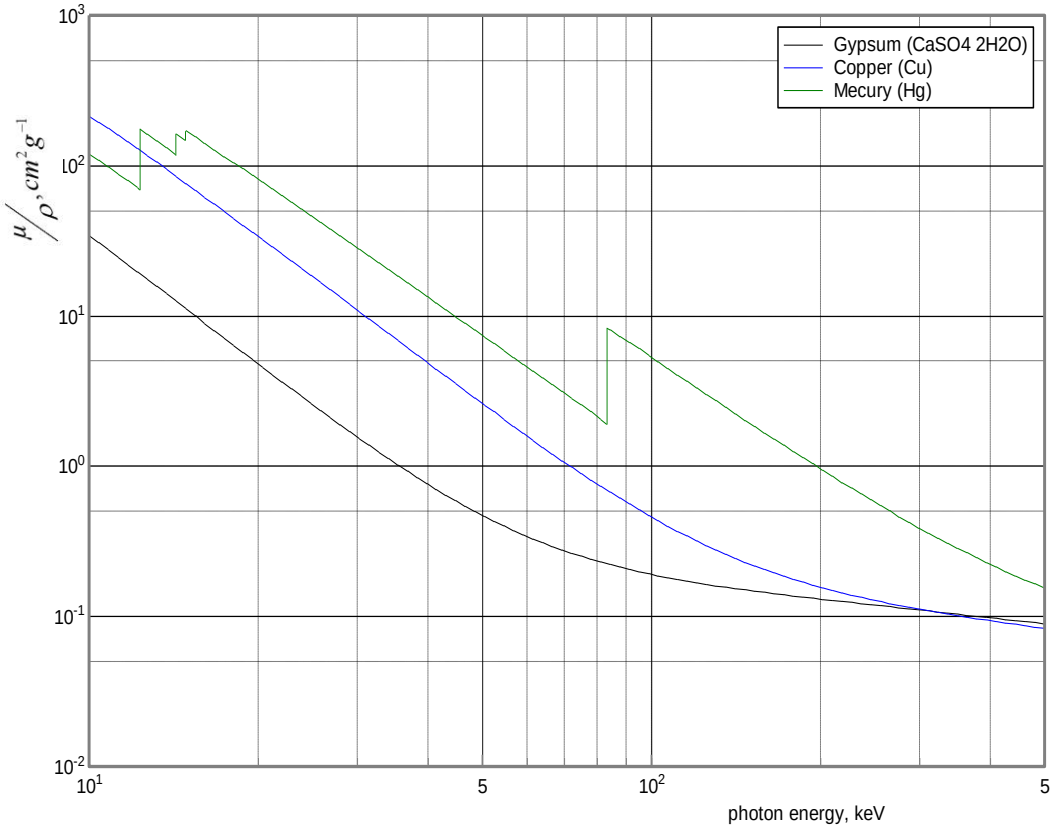

Figure 3.12 – The attenuation coefficient relationship between gypsum, copper, and mercury.

3.3.2 X-ray Lens and Detector

Detection of photons is accomplished with an array of different magnification lenses and a CCD (Charge-Coupled Device) detector shown in Figure 3.13. X-ray photons from the microfocus x-ray generator are absorbed at a certain level by the sample, and then pass through the detector lens. The x-ray lens transforms the arriving x-ray into optical light and magnifies for a certain resolution at the detector. Currently, there are four lenses setting on a turret which allows for six combinations for different levels of magnification. One lens is applied in one single scan. However, the lens can be switched by the turret rotator in a row between different scans.

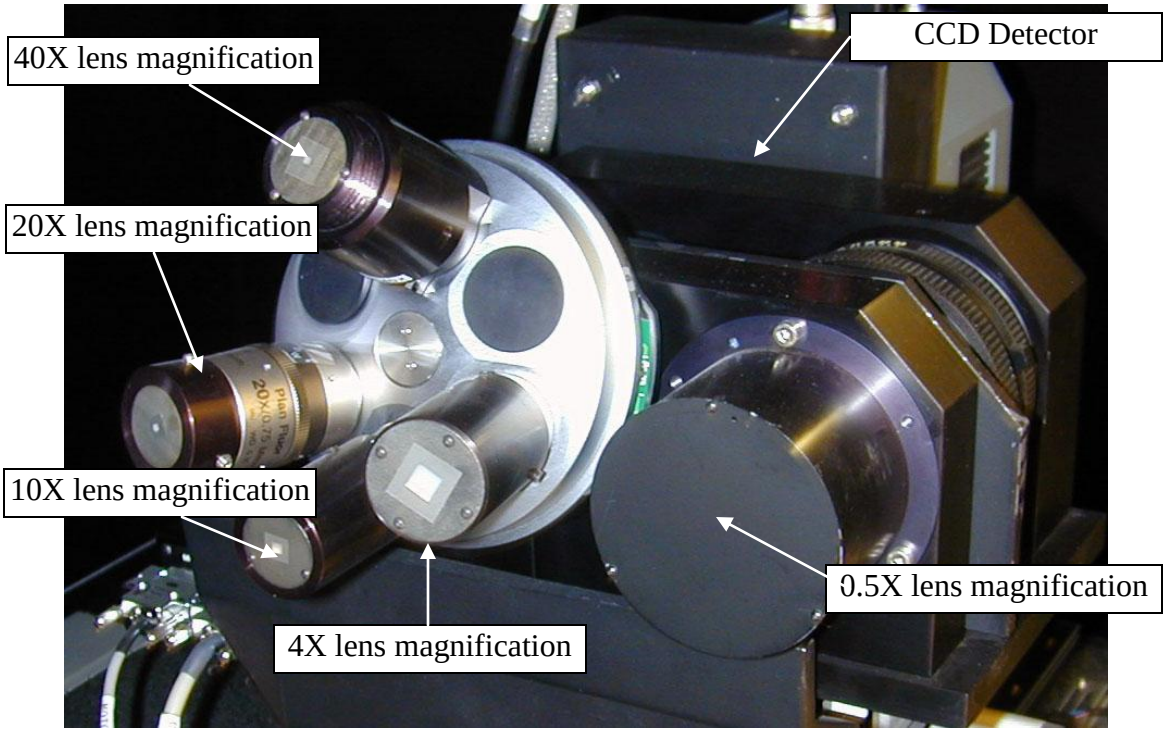

Figure 3.13 – The magnification lens set and detector of XRadia Micro XCT 400 system.

The five x-ray lenses on the turret are 4X, 10X, 20X, 0.5X and 40X in the option list. Each lens has its own magnification scale and resolution. The 40X state can reach a reconstructed voxel resolution to 0.86 micron. However, the true resolution, which is the maximum resolution that the two boundary voxels can be identified and differentiated by image processing software, is less than the reconstructed voxel resolution. Table 3.5 lists a range of true resolutions corresponding to different lens and magnification.

Table 3.5 –List of magnification, resolution with field of view and the distance.

Lens	True Resolution	Common used Resolution	Field of View	Min. Distance (Source / Detector)
4X	~4.5 microns	~5 microns	5mm*5mm	-44mm/8mm
10X	~1.8 microns	~2 microns	2mm*2mm	-44mm/8mm
20X	~1.4 microns	~2 microns	2mm*2mm	-44mm/8mm
0.5X	~30 microns	~30 – 50micons	4cm*4cm	-70mm/44mm
40X	~1.4 microns	~2 microns	1mm*1mm	-44mm/8mm

Magnification is decided by a consideration with mostly resolution, field of view, sample composition and exposure time. To visualize an identicle particle, the minimum required voxels number is 8, equal to a 2 by 2 by 2 cubic volume. Under this circumstance, the minimum grain size in a sample for 0.5X is 100 microns, 10-20 microns for a 4X scan, and 5 microns for a 10X or 20X scan.

Figure 3.14 shows a schematic diagram of x-ray path from source penetrating sample, and then with the lens on the detector. Lenses not only magnify the field of view but also transform x-ray into optical light by using an x-ray light valve. After the x-ray has been converted into optical light, the light of the beam is measured by a CCD sensor which has a 2048x2048 pixel array with 16 bits of color depth. Light intensity signals are digitalized and assembled into a radiograph image, and then sent to an ergonomic station for further processing.

The geometry for magnification and detector capture of photons is shown in Figure 3.14. The lens on the detector will transform x-rays and magnify the image by different magnifications. The lower magnification means more x-ray photons will be measured on the detector, with lower resolution and larger field of view; alternatively, higher magnification will have fewer x-ray photons captured by detector, higher resolution, and a smaller field of view.

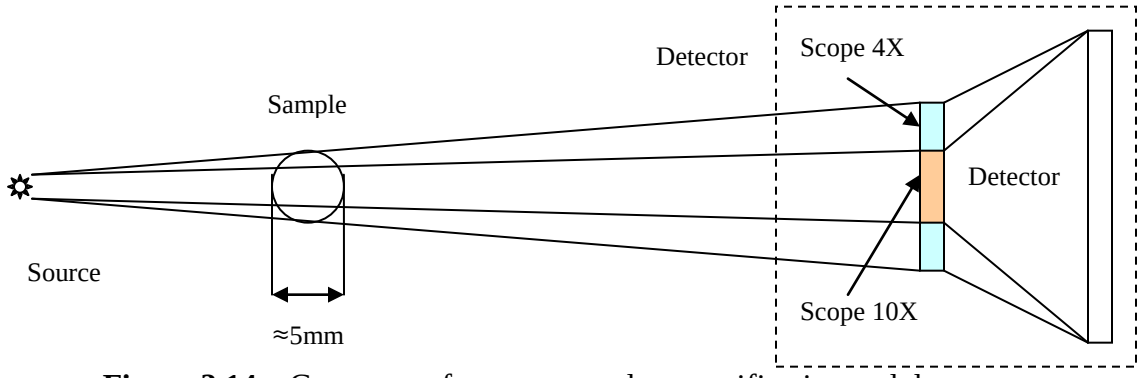

Figure 3.14 – Geometry of source, sample, magnification and detector.

The light intensity reading is capped by detector color depth. The 16-bit detector is able to identify the color depth levels from 0 to 65535 in an unsigned short format. Thus, the maximum reading of x-ray intensity cannot be over 65535. The detector can identify 65536 different phases in the scan. A CT number can be assigned in this range according to the light intensity measured on the detector. However, if the light intensity is too high caused by high level source energy or long exposure time, the reading on the detector will reach the maximum value. An artifact is called overexposure which is a malfunction of image acquisition of light intensity on detector. The detector can not differentiate between mineral phases because the light intensity reading is more than the maximum number, and the radiograph will show all white pixels to represent the overexposure region. This artifact mostly affects the use of image reference, which is an image acquisition of air having the lowest mass attenuation coefficient and highest light intensity during the scan. If the reference can not perform a correct light intensity reading of air, it will cause reconstruction error. References will be discussed in Section 3.3.8.

Image resolution is also an important issue of the HRXMT scan. Minor characteristics at the micron level like small cracks, porous structures, and boundaries of two different phases require the highest resolution scans to visualize the features on the image. The maximum image resolution does not only rely on the magnification, but also depends on the quality and the setting of the detector. The detector is an array of numerous CCD components transforming optical light intensity into electron signals (XRadia, pp. 283-284, 2010). Thus, the scan image can be shown on the screen as a “projection”, which means a single sample vertical cross section image acquired on the detector. The maximum image size that the detectors can acquire is 2048x2048 pixels

according to the XRadia MicroXCT 400 specification. Equation 3.4 shows a calculation of field of view under different binning and magnification conditions.

$$\text{Maximum Resolution} \times \frac{2048 \text{ pixel}}{\text{Camera Binning}} = \text{Expected Field of View.} \quad (3.6)$$

For example, a 4X magnification single tomography image is having 4.85 microns resolution under source/detector distances 60mm/-20mm, and shot in camera binning 2, the expected field of view is:

$$4.85 \text{ micron} \times \frac{2048 \text{ pixel}}{2} = 4.9664 \text{ millimeter} \quad \text{(XZ plane)}$$

Binning is a process of combining charges from adjacent pixels in a CCD during readout (XRadia, pp. 175, 2010). It is also a concern of image resolution. Camera binning can be set in the XMController be fore the scan. Under a binning 1 condition, the image resolution pixel is assembled by CCD components one by one on the detector; under a binning 2 condition, the pixel resolution is assembled by 2 CCD components on the detector in each dimension. Thus, the pixel resolution is reduced to 1/4 in binning 2 (X plane times Z plane), but the light intensity is 4 times than that for binning 1 due to the multiplications.

Although the actual field of view is changed by the distance of source and detector, this gives a basic idea of the maximum size of image that can be acquired for the sample with specific magnification. The distance also affects the center shift correction which will be discussed in Section 3.4.1.

3.3.3 Distance Specifications

Mass attenuation coefficient increases with an increase in x-ray photon travel distance according to equation 2.4. In other words, the further the distance between x-ray source and detector, the lower the x-ray intensity that will be measured. Under this consideration, a combination of distance, energy level and exposure time can be adjusted to obtain a better image quality.

For scans with overexposure in certain conditions such as high energy level or low magnification, the distance between source and detector can be extended in order to decrease the x-ray photons captured by the detector. In a high linear attenuation coefficient scan, dense materials require a high energy level in order for enough x-ray photons to penetrate through the sample to the detector. This higher x-ray intensity will cause overexposure on low density material in the sample or the reference. The x-ray intensity can be reduced by extending the distance of sample-to-detector without losing the x-ray photons that penetrated the dense material under a high energy level scan. On the other hand, a low magnification scan also has the problem of high x-ray intensity due to the large field of view used for x-ray capture. The x-ray intensity can be reduced by moving away from the source, and the detector still can maintain good x-ray intensity at minimum exposure time.

Variation in distance is also useful to improve the image contrast, which means the difference of x-ray intensity reading of each pixel visualized in grey scale. To differentiate each pixel and mineral phases, the two adjacent pixels have to differ by 10%, and over 3000 counts must be achieved in order to obtain enough x-ray photons for further image analysis. Two ways to achieve a good contrast include: extend the exposure

time, which will be discussed in a later section, and adjust the distance between source, sample and detector. A larger ratio of the distance of source-sample to the distance of sample-detector gives better image contrast at a high energy level and long exposure times. However, the x-ray intensity counts are also reduced in this regard. To obtain an image with good quality contrast and enough counts of x-ray intensity, a combination of distances and exposure time is necessary.

The spatial resolution and field of view will change with the distances shown in Figure 3.15. As the figure shows, the resolution increases with a decrease in the field of view by moving the source close to the sample; on the other hand, the resolution decreases with an increase in the field of view by moving the detector closer to the sample. Although the geometry of HRXMT is considered as parallel beams to reduce this effect to minimum, distances still change the resolution and field of view, slightly. More details of field of view will be discussed in Section 3.3.5.

A source-to-sample / sample-to-detector distance ratio of 4:1 to 7:1 is suggested by XRadia to obtain good image contrast. From a practical point of view, the distance has to be as close as possible to obtain x-ray counts above 3000 for high linear attenuation coefficient including thick and high atomic number elements presented in the sample.

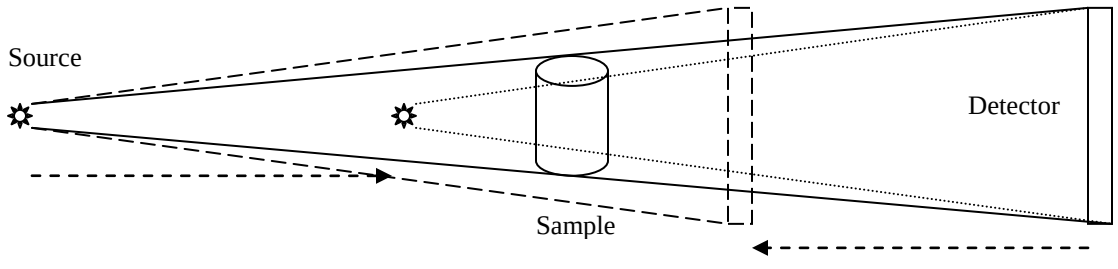

Figure 3.15 – Change of field of view and resolution by moving source/detector distance.

3.3.4 Filter Options

A filter is a thin, flat film or foil put between the source and detector. It helps to reduce a specific element effect. Due to the fact that the energy output is not stable, but varies according to a wave function in a polychromatic x-ray source, low energy x-ray photons are also projected in a high energy level environment. Thus, the mass attenuation coefficient of a material with low x-ray attenuation is not so "accurate" when a low energy x-ray photon penetrates it. Minerals that have low mass attenuation coefficient can be penetrated by low energy level x-ray photons in a high energy level environment while minerals that have high mass attenuation coefficient are not. X-ray intensity readings of low mass attenuation coefficient thus are higher than expected. In this case, a filter is introduced to remove the selected level of x-ray photons. The filter can absorb x-ray photons below its own attenuation level with the following advantages.

First, the various low energy x-ray photons are "filtered" and the reading of low attenuation material is more accurate and uniform in the resulting image. Second, the image contrast is more focused on the range of higher x-ray attenuation material, and it is more easy to identify the difference between two high x-ray attenuation materials. Third, a longer exposure time can be applied on the scan using thicker or heavier filters to measure the very high x-ray attenuation materials such as gold, lead and mercury. However, the absorption also leads to a reduction of all energy level x-ray photon penetration, and reduces the contrast among low x-ray attenuation materials. A consideration of the application of filters is decided by the objective mineral x-ray attenuation.

High x-ray attenuation minerals, e.g. mercury, are difficult to identify in a low energy level scan. While the energy level is raised by elevating the source voltage or moving the source and detector closer, the exposure time will decrease, preventing the reference overexposure. Thus, scans for mercury require a thicker or denser filter combined with 3 pieces of 1 mm glasses, which reduces total energy level by 30% and removes low energy x-ray photons, while keeping the high energy x-ray photons for penetration of mercury minerals. In a lower attenuation mineral scan, e.g., copper, apply the filter such as 150 micron thickness glasses for filtering the silicate minerals, and enhance the image quality on copper minerals.

X-rays are generated in two ways. First, if the electron interacts with an inner-shell electron of the source material target, the characteristic x-rays can be produced. These x-rays result when the interaction is strong enough to ionize the target atom and remove the inner-shell electrons. The appearing hole will be filled by an outer-shell electron, which will emit x-ray photons during the transition process (Casteele, 2004).

The second part of x-ray production is initiated by electron kinetics. The electron loses kinetic energy passing through the nucleus of an anode atom. Energy will be released as x-ray photons are produced. These types of x-rays are called “Bremsstrahlung”, which provides continuous x-ray spectrums in Figure 3.16. X-ray photons below the characteristic energy level are not required and may cause noise in samples having low density materials (Favretto, 2009).In order to reduce the low energy x-ray photons, a plate material (filter) can be placed to remove x-ray photons below some specific energy. The filter effect in Figure 3.16 shows a significant decrease of x-ray intensity of the low energy x-ray photons.

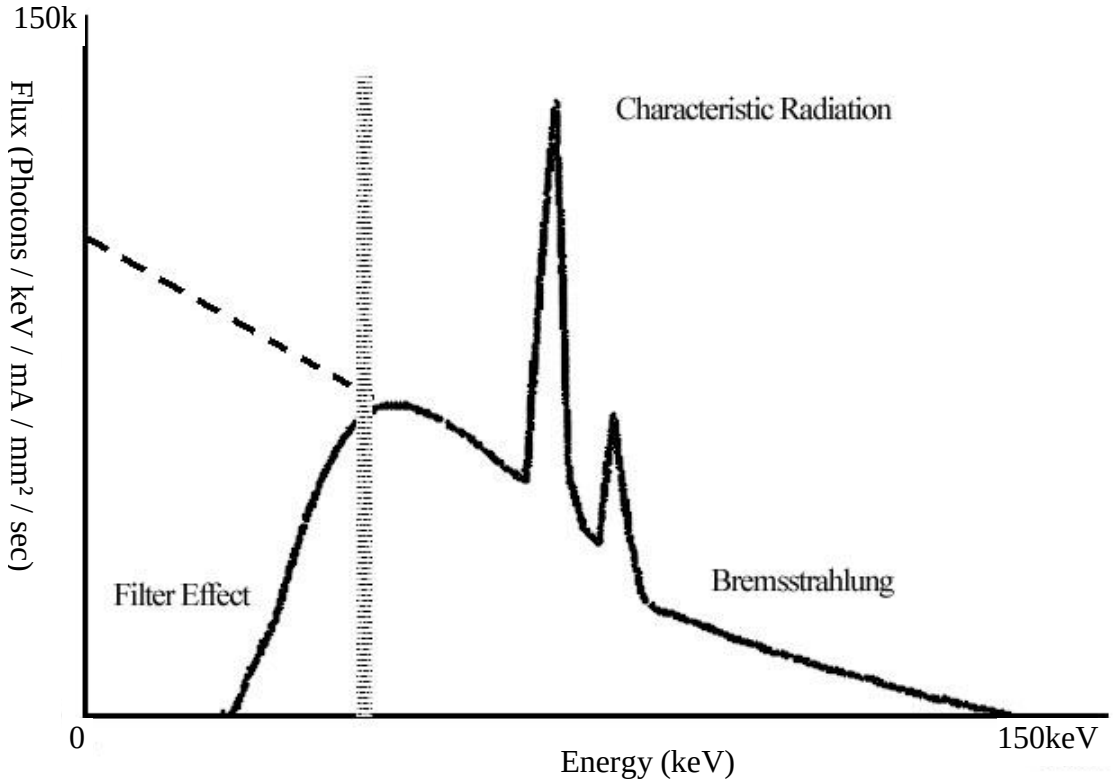

Figure 3.16 – The typical x-ray energy spectrum.

Filters can be placed before (between source and sample) or after (between detector and sample). The previous generation XCT is used to put the filter after the sample to cut down the receiving energy level on the detector, and apply longer exposure time for a high attenuation material scan. For most scans taken in the last generation HRXMT, the filter was placed at the output window of the source covering all projected x-ray photons. The advantage of this method is the noise of attenuation stimulated by low energy x-ray photons generated by the source is dramatically reduced.

A "Cut-off" energy level has been introduced to determine when a filter should be used (ARACOR, 2000). The cut-off energy is the linear attenuation coefficient of the filter material. X-ray photons below the energy level will be absorbed, in other words,

"filtered" by the material. Figure 3.17 shows a simple attenuation-coefficient / energy graph of a mineral sample which contains iron, silicon and carbon calculated by XMuDat. According to equation 2.1, we can have the mass attenuation coefficient of passing through x-ray photons less than 1%:

$$0.01 = e^{[-\mu(E_x)\rho x]} \tag{3.7}$$

Rearranging equation 3.7 we can have:

$$\mu[E_x] = -\frac{\ln(0.01)}{\rho x} = \frac{4.6}{\rho x} \tag{3.8}$$

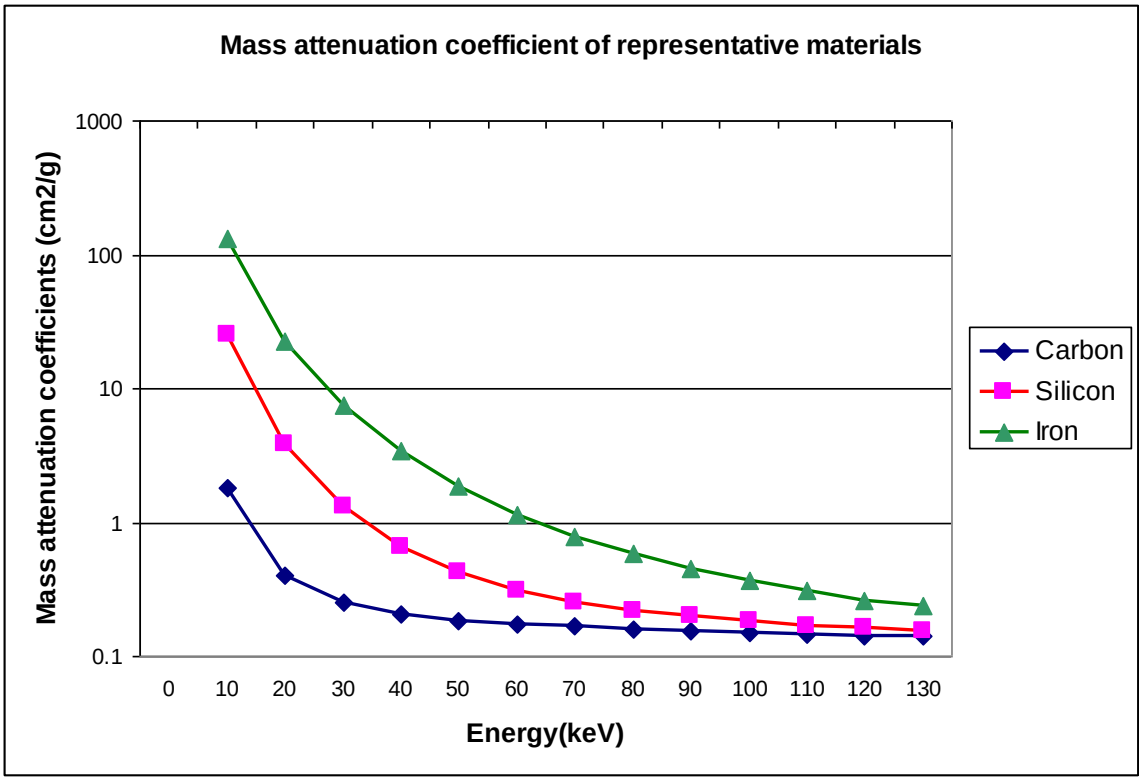

Figure 3.17 – Mass attenuation coefficient / energy relationship of iron, silicon and carbon.

Assume that the sample is an iron powder, and the sample diameter is 5 millimeter; we can calculate the attenuation coefficient and find the curve of iron corresponds to 55keV in Figure 3.17.

$$\mu[E_x] = \frac{4.6}{\rho x} = \frac{4.6}{\left(5\,g/cm^3\right)(.5cm)} = 1.8\,cm^2/g$$

Table 3.6 shows a list of filter sizes and properties (ARACOR, 2000). To select an adequate filter, the cut-off energy level should be higher than for the sample. The filter absorbs x-ray photons below 55keV, and the 0.04" brass filter with a cut-off energy of 62 keV would be used for this sample scan.

Table 3.7 presents an often used filter list for selected scan conditions. The scan conditions are fixed at two energy levels with the HE (High Energy) and LE (Low Energy) filters as suggested by XRadia (XRadia, pp. 87, 2010). Glass/Quartz (SiO_2) performs a similar x-ray absorption behavior to silicate minerals frequently called gangue minerals. Most silicate minerals have low densities and low mass attenuation coefficients.

Table 3.6 – Candidate filters.

Filter	Mass(g/cm2)	Energy Cut-off(keV)
None (carbon cover)	0.269	8.4
0.005" Al	0.0342	11.5
2x(0.005") Al	0.0683	13.5
0.020" Al	0.1346	16
0.125" Al	0.862	30
0.500" Al	3.429	40
0.010" Brass	0.217	48
0.040" Brass	0.854	62
0.001" Fe	0.020	17
0.002" Fe	0.040	21
0.005" Fe	0.1	29

Table 3.7 – Source filter selection for 10X, 20X and 40X lenses, by x-ray source.

Transmission@80kV (90kV X-ray Source)	Transmission@140kV (150kV X-ray Source)	Source Filter
>0.63	-	No filter
0.44-0.63	-	LE #1
0.34-0.44	-	LE #2
0.28-0.34	-	LE #3
0.21-0.28	-	LE #4
0.14-0.21	-	LE #5
0.08-0.14	-	LE #6
-	0.18-0.30	HE #1
-	0.08-0.18	HE #2
-	0.06-0.08	HE #3
-	0.04-0.06	HE #4
-	0.03-0.04	HE #5
-	<0.03	HE #6

In the mineral scan, the filter is not only used for reducing low energy photon noises, but also to reduce the total x-ray intensity on the detector by 10% to 30% at the same time. The filter decreases the contrast of different minerals, but ensures no overexposure error. A 150 micron glass filter is used for scans of heavy metals such as copper and iron. In some high atomic element scans like gold, and lead, the 1mm glasses x3 are combined together as a filter. Table 3.8 shows the reduction percentages of these filters. Images are taken as reference shots with 4X magnification, and distance of source /detector are -60mm/20mm. To characterize specific elements and minerals in the sample, it is necessary to use a fixed filter to maintain a steady x-ray intensity count. The 150 micron glass is the optimal choice for the copper minerals, which are of frequent interest.

Table 3.8 – Center x-ray intensity readings of different filters in HRXMT scans.

Filter/Exposure Time	60kV, 10secs	80kV, 5secs	Reduced percentage
No Filter	33014	33812	0
150 micron meter Glass	25691	27000	~21%
1 mm Glasses x3	11596	19201	65% / 45%

3.3.5 Field of View

The Field Of View (FOV) is determined by designed magnification and distance for source and detector. The first generation micro CT has limited FOV because the focal x-ray source and the detector are fixed. The sample has to be moved closer or away from the source to obtain a better FOV and cover the region of interests. Thus, the FOV generally depends on the spatial relationship of source, sample and detector. In the HRXMT (Micro XCT 400), the design with parallel beam helps reduce the effect of distance on the FOV, and selection of magnification also helps focus the FOV on a region of interest in order to increase the image resolution. The FOV is more flexible with a better image quality and x-ray intensity can be achieved by moving the source and detector. It is very important to cover all sample material (XZ plane, see Figure 3.3) in the FOV. Figure 3.18 shows a sketch of scanning geometry where the sample is larger than the FOV. Beam A traverses the sample and measures the x-ray intensity on the detector at angle 1 (solid lines). The thickness of the sample outside the FOV is unknown. At angle two, beam B traverses a different thickness of the sample outside the FOV (dotted lines), where the material and thickness in FOV remain the same.

According to equation 2.4, the x-ray intensity will perform different counts while the material property and thickness have not changed. The error is also shown in Beam B where the gray part of the sample is denser than other regions. However, it is not shown in the FOV and the attenuation coefficient of the material will not be measured correctly. Although the reconstruction algorithm can process the image with correction and reduce the errors at a minimum, the irregular shape and heterogeneous property of sample will cause misinterpretation of the mass attenuation coefficient.

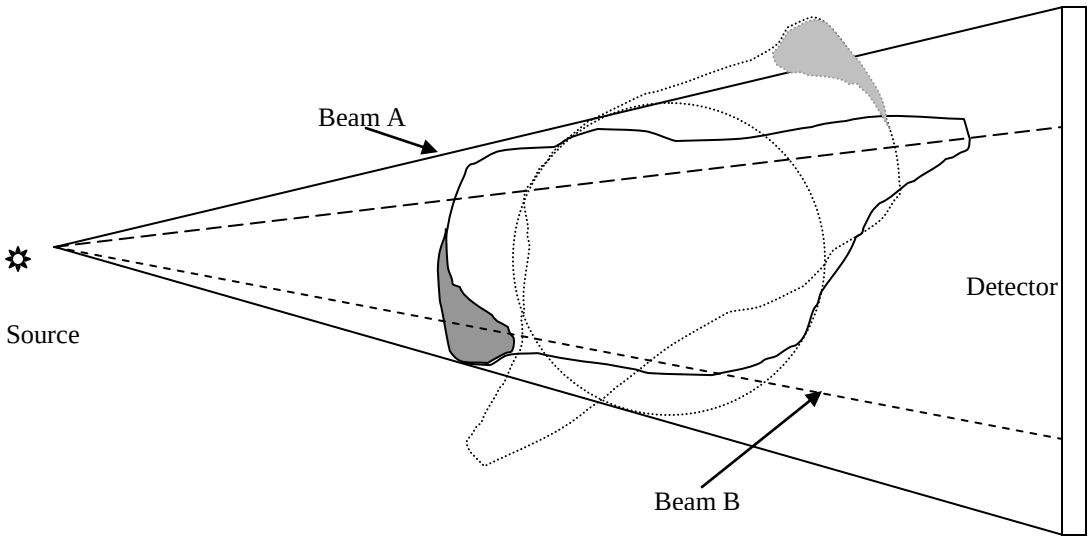

Figure 3.18 – Geometry of irregular shape, heterogeneous sample in a smaller FOV.

An artifact called “Beam Hardening” is also considered in the adjustment process to establish the FOV. This artifact can be corrected in the reconstruction stage using an algorithm and correction factor. However, sample material which is not in the FOV will cause misinterpretation and more difficult to correct. In order to avoid this effect, the region of interest has to be just equivalent to or smaller than the FOV. More details of beam hardening will be discussed in later sections.

Figure 3.19 shows the difference of FOV for one sample with different magnification. The sample is particle based and prepared in a syringe tube. Images are taken at 80kV with source/detector distances equal to -60mm/20mm, exposure time equal to 10 seconds, and with a 150µm glass filter. The left image is taken under 4X magnification having a FOV $(5102.82)^2$ µm² with center point x-ray intensity reading equal to 16942; the right image is taken under 10X magnification having a FOV $(2021.77)^2$ µm² with the center point x-ray intensity reading equal to 2891. Both images are taken in the same position.

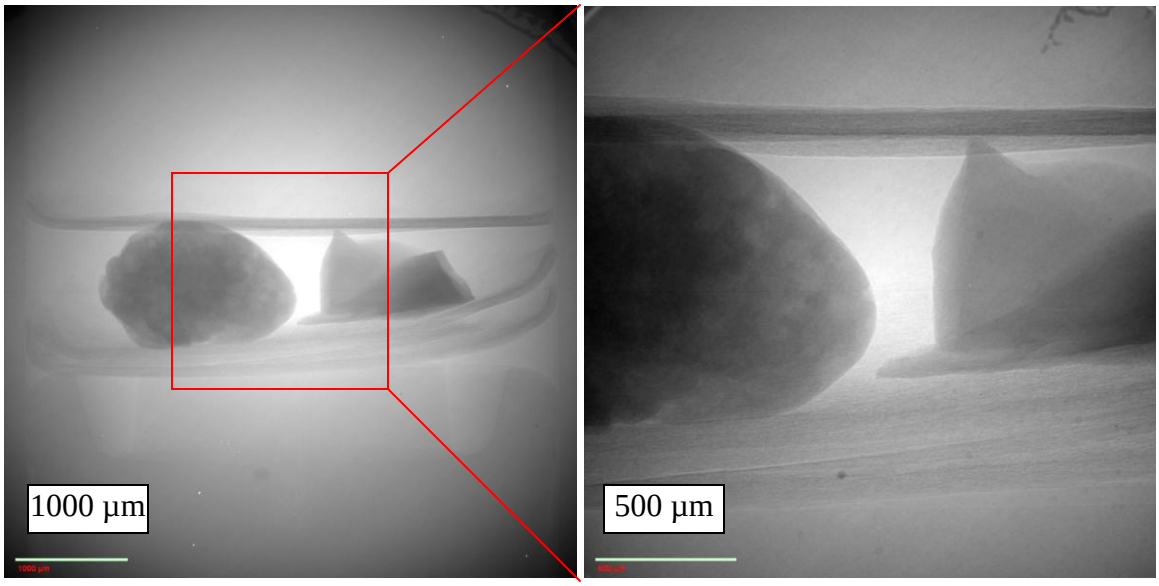

Figure 3.19 – A few particle samples sealed in an approximately 5mm diameter syringe.

An ideal condition is where the sample image is equivalent to or a bit smaller than the field of view. To achieve this condition, first the required resolution and sample size are to be considered according to Section 3.2.2 by using different magnification. Then the distance between source and detector is adjusted to obtain a better FOV. Make sure the sample or objective minerals stay in focus in the FOV for every angle in order to acquire enough sampling without much deviation. Rotate the sample stage by -90 degrees to 90 degrees in order to confirm the sample is always in the FOV for the scan.

3.3.6 Exposure Time

Exposure time is a decisive factor for the CT scan. Material density and elemental composition decides the energy level (Voltage), and exposure time decides attenuation coefficient reading for the sample. For a heavier, thicker or higher atomic number material, a longer exposure time is required to collect enough x-ray photons passing

through the sample. However, collateral effects like longer total scan time would cause overexposure of the reference.

Table 3.4 in Section 3.3.2 has already provided a basic use of exposure time and maximum exposure time without overexposure, and similar information was presented in the voltage section. The overexposure effect will be described in the reference setting. To decide a proper exposure time, the first consideration is the x-ray intensity counts. The minimum reading of the objective structure/mineral phase is required to be at least 3000, with a 10% difference in counts between phases. To obtain higher x-ray intensity counts on a high density/atomic number material, or a large sample size, the exposure time can be extended before the artifact of reference overexposure. The optimal operating exposure time is to be determined by the scan objective and image quality. Table 3.9 provides a list of optimal exposure time for different scan conditions for 150 um glasses filter and 1000 projections. The key points to determine exposure time are always based on three considerations: 1) enough transmission of x-ray photons to achieve more than 3000 counts on the detector; 2) reference is correctly acquired without over-exposure; 3) less scan time in case of any mechanical issue such as sample tilting, power fluctuation or detector failure.

Table 3.9 – Optimal exposure time for different scan conditions

Mineral	Scope	Volatege	Distance (mm)	FOV	Exposure Time	Total Scan Time
Gypsum	0.5X	60kV	-125/125	>5cm	3 seconds	50 minutes
Copper	4X	80kV	-44/20	5.2mm	9 seconds	4 hours
Copper	10X	80kV	-44/20	2.0mm	30 seconds	10 hours
Foamboard	4X	40kV	-120/20	4.2mm	10 seconds	4 hours
Oilshale	4X	80kV	-60/30	4.8mm	15 seconds	6 hours
Nickel ore	0.5X	100kV	-250/75	>5cm	1 second	1.5 hour

Exposure time (E) is a part of the total scan time. Mechanical movement time like shutter, sample rotation and reference scan time, or data digitization time like CCD data transfer, are also included in the total scan time. For each projection, the rotation/shutter time (R) is about 1 second, and the CCD data transfer (C) takes about 4 seconds. For one reference image preparation and acquisition (*ref*), it takes about 30 seconds to move the sample aside, take the shot and then move back. The estimated total scan time can be calculated by equation 3.9.

$$TotalScanTime = (E + C + R) * F + E * (ref) \tag{3.9}$$

F is the total projection counts. For example, a scan with 1000 projections and an exposure time of 9 seconds, would come to a total time = (9+4+1)*1000+9*(16+30) = 4 hours, the same time as the time specified in Table 3.9.

3.3.7 Projection Counts

The projection counts greatly affect the quality of the reconstructed image. In general, the radiograph set (projection) is collected and transformed using the Fourier Slice Theorem (Casteele, 2004). Each radiograph is converted into a linear regression of x-ray intensity in the Fourier frequency domain as shown in Figure 3.20. After all radiographs have been collected, the 3D image is "reconstructed" using the back-projection method which is the reverse of the Fourier Transform. Thus, the reconstructed image can be visualized as a 3D view with linear attenuation coefficients attached as CT numbers. The image is displayed by phase contrast based on the grey scale established for different materials.

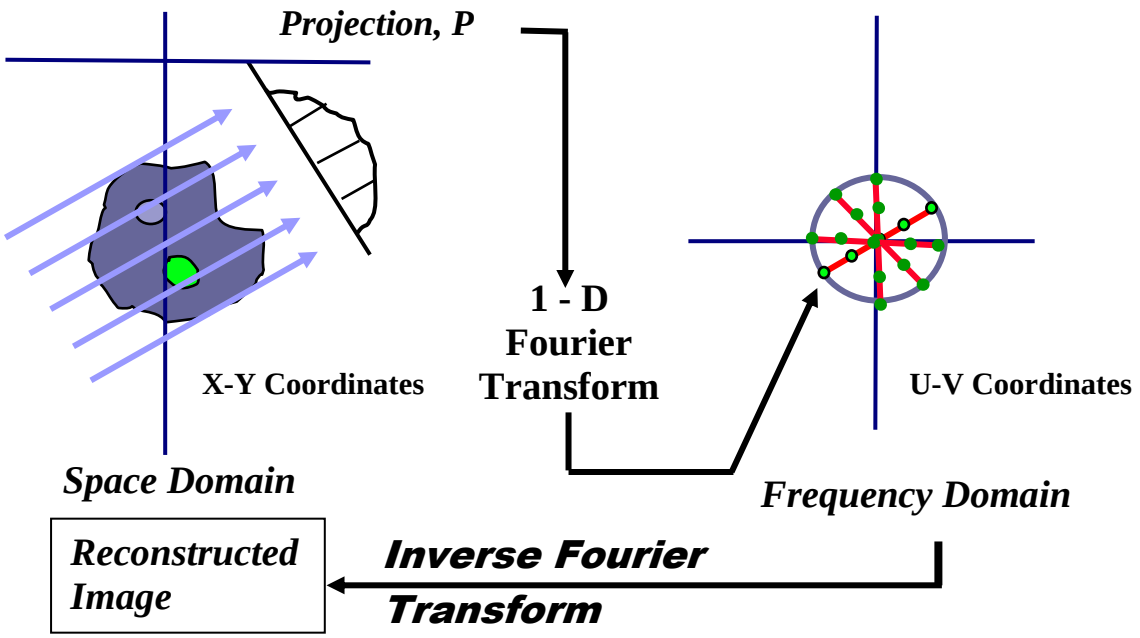

Figure 3.20 – Image processing from tomographic projections to image reconstruction.

The number of projections, in other words, "sampling", decides the voxel composition in the reconstruction stage. Generally, each voxel is reconstructed by projection from each angle in order to acquire enough image quality. In this consideration, a scan result giving an image dimension of 1000x1000x1000 requires 1000 projections. If the sampling is less than the voxel counts for each dimension, the image still can be reconstructed, however losing quality and sharpness of the result. This is also called "Undersampling". In the practical scan procedures, the full number of projections is used on detailed scans for such features as internal structure visualization, fine particle examination and mineral grain characterization; less number of projections, like 360 projections for a full rotation scan, is used for a quick view of sample features, such as high contrast mineral composition and CT standard scans. Figure 3.21 shows a bone particles sample scan using different numbers of projections and then reconstructed under the same condition.

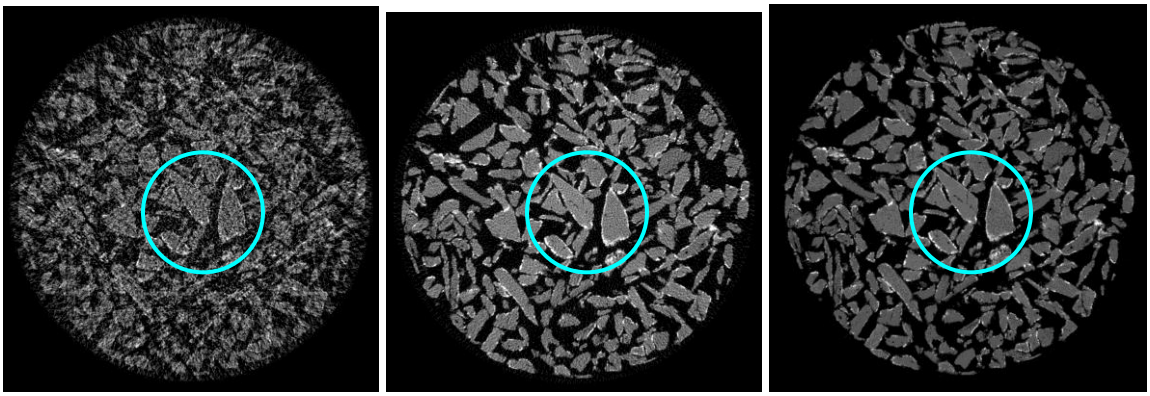

Figure 3.21 – The sample is scanned with three different numbers of projections.

In Figure 3.21, the left sample image is scanned at 36 projections and results in a large number of streaks and noises from reconstruction error at the circled areas. The particle in the circled area in the middle image, which is scanned at 360 image projections, has less noise. The right image, which is scanned at 1000 projections, has the best image quality and the most consistent linear attenuation coefficient of all three. The minor internal structure for the right image is obviously sharper and clearer than it is in the left image. To acquire a stable and correct result, at least 1000 projections are required during the scan procedure. However, there are some advantages to using less sampling scans depending on the scan objective. For example, a CT standard scan requires the mass attenuation coefficient of the material rather than internal structure. Thus, the prepared sample is filtered and selected as pure as possible before the scan to obtain a most accurate reading. In this respect, the scan does not require many projections because the mass attenuation coefficient has no significant variation in small and large number of projections. Another advantage is to reduce the scan time and file size. In a preliminary scan, the objective of the scan is to measure the linear attenuation coefficient and internal structure, approximately. If the result shows valuable information, a detailed scan for further study with the full number of projections will be done.

3.3.8 Consideration of Reference States

Because the environment for the HRXMT scan is neither in a vacuum nor isolated, reference states are measured to remove x-ray attenuation of background, air and other effects associated with the lens like dirty spots and dust. There are a few ways by which the reference state can be established: single reference state, multireference states and an averaged reference state. Multiple references are taken and applied for each radiograph during the scan process to establish the same condition for the reference state as the corresponding radiograph. The reference state can be acquired after each one or a few of the radiographs have been taken to obtain the background x-ray attenuations, same as that measured during radiograph acquisition. This method is suitable for unstable environments when there is variation of x-ray intensity caused by power fluctuation, movement of the atmosphere/air, where background x-ray intensity is not fixed. The multi-averaged reference state is a set of all reference states collected during the scan and then integrated into one image. This method is suitable for regular scans to save time-taking reference scans. Single reference is usually applied on scans of huge sample size which is unable to be removed from the field of view during the automatic reference shooting. The reference state can be shot before or after the scan following the same scan condition. This method spends the least time, and also results in the least accuracy in correction for background x-ray intensity. Two modes are provided for the reference on projection/tomography images. Figure 3.22 shows a series of images of projection using different reference modes. The scan conditions are set at 4X magnification with 9 seconds exposure time; source voltage is set at 80kV; distance between source and detector are -44 mm and 20mm; camera binning is set at 2 with a 150 mm glass filter.

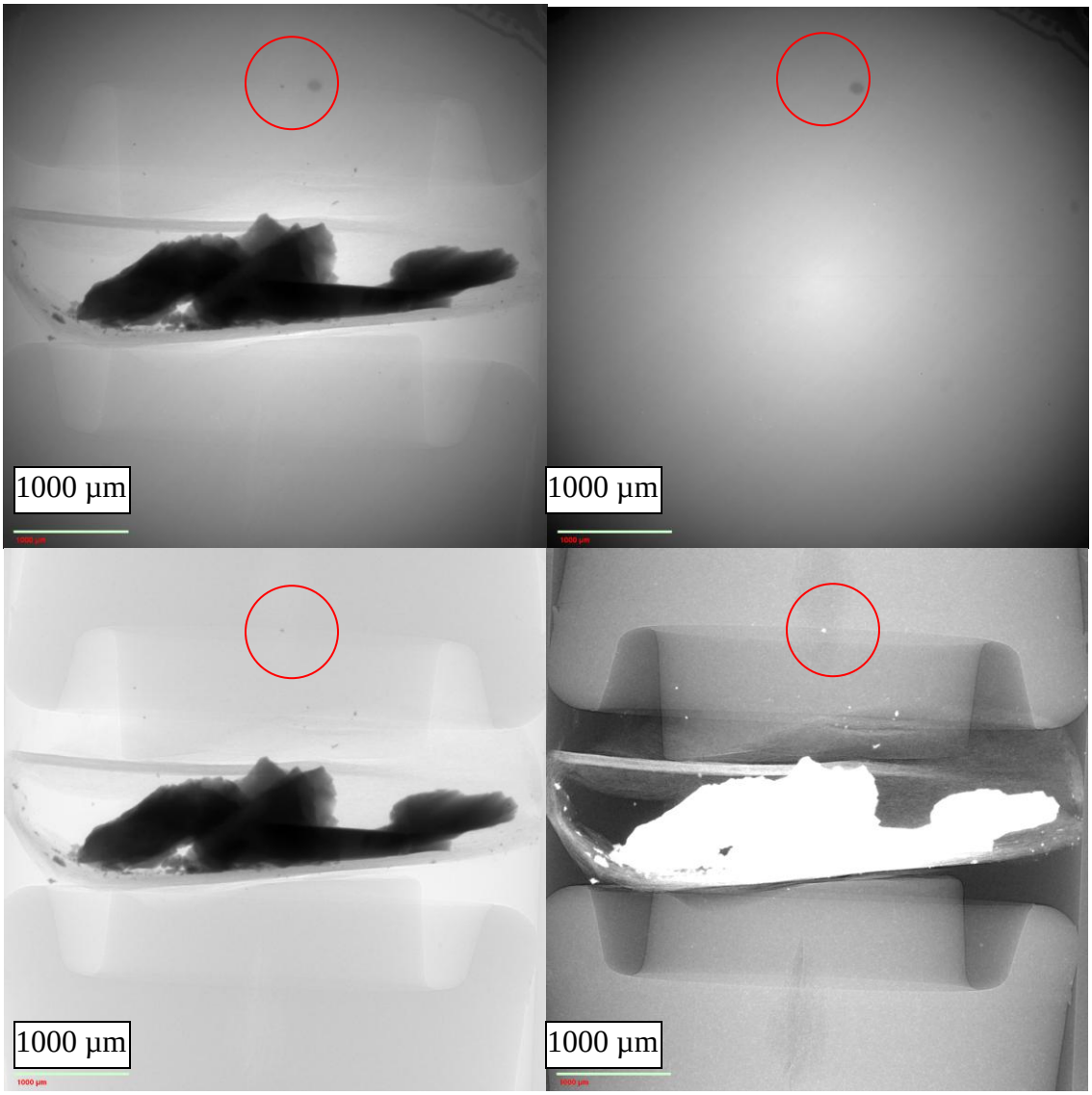

Figure 3.22 – Images of different reference states.

Figure 3.22 shows projection images of different reference states. On top-left is the original radiograph without reference applied; on the top-right is the reference; on the bottom-left is the radiograph applied with the reference with absorption mode and on the bottom-right is the transmission mode. The circled area is dust on the filter. The "Absorption" mode, which means the x-ray attenuation coefficient of each voxel is obtained when the intensity in the reference image is subtracted for the detector reading

corresponding to the same coordinates, equals the x-ray energy absorbed by the sample and is shown in the bottom left image. Another mode is “Transmission”, which is shown in the bottom right image. This mode is contrary to the absorption by displaying the “transmitted” x-ray intensity. A control option menu for reference in the XMController can switch the method to different modes.

In a reference acquisition shot, the sample stage will move to the end of the X axis away from the field of view, and then a few reference shots are taken. References images are saved as a multireferences tomography file, and an Averaged Reference projection, with the tomography files in the same folder. The multireferences shots can be applied on every projection image according to the time sequence, or be accumulated and averaged as a single reference applying to all acquired projections. In the controller application, both options “Reconstruction after scan” and “Collect reference but no reconstruction” can acquire references. XMController provides a reference collection setting which can be manually modified by intercepts and slices (XRadia, pp. 87, 2010). The first option changes the interval of projection acquisition for each reference shot that has been taken; the second option decides how many reference images have to be acquired for each reference shot. Multireferences and averaged references can be applied on most sample scans.

However, if a sample is too big to move away from the field of view, a single reference is taken after the sample is removed from the stage. This method is usually applied on 0.5X magnification because the samples are large and not able to be moved out of FOV shown in the left image in Figure 3.22. Correction with a single reference is the same as correction with an averaged reference.

A phenomenon called “overexposure” sometimes happens during the scan. The reference projection loses its function and the detector becomes saturated because the exposure time is too long. Whether using the absorption or transmission method, the sample mass attenuation coefficient can not be obtained by subtracting air and dust spots from the reference projection.

Figure 3.23 shows a comparison of reference projections and sample projections for different situations. Two errors were encountered for the measurement of reference projections: at the left image is the normal reference projection and in the middle image, overexposure has occurred. To avoid this problem, lower voltages, longer distances and less exposure time can be used to help reduce the x-ray intensity of the reference projections. In the right image, the sample is not totally removed from FOV when acquiring reference state. A single reference state can be applied later after removing the sample in the field of view. Generally, reference is a main factor used to decide the settings above, and has to be checked before the scan by moving away the sample and taking a single reference shot to evaluate the center x-ray intensity. All pixel readings must be lower than 60000 with a 10% error.

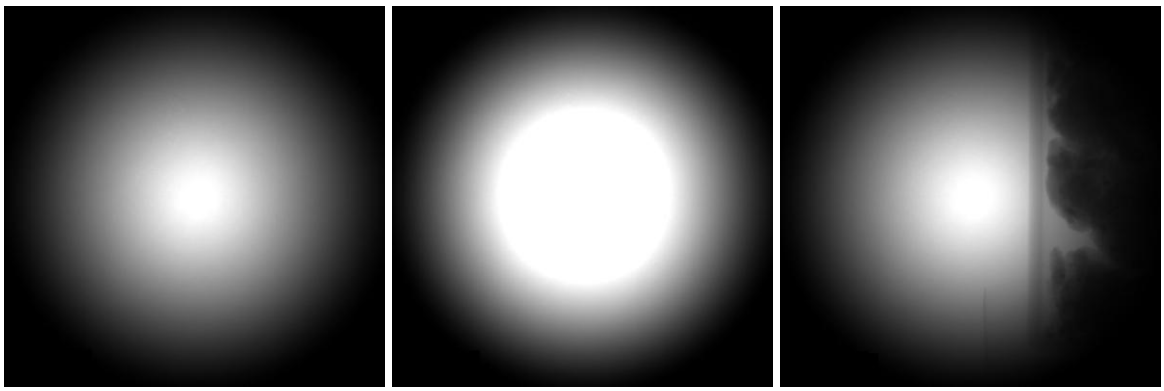

Figure 3.23 – Two errors encountered for the measurement of reference projections.

3.4 Reconstruction Considerations

After the projections have been acquired from every angle during the scanning, a reconstruction process is required to establish the sample image in 3D. XRadia provides an application called "XMReconstructor" for this purpose. It helps users evaluate and determine which variables to vary in order to obtain the best image quality, and reduce the artifacts. In the following sections, reconstruction conditions will be discussed based on the options provided by the XMReconstructor.

3.4.1 Center Shift

The field of view is not always centered on the object and deviates from the center line. Thus, the image will be reconstructed with artifacts shown in Figure 3.24. The image on the left is clear and focused with a good center shift (-8); the image on the right is not center shifted or has a bad shift (10). Such artifacts are caused by the center shift, an offset from the center line of the detector (XRadia, pp. 155, 2010). To correct this artifact, we can adjust the offset distance and acquire a higher quality image.

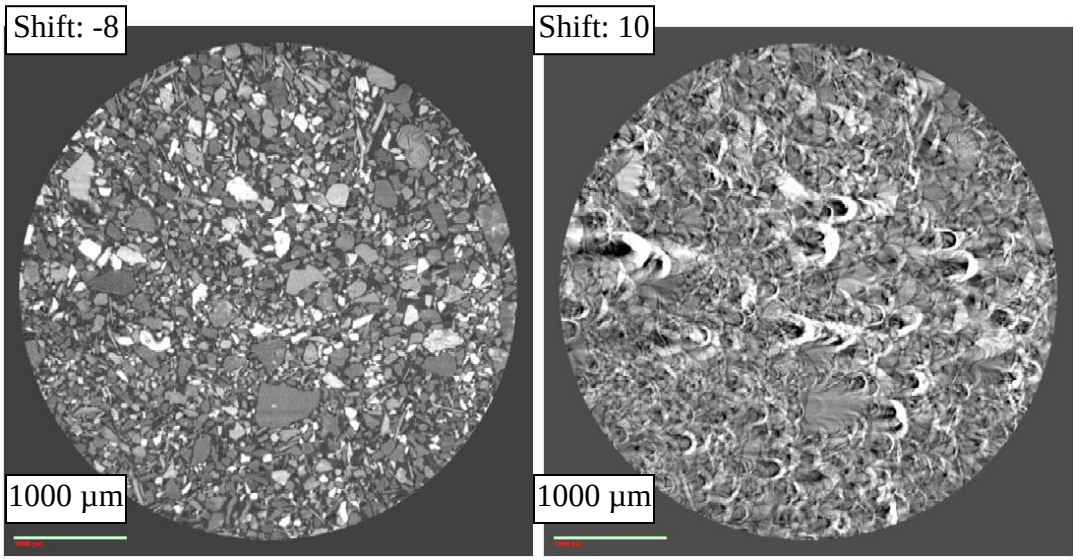

Figure 3.24 – Images of different center shift correction.

The center shift occurs on the XZ plane because the sample stage rotates on the Y axis (see Figure 3.3). To acquire an image with the appropriate center shift, the XMReconstruction provides a function for center shift adjustment to shift the center axis from -10 to 10 (shift range) with a step size equal to the voxel resolution. Figure 3.25 shows two different image patterns which were scanned at 180 degrees (left image) and 360 degrees (right image). In a sample scan with a homogeneous single phase material, or high resolution scan with tiny specific features, it is very difficult to identify the center shift. In order to enhance the image contrast and material phase differences, we can move the XZ plane on the Y axis to find out some specific features, or adjust the histogram to enhance the contrast of the image.

The histogram is a function in XMReconstructor that adjust brightness and contrast of each image. This function will find the highest and the lowest CT number, which is the scaled x-ray linear attenuation coefficient, and then assign the brightness of each voxel by the range. It can be chosen using local histogram (brightness scaled by current image), or global histogram (brightness scaled by whole image set).

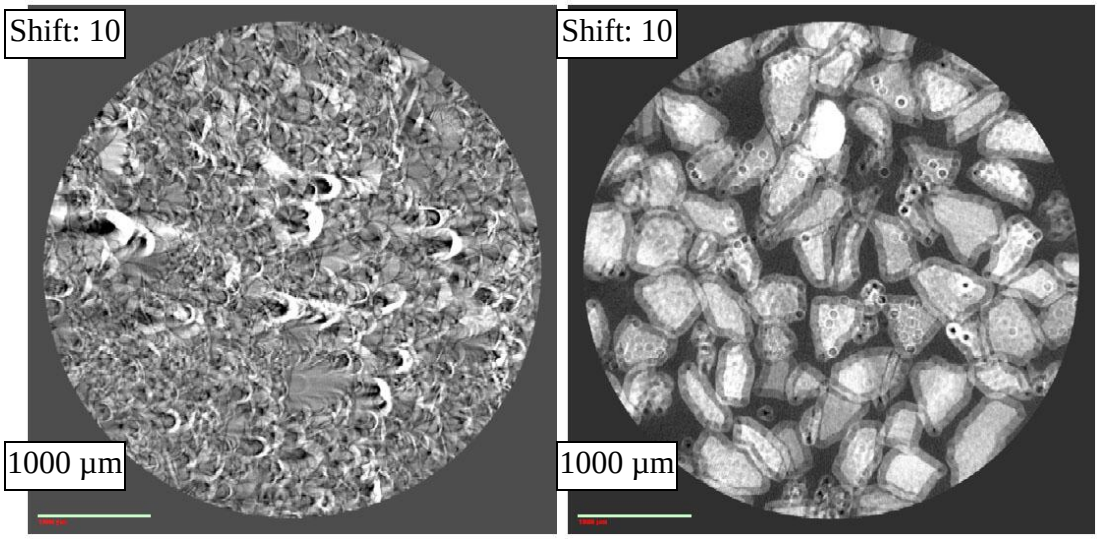

Figure 3.25 – Center shift images scanned at 180 degrees and at 360 degrees.

Figure 3.26 shows the same XZ plane with different levels of the histogram. The histogram function in the XMReconstruction can be applied in order to adjust the brightness and contrast of the image. The circled part is a dense (bright color) mineral that can help determine appropriate center shift. The dense mineral phase has been emphasized in order to more easily determine the center shift. Rotation center in the XMReconstructor provides a default range of center shift from -10 to 10. Sometimes the center shift value does not fall in this range. The user can increase the range and redo the preview until a clear image with an appropriate center shift value is obtained. Once the center shift amount is obtained, the number can be applied for the next calibration of beam hardening correction. It is noted that the center shift value will be the same in every scan if the magnification lens or the distance of detector are not changed. In this respect, the center shift can be recognized as a deviation of detector position. If the center shift is too large and reduces the field of view dramatically, a recalibration process is needed to readjust the detector position and be moved back to the center line.

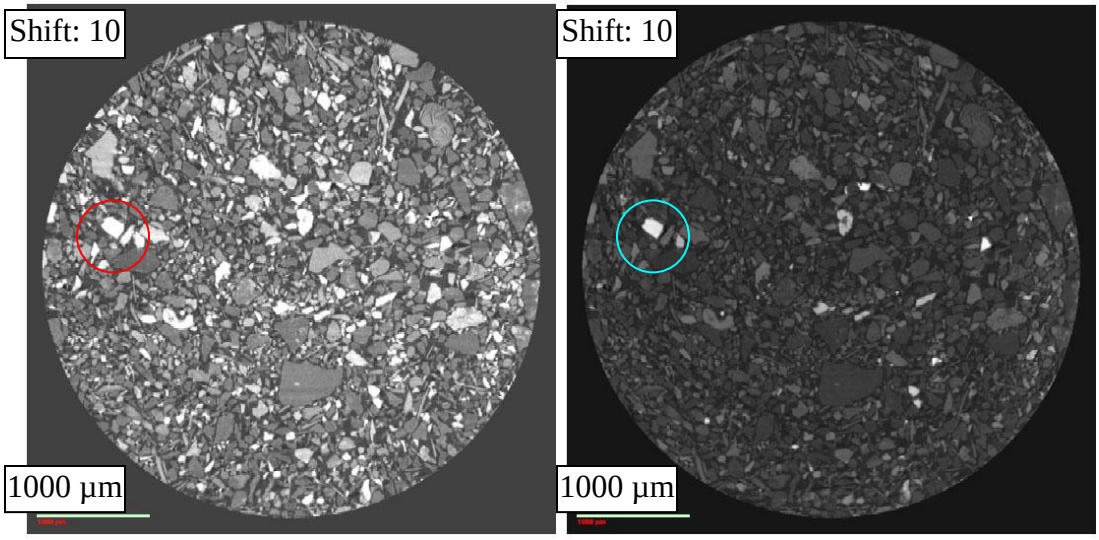

Figure 3.26 – Two match planes are displayed under different histograms.

3.4.2 Beam Hardening

When a polychromatic x-ray source projects x-ray beams through a homogeneous cylindrical object in space, the object absorbs some x-ray photons, and the rest of the x-ray photons will pass through the sample and their intensity can be measured on a detector. The amount of x-ray energy attenuated by an object is based on equation 2.4, and affected by the transmission distance x under specific circumstance. The polychromatic source emits x-ray beams at different energy levels, including high and low energy levels other than characteristic x-rays which were mentioned in Section 3.2.3.

Although filters can remove low energy level x-ray beams, the dispersed energy levels of x-ray beams cause various attenuation coefficients of one specific mineral phase based on equation 2.4. As mentioned, x-ray intensity is also affected by the distance through which the photon passes. Thus, the obtained linear attenuation coefficient of a homogenous material is not uniform in every place. The measured linear attenuation coefficient is lower in the center, where the x-ray passing distance is longer, and higher at the edge, where the x-ray passing distance is shorter. In other words, the x-ray beam looks “Hardened” at a higher energy level in the boundary area (ImpactScan, 2005).

Figure 3.27 shows a practical beam hardening image for which the CT number profile is shown across the object. This sample is a cylindrical steel rod made of uniform material. The left image is a cross section view of the rod sample, and the right image is a CT number distribution of the line across the rod in the left image. Theoretically, the homogeneous rod should perform a uniform CT number reading in the profile. However, the profile illustrates a higher reading at the edge. This effect is also called “cupping artifact”.

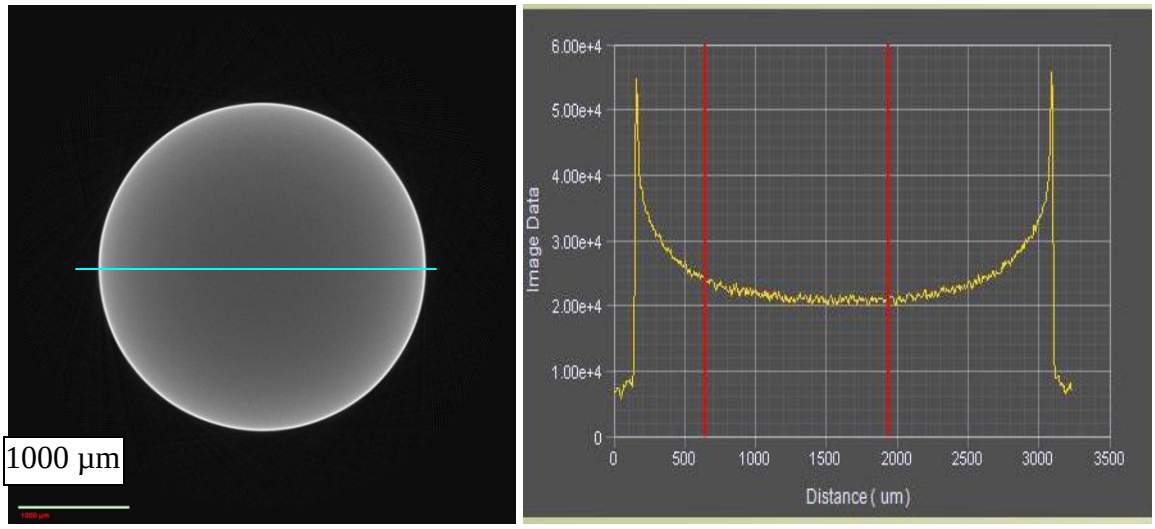

Figure 3.27 – Beam hardening artifact and measured CT number.

Correction can be applied by calibrating the CT number profile, or using a software algorithm to remove the artifact. XRadia already has a function in the reconstruction software stage in which one inputs a beam hardening number to determine the depth of beam hardening correction of the image. A series of images using different beam hardening numbers in a certain range are provided by XMReconstructor. The user can compare the images and determine an appropriate beam hardening number that gives a high quality image. Once the number is decided, the reconstruction controller will put a beam hardening correction in the setting automatically.

This artifact is usually more obvious if a sample contains high density or high atomic number materials. To obtain sufficient x-ray intensity counts on the detector, the required x-ray energy level is usually higher, and the exposure time is also longer. In this respect, the dispersed x-ray energy affects the difference of reading by travelling distance is even more significant. Another situation is the irregular shape of a sample, or if the sample size is larger than the field of view. The mass absorption of x-ray energy is

dramatically defined by the path, which means the x-ray travel distance, or the thickness of the sample. Specific shapes such as rectangle, cube, thin-film, or a sample which has numerous parts not in the field of view, would also cause this artifact to be more difficult to correct in the reconstruction.

Figure 3.28 shows a series of images of one sample scan using different correction numbers. The particle composition is different on the image using different beam hardening number. A copper ore sample is scanned under 80kV, 4X, 10 seconds exposure time, and then reconstructed with different beam hardening correction. The image at the left is a cross section view and reconstruction using a beam hardening number at 3. Images at the right are of the circled area from the left image and reconstructed using different beam hardening numbers. Images from top left to bottom right are reconstructed using beam hardening number 0 (top left), 1(top right), 2 (bottom left) and 3 (bottom right).

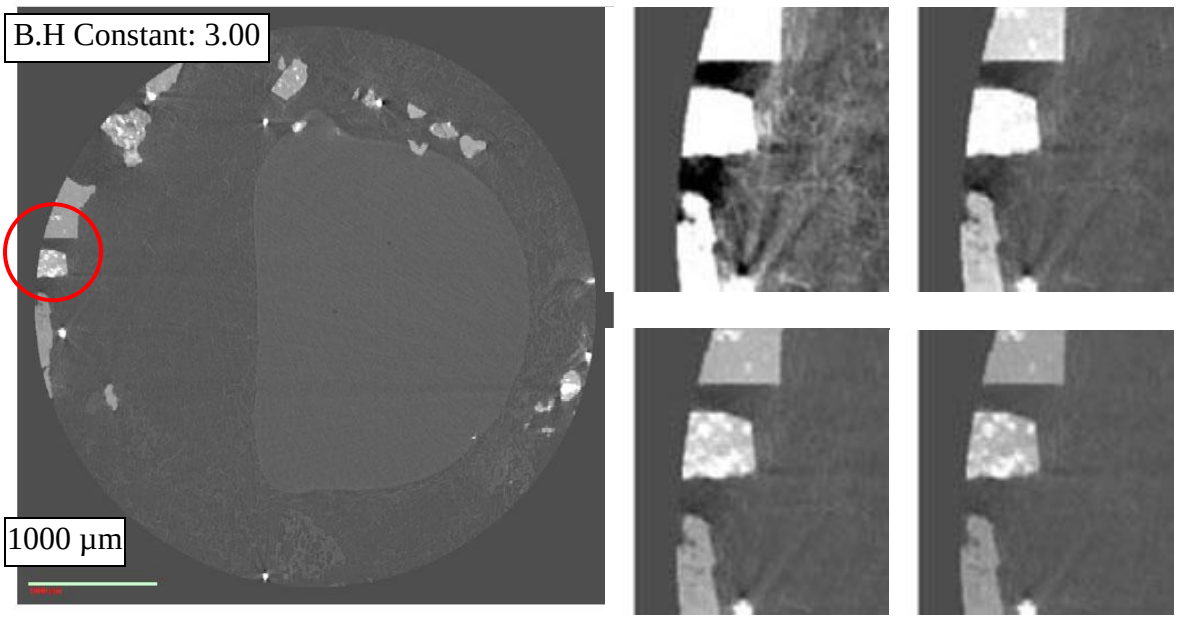

Figure 3.28 – Sample is scanned and reconstructed with different beam hardening correction.

Comparing each image in Figure 3.28, the image using 0 as a beam hardening number has a significant white boundary that covers almost all features in the boundary area. Images using 2 and 3 as the beam hardening number reduce this artifact dramatically. The mineral phases in the circle area are now significant with beam hardening correction. However, using 3 as a beam hardening number does not enhance the sharpness in the circle areas, but changes the reading of attenuation coefficient in the center. Streaks and internal structure in the main grain are also removed using high beam hardening number. It is apparent that beam hardening correction is capped, usually from 0.5 to 2. Numbers higher than 2 usually have no significant correction, but have the attenuation coefficients slightly affected with correction due to beam hardening.

3.4.3 File Conversion

File conversion is an important part of CT data storage. The tomography file is not saved in a geometry of vectors, but in a geometry of voxels. Thus, the scan resolution and color depth decide the file size and format. The CCD detector has a sensitivity of color depth in a 16-bit grey scale, which means the reading is between 0 to 65,535, positive integers. A single projection image in two dimensions is captured by the detector, visualized by XMController on the screen and then saved as a tomography file pattern with extension .XRM. The XRM file contains information of coordinates, angles, exposure time, source voltages, distances, etc. Datasets that contain a collection of projection images are saved with the extension .TXRM. This dataset of projections with the extension .TXRM can be reconstructed by XMReconstructor to form two-dimensional slices oriented in the XZ plane. Slices generated from the .TXRM file are

stored in a file with the extension .TXM, which is able to be processed with the XMController and XM3DViewer.

In the XMController, the TXM file can be exported as the following formats: 8-bit tiff, bitmap, jpeg, 16-bit raw tiff, single XRM image and binary files (.bin). The Binary file (.bin) format is the same format as the .raw file with simply different extension. The .raw file is a common file type in image processing and accepted by most software applications. The advantages of .raw file type are easy-accessibility, fast-process and no data loss during interpretation. When an image file is generated, a header file is included with necessary information such as width, height, resolution and data type.

When the TXRM file is being reconstructed in the XMRreconstrutor, a data output file format has to be chosen in the following options. According to the specification of Micro XCT 400, the maximum color depth of the CCD detector is 16-bit; for each voxel, x-ray attenuation coefficient is saved in a binary type unsigned 16-bit length string. Unsigned short 16-bit file type provides a same number range in 2 bytes length as detector assigned, which keeps the attenuation coefficient unchanged. The format float 32-bit is using 4 bytes space to store each voxel reading with floating point precision for certain purposes. Unsigned byte is an 8-bit file type providing 1 bytes space from 0 to 255 integers for rescaled attenuation coefficient numbers using global minimum/maximum intensity, or bided by input intensity range. Equation 3.11 shows a calculation of raw file size according to the image dimension and file format.

$$x \times y \times z \times fileformat = filesize(byte) \tag{3.11}$$

For example, a tomography file has been reconstructed and converted into an unsigned short 16-bit .raw binary file in a 1012x1024 dimension (XY plane) with 1014 slices (Z axis); the file size can be calculated as 2 gigabytes, approximately.

$$1012 \times 1024 \times 1014 \times 2 = 2101592064\ (bytes) \cong 1.95726\ (gigabytes)$$

Table 3.10 shows files for regular scan conditions with a header file and different file sizes. Unsigned short file type (2 byte) stores the attenuation coefficient numbers the same as the depth of the CCD detector (16-bit); however, unsigned byte file format (1 byte) reduces half of the data size for data storage. The advantage of the unsigned byte is less disc space consumption, especially for the scan which does not have many mineral phases, or for the scan which is focused on internal structure. The unsigned byte file is finally burned into a DVD disc with the projection files as backups. These two files just fit a regular DVD size format (4.7GB).

Smaller data size does not only help save storage space but also allows low-end computers to process the image file under the system limitations. It is favored to use unsigned byte format to store a final .raw file. File conversion can be done from unsigned short to unsigned byte using MIPAV (MIPAV, 2007). The .raw file can be converted from 16-bit unsigned short to 8-bit unsigned byte and rescaling. The scale is usually a range multiplied by 255 in a specific ratio focused on the range of objective mineral attenuation coefficients. Figure 3.29 shows a comparison of CT number at the same voxel in unsigned short and unsigned byte. The image is extracted from the scan in Table 3.10, and the conversion ratio is 40. The CT numbers are different in the left image, 42744 (16-bit, unsigned short) and in the right image, 166 (8-bit, unsigned byte).

. **Table 3.10** – Scan conditions and header file of BLP-1 scan.

Projection Acquisition	
Sample Name	BLP_1_+75µm
Date	February 12th, 2010
Total Scan Time	4 hours
Objective	4X
Source Settings (kV/W)	80kV/10Watts
Pixel size (µm)	4.85 microns
Start and End Angle	-95 degrees to 95 degrees
Number of Views	1000
Time per View (sec)	9 seconds
Source/Detector Positions	-44mm / 20mm
Camera Binning	2
Physical Filter	150 µm glass
Source Drift	-8
Reference Type	Averaged Multi-References
Secondary Filtered Reference Details	None
Software Filtering	None
Image Reconstruction	
Recon Binning	1
Ring Removal	None
Beam Hardening	0.5
CT Scaling or Max/Min counts	Copper Ore Standard
Header File	
Image Taken (Z axis)	1024
Width (X axis)	1008
Height (Y axis)	1024
Data Type	Unsigned Short
Pixel Size	4.85 micron
Voltage	80
Current	125
Exposure Time	9 seconds
File type and size	
Single Shot Tomography (.xrm)	4,128 K
Single Shot Tomography (.jpg)	339 K
Total Projections Tomography (.txrm)	69,724 K
Reconstructed File (.txm)	2,089,260 K
Binary File 16bits Unsigned Short (.raw)	2,089,260 K
Binary File 8bits Unsigned Byte (.raw)	1,033,630 K

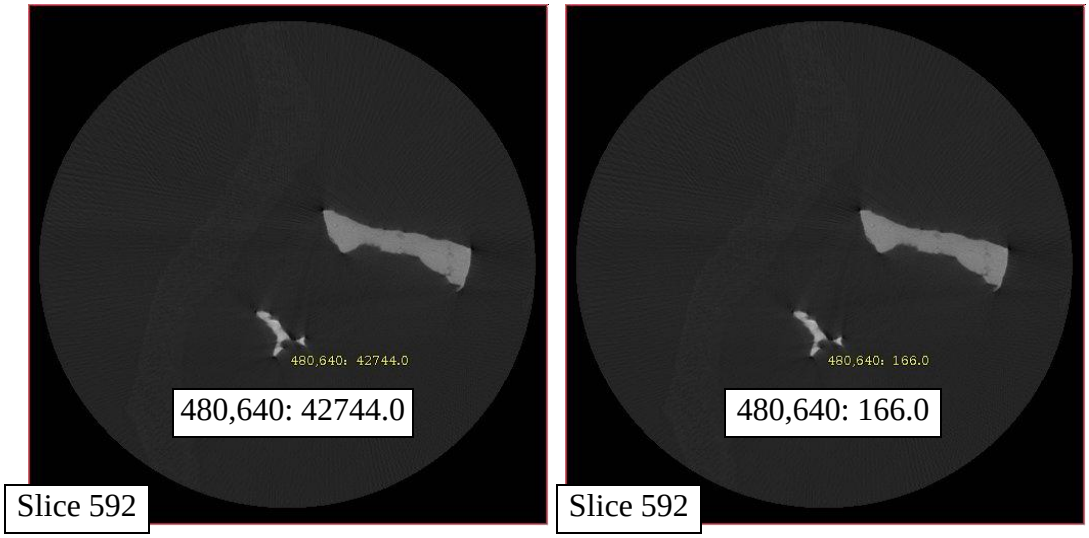

Figure 3.29 – A cross section on XY plane having same coordinates but different data format.

3.5 Scaling of Attenuation Coefficients for Mineral Identification

Computerized Tomography Standard (CT Standard) is an important tool in Micro XCT 400 to classify and quantify sample mineral composition and characteristics. In the reconstruction phase, CT numbers are assigned according to the mineral attenuation coefficient, and distributed in the range of highest and lowest readings. This scaling method is called Global Scale, which gives a CT number of each voxel according to the relationship to the maximum and minimum attenuation coefficient. It is very convenient to distinguish different mineral phase while using the global scale. However, if the mineral sample was some minerals having very high or low density elements, it will cause scale variation. Materials having very high and very low attenuation coefficients extend the range of the scale, and compress the scale range of CT numbers in between. The image contrast of objective materials is also reduced. In this case, a standard must be set in order to exclude overestimated and underestimated elements which extend the scale, and focus on objective materials.

On the other hand, a standard also helps to quantify mineral composition by measuring a standard material's density and mass attenuation coefficients. While a standard material has been scanned and has a fixed CT number under specific scan conditions, mineral density can be correlated to the mass attenuation coefficient and a linear regression of the density-mass attenuation coefficient relationship can be made. Thus, mineral phases having mass attenuation coefficient close to the standard material are able to be identified, relatively easily. If the mineral composition of a sample is known, the density and the amount of each mineral phase can be calculated by counting the CT number of each voxel. To apply a CT standard on the scan, at least one CT standard has to be made, and the sample scan must follow the same condition as the CT standard has, then a CT number is assigned for each voxel using the CT standard scale during the reconstruction phase. In the following section, a few copper minerals are introduced to show the operating procedures to establish a CT Standard.

3.5.1 Calibration Using Mineral Standards

In many cases, copper minerals are a common mineral phase of interest. A CT standard has to be set for the mineral characterization in subsequent analysis. The left image in Figure 3.30 shows a set of mineral samples including pyrite (FeS_2), chalcopyrite ($CuFeS_2$), bornite (Cu_5FeS_4) and covellite (CuS). These are the most common copper mineral types with characteristic mass attenuation coefficients.

To establish a CT standard, mineral samples must be homogeneous consisting of a single mineral phase. Impurity and heterogeneous internal/external structures will cause the attenuation coefficient to vary. In this example, four pure particles of each mineral type was hand picked and sealed in the sample container (Syringe).

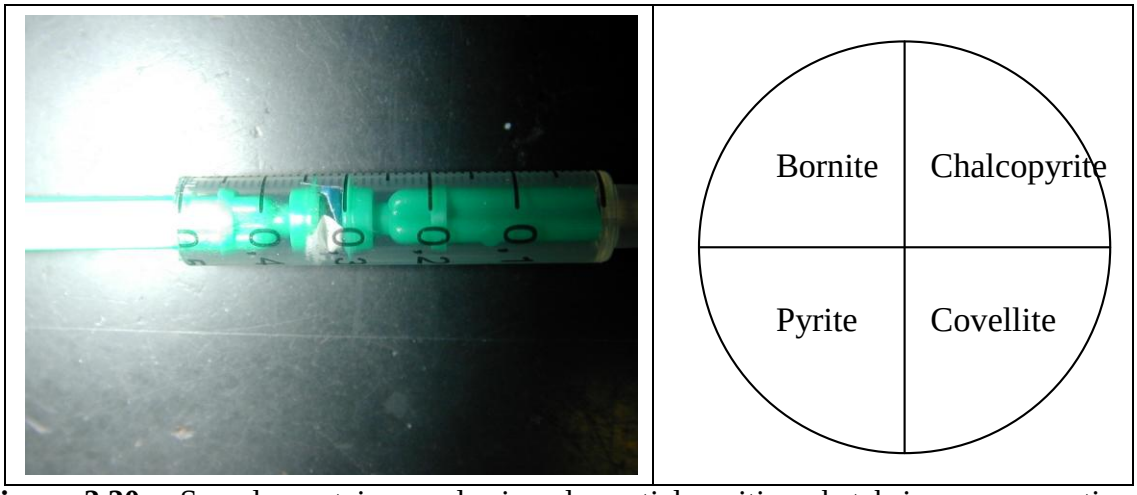

Figure 3.30 – Sample container and minerals spatial position sketch in a cross section view.

Four different mineral particles were sealed in the sample container at different locations, and their characteristics are listed in Table 3.11. Also, Figure 3.31 shows a mass attenuation coefficient relationship for the four individual minerals at a certain energy level using XMuDat. Lines from top to bottom are listed corresponding to bornite, covellite, chalcopyrite and pyrite. The mineral's effective atomic number can be calculated by equation 2.3 and the densities can found on http://www.mindat.org/ (Ralph and Chau, 1993). The density we used here is the theoretical one (calculated by atomic structure) for use in equation 2.3. In Figure 3.31, the results of XMuDat show that pyrite has the lowest mass attenuation coefficient and bornite has the highest one. This graph provides the idea of the CT number relationship and allows for the identification of each mineral phase.

Table 3.11 – List of copper minerals properties.

Name	Chemical Formula	Effective Z Number	Density
Pyrite	FeS_2	21.8459	4.99 g/cm^3
Chalcopyrite	$CuFeS_2$	24.7988	4.2 g/cm^3
Bornite	Cu_5FeS_4	26.4213	5.09 g/cm^3
Covellite	CuS	26.0074	4.7 g/cm^3

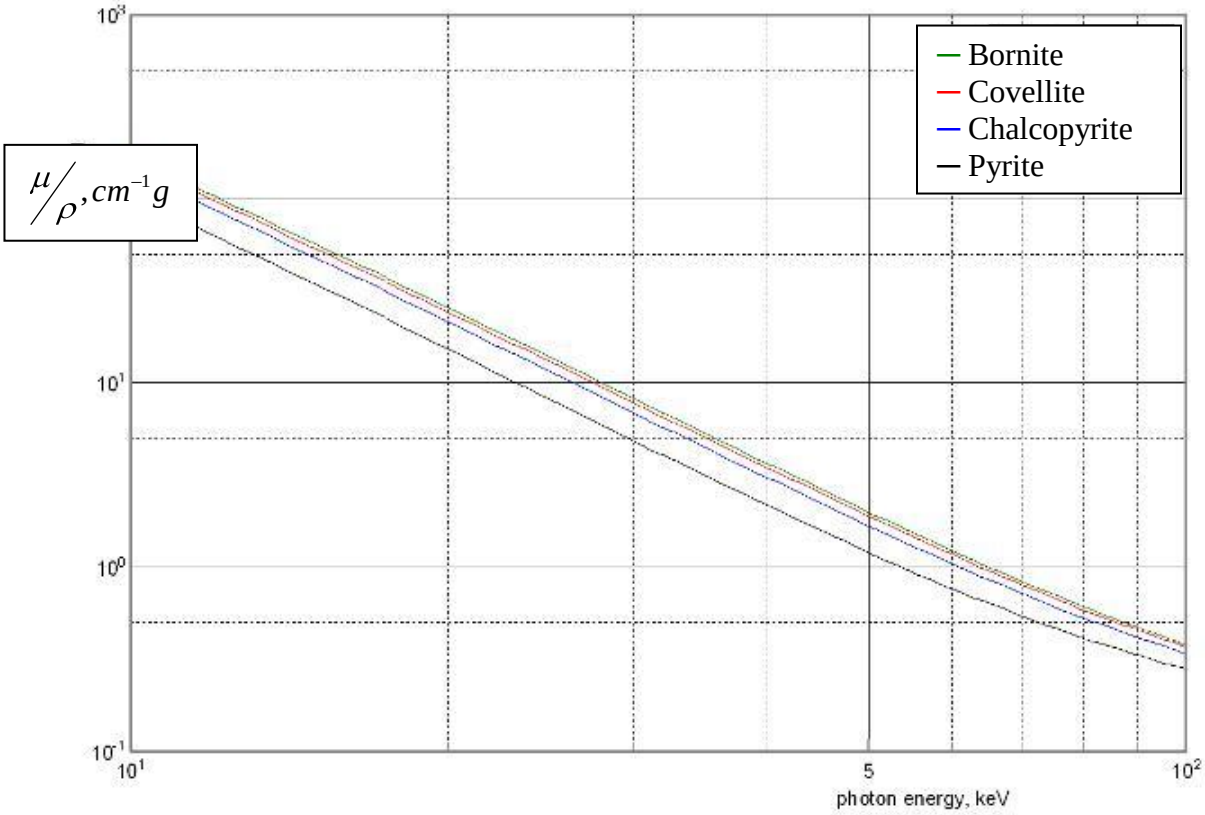

Figure 3.31 – Mineral mass attenuation coefficient relationship of 4 specific minerals

First, the scan conditions have to be set. To establish a universal scan condition for common copper mineral scans, the energy level has to be determined. The energy level for copper mineral scans usually starts from 60kV to 150 kV with different mineral composition and sample thickness. Several CT standard scans can be set according to different requirements. In this case, the x-ray source voltage is set at 80kV/10watts. All four minerals will gain enough x-ray photon penetration and the x-ray intensity can be measured on the detector.

The magnification is set at 4X to obtain an image resolution of 5 micron per voxel. The source and detector distances are set at -44mm and 20mm in order to have a better field of view and enough x-ray photon counts. The exposure time is set at 9 seconds per image acquisition providing at least 10,000 x-ray intensity counts on each voxel to obtain

a good contrast with different mineral phases. The sample is sealed in a 5mm diameter syringe.

Since the main objective of the scan is to acquire the linear attenuation coefficient of each mineral rather than the inner structure or high resolution result, the number of image acquisitions is set at 189 images in order to get a fair quality of inner structure and enough sampling for image reconstruction. The scan is taken at half rotation and one image acquisition in each degree.

The reconstruction is following the normal settings except the beam hardening. The beam hardening number is set at 1 to avoid the beam hardening effect at the image boundary area. Table 3.12 shows the scan details.

. **Table 3.12 –** The bornite standard scan conditions in 80kV, 4X magnification.

Sample Name	Bornite Standard, 80kV, 4X
Date	May 21th, 2010
Total Scan Time	1 hour
Objective	4X
Source Settings (kV/W)	80kV/10Watts
Pixel size (μm)	4.85 microns
Start and End Angle	-94 degrees to 94 degrees
Number of Views	189
Time per View (sec)	9 seconds
Source/Detector Positions	-44mm / 20mm
Camera Binning	2
Physical Filter	150 μm glass
Source Drift	0
Reference Type	Averaged Multi-References
Secondary Filtered Reference Details	None
Software Filtering	None
--	--
Recon Binning	1
Ring Removal	None
Beam Hardening	1
CT Scaling or Max/Min counts	Global Scaling

After the tomography images have been acquired, the global scaling is applied to have primitive images in the reconstruction phase. The reconstructed 2D cross section images are shown in Figure 3.32. The four mineral particles have different linear attenuation coefficients.

According to Figure 3.31, bornite has the highest reading which is presented on the top-right particle, while pyrite has the lowest reading for the top-left particle. Chalcopyrite and covelllite can also be identified by the location compared to the other minerals. Recalling Figure 3.30, we can identify each particle by the spatial relationship and corresponding position. Figure 3.32 shows a 2D cross section image and a 3D volumetric image generated by HRXMT result.

In Figure 3.32, the left image is the cross section view of the reconstructed image. (1012x1024, slice 480), and the right image is a volumetric image. The 3D image is flipped on the X axis and the corresponding minerals are labeled. The next step is to set up a CT standard in the XMController.

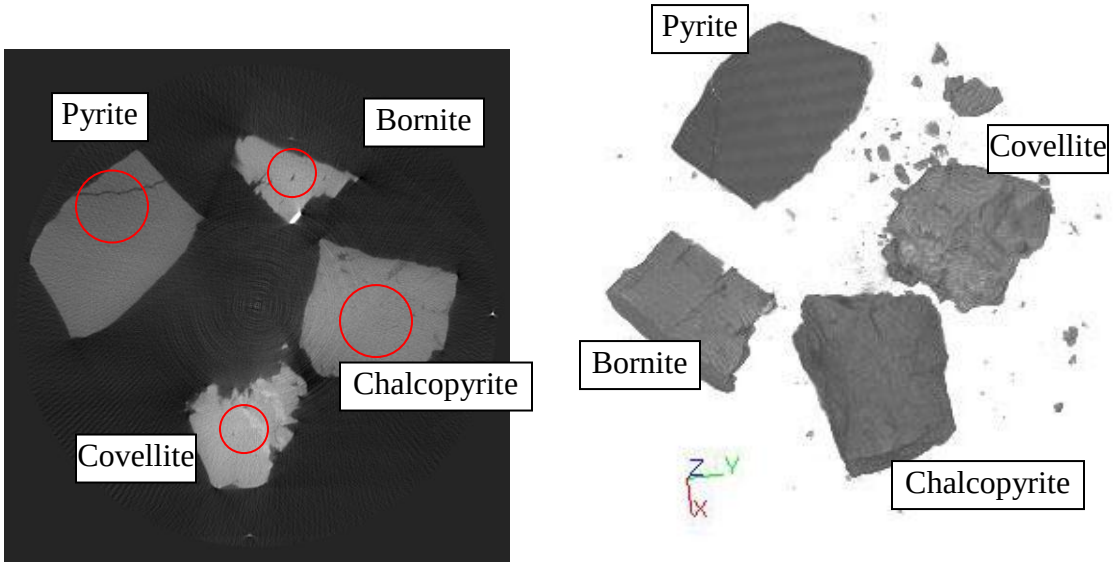

Figure 3.32 – The cross section view and a volumetric image.

First, the bornite mineral is picked to demonstrate the operating procedures. A region of interest (ROI) has been selected including a portion of the bornite particle and a portion of air. This function can be found in the XMController in Figure 3.33. In Figure 3.33, the ROI selection icon can be found in area A. The XMController provides different kind of ROI tools including circle, rectangle and polygon; the selected ROI region on image can be found in area B. Note the selected region is covered by pure bornite area, and will obtain simply bornite CT number reading in the calculation; the ROI calculation is in area C in the Process menu. This function calculates the histogram of the ROI including multiple slices, and gives a full list of the attenuation coefficient for each voxel.

Readings in the ROI will be calculated and cumulated using all slices of view to have an averaged CT number reading. Considering the ROI may contain mineral phase and air phase, the CT number value distribution will be plotted using the "Mean" value method to obtain a moderate result. Other options such as "Median", "Minimum", or "Sum" can be selected according to user's purpose. Figure 3.34 shows partial CT number readings of the sample. Area A and Area B in Figure 3.35 have the highest and the lowest readings. To enhance these regions, the ZOOM function on the graph is used to display the peak value and the flat line value shown in Figure 3.35. The peak number at area A in Figure 3.35 represents the CT number readings of the bornite particle, and the flat line value at area B in Figure 3.35 represents the CT number readings of air. Values are recorded as 43,250 and 10,050.

These two CT numbers represent the attenuation coefficients of bornite and air. To characterize and to quantify the materials, a CT scale has to be established and the procedure will be performed in the next step.

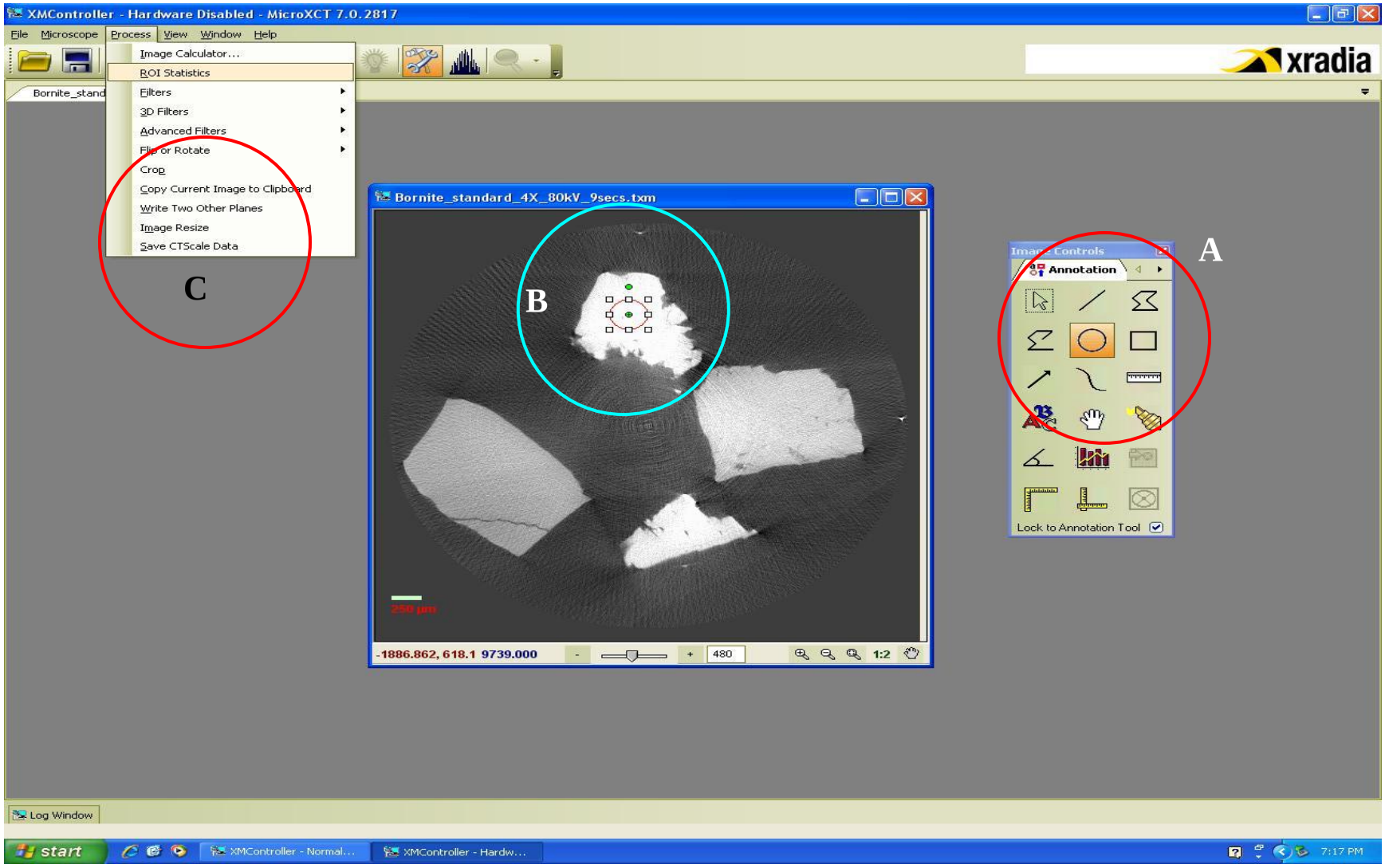

Figure 3.33 – The ROI functions of the XMController are shown in area A, B and C. Image is shown as example of option and menu location.

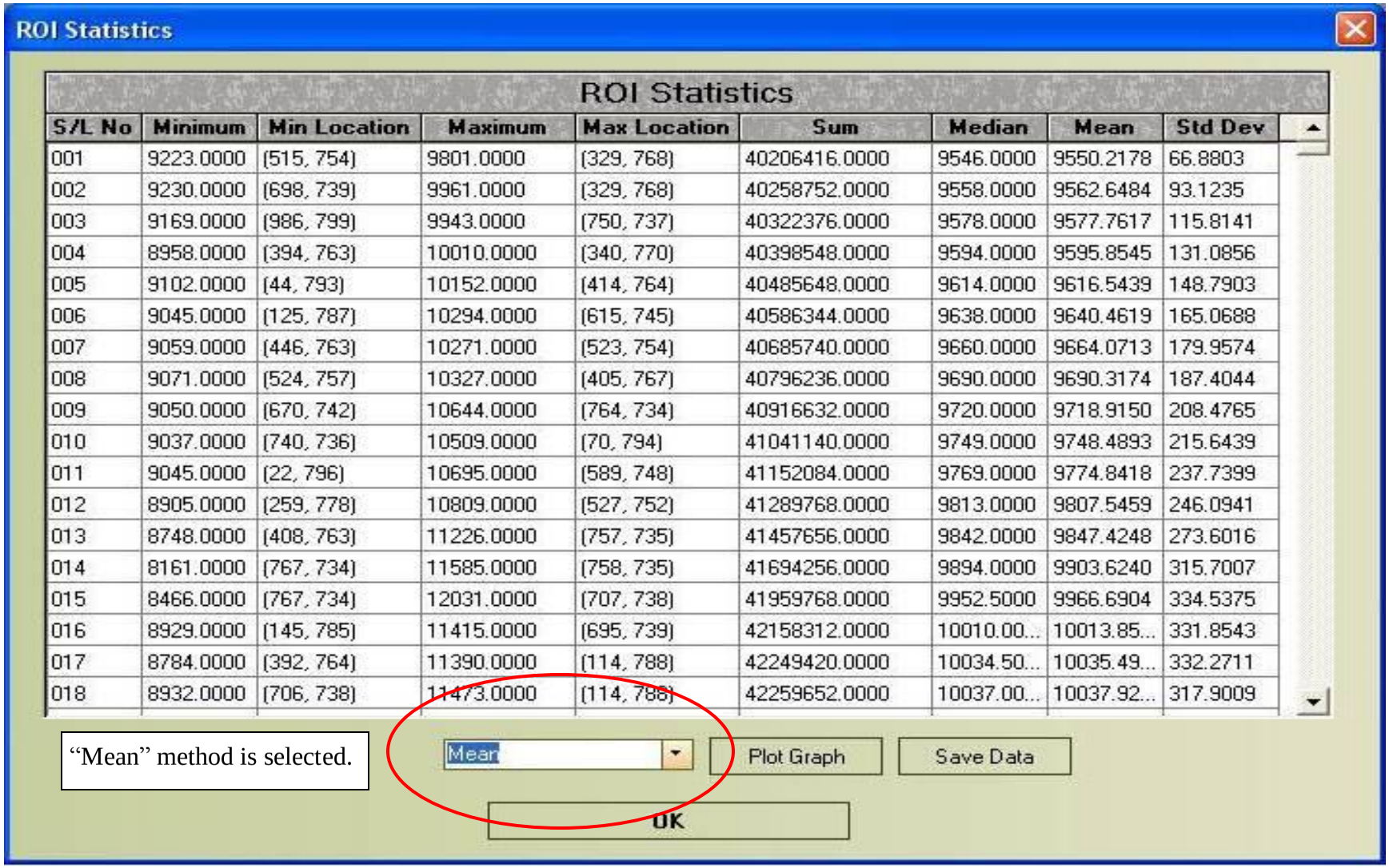

Figure 3.34 – The ROI statistic of bornite particle.

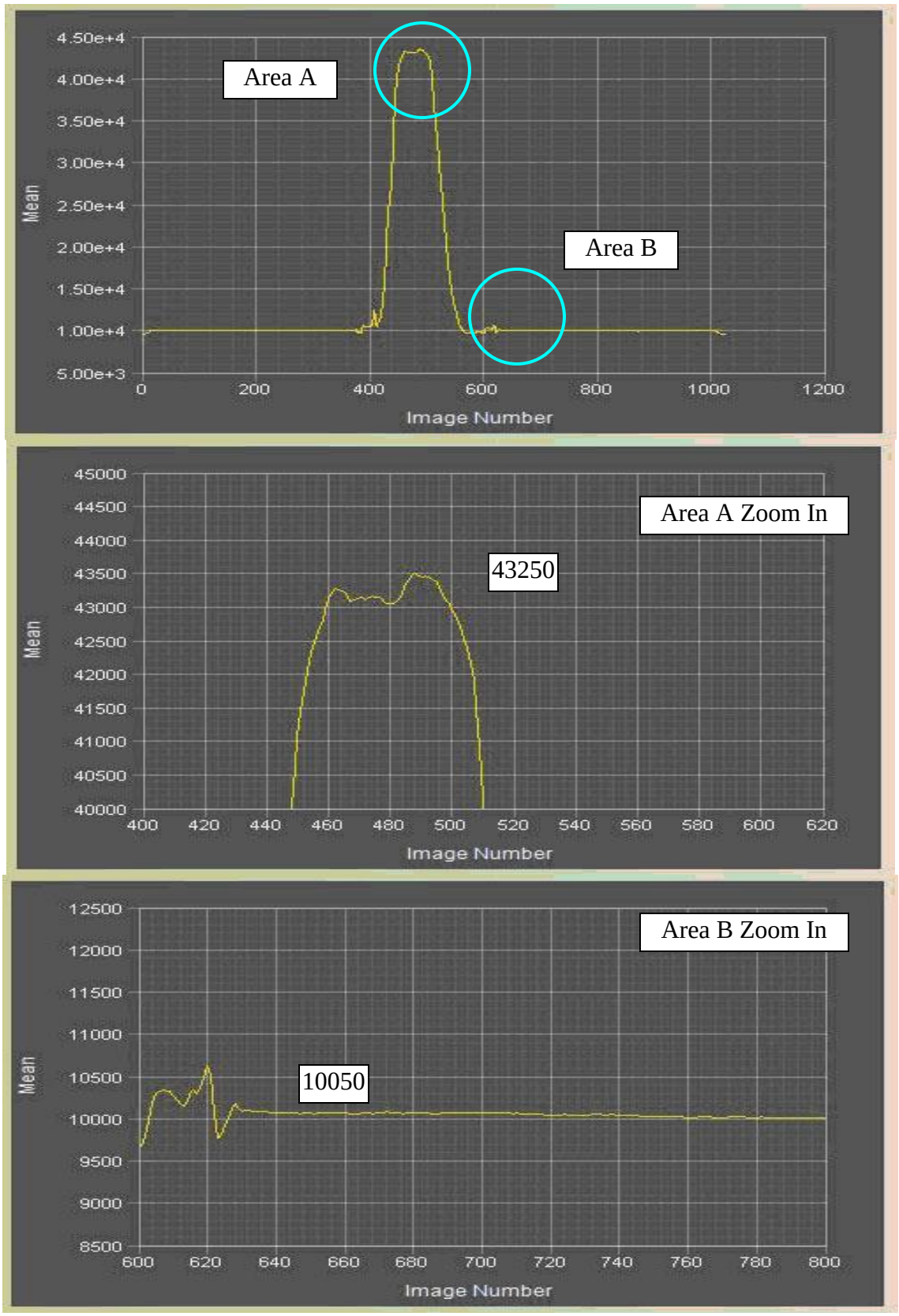

Figure 3.35 – The CT number distribution graph for bornite particle.

Table 3.13 shows the CT number readings of all four minerals. The CT Number (Original) is the measured CT number counts of each mineral phase without CT Scale; the CT Number (Rescaled) is the measured CT number counts using CT Scale in the reconstruction. The rescaled CT numbers are relatively easier to identify each mineral phase, and also focus the CT numbers in the specific range. The CT number readings will no longer be affected by the high density materials in the sample, which usually changes the global CT number scale dramatically. To rescale the CT number in the reconstruction, a new CT Scale has to be established.

Figure 3.36 shows the "Save CT Scale Information" window for configuring a new CTScale. The CT Numbers (Original) of all four minerals in the sample are required. First the name of CT scale is given using the naming rule with magnification, voltage, exposure time and beam hardening number. Number of Inserts is set at 2 using air and bornite. More than two inserts are able to be added. The CTScale is set after pressing OK. Now, a new CT standard can be found in the XMReconstructor for a scan using the same conditions that were established for this standard. In Figure 3.37, the CT scale option for the bornite standard is ready now and the specific range of the bornite CT standard is shown. All scans following the same conditions can be reconstructed using this scale.

Table 3.13 – CT number distribution/frequency of each mineral phase.

Name	Chemical Formula	CT Number (Original)	CT Number (Rescaled)
Air	O_2, N_2, CO_2	10050	0
Pyrite	FeS_2	14250	2750
Chalcopyrite	$CuFeS_2$	34000	3800
Covellite	CuS	39700	4750
Bornite	Cu_5FeS_4	43250	5275

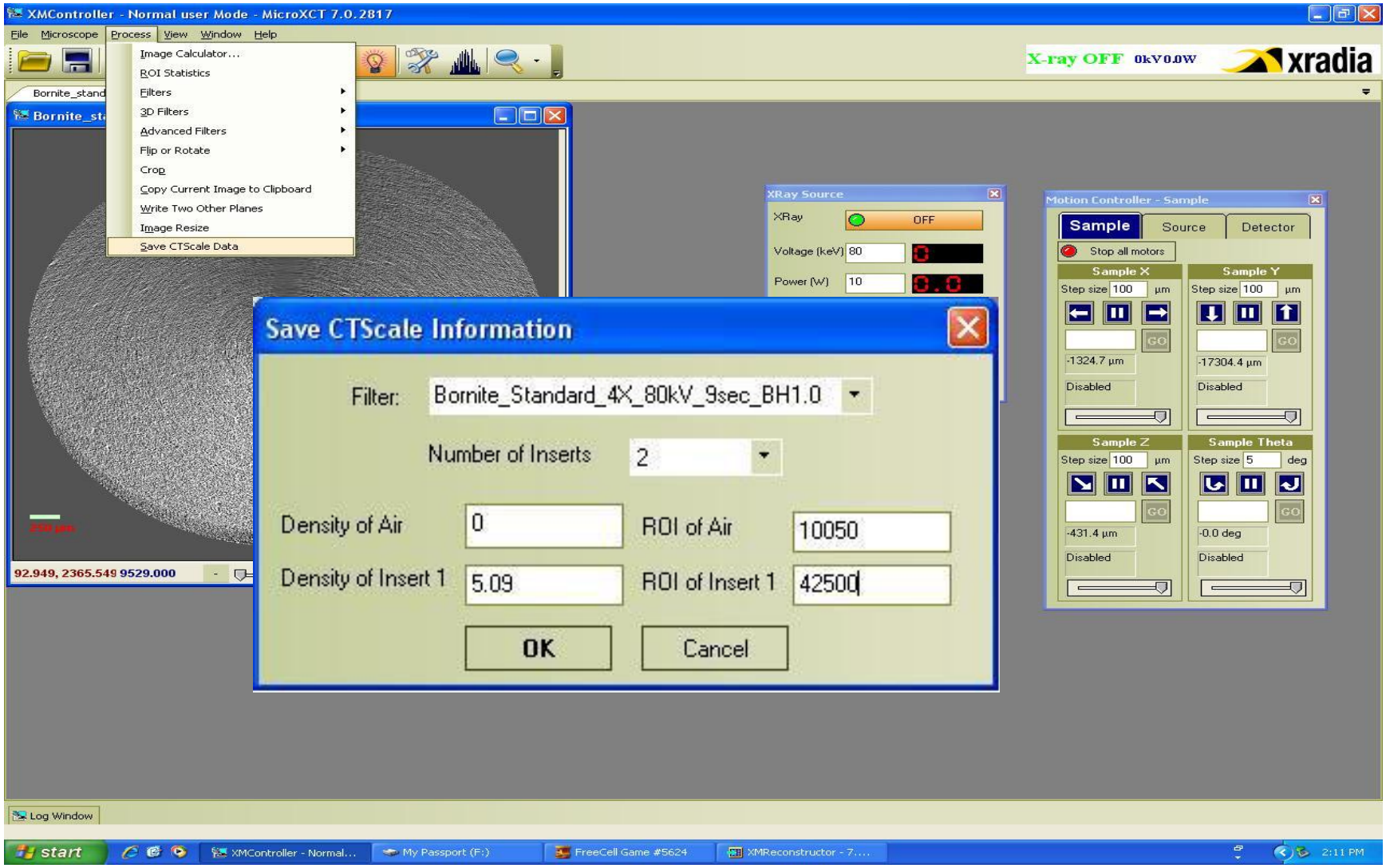

Figure 3.36 – CTScale setup window in the XMController. Image is shown as example of option and menu location.

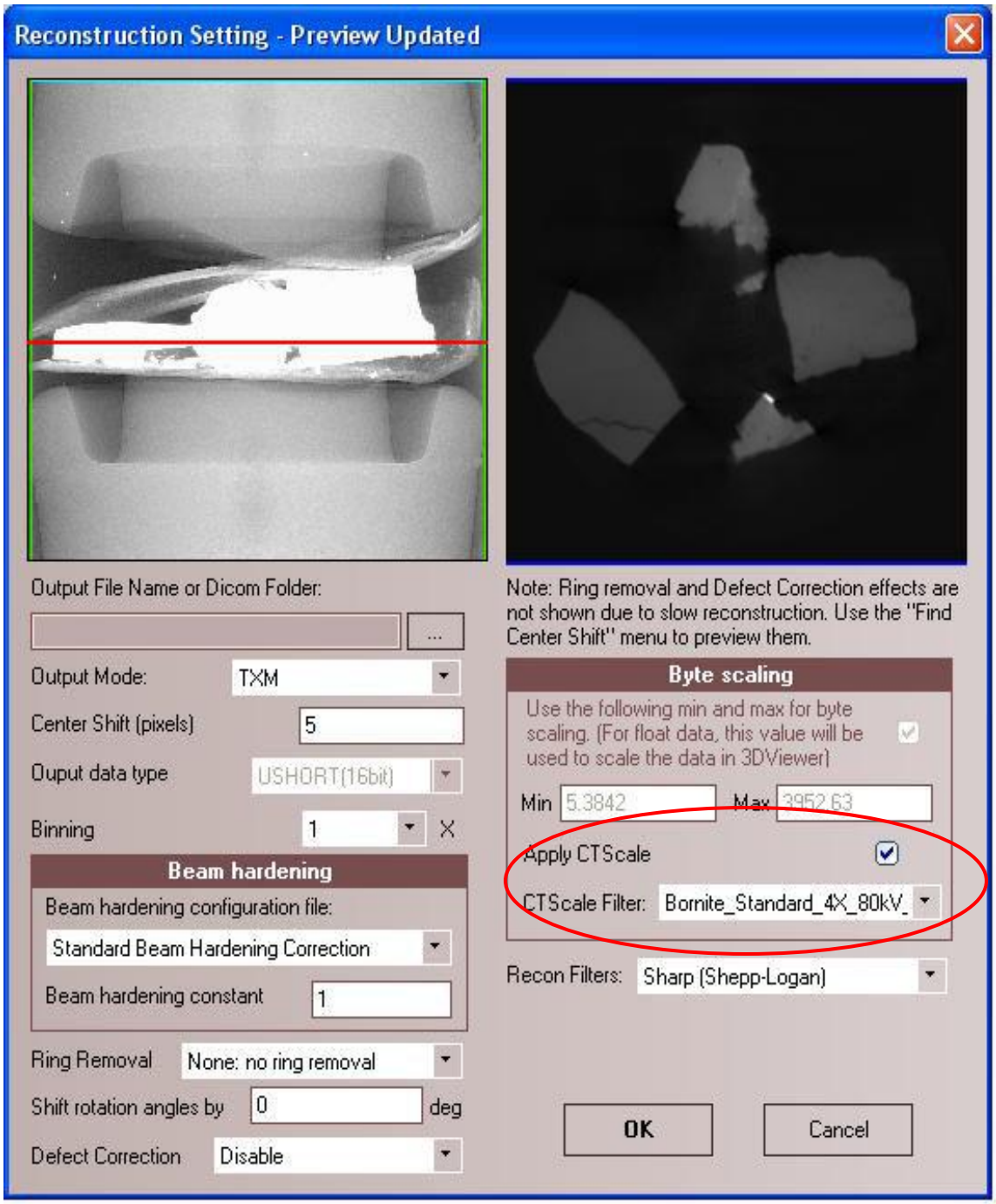

Figure 3.37 – CT Standard can be applied in the XMReconstructor.

After the reconstruction is finished, the image has been rescaled by the CT standard. The top-right image in Figure 3.38 shows the CT number of the bornite particle has changed from 43250 to 5275, and air from 10050 to 0. The rescaled ranges are determined by the valley value of each CT number of minerals. Figure 3.38 shows the CT number histogram maps using the same ROI function as in Figure 3.35 as for all four minerals after reconstruction using the CT standard. According to Figure 3.38, by the mass attenuation coefficient relationship, pyrite has the lowest CT number and bornite has the highest one, with chalcopyrite and covellite in between. Hence, minerals can be identified due to this relationship in the scan.

The CT number distribution map can be exported and transformed into an excel worksheet using ImageJ. ImageJ is an opensource software for image processing (ImageJ, 2011). The total number of voxels with a given CT number is exported as an excel file. As we know, the CT number map is a normal distribution, and air is the most prominent material in the scan occupied from 0 to 1632. So, for voxels having CT number lower than 1632 are to be seen as void and noises and be removed from the excel table. The CT number distributions are plotted by importing the readings to excel. All four minerals can be characterized by their unique CT number value in a simple, direct view. The CT number distribution map of each mineral in the scan is shown in Figure 3.39.

Mineral characterization and quantification is achievable by calculating the amount of voxels and frequency. Scans are taken with a mono-sized sample and good image quality without artifacts, such as smearing, beam hardening and full sampling, will also increase the reliability.

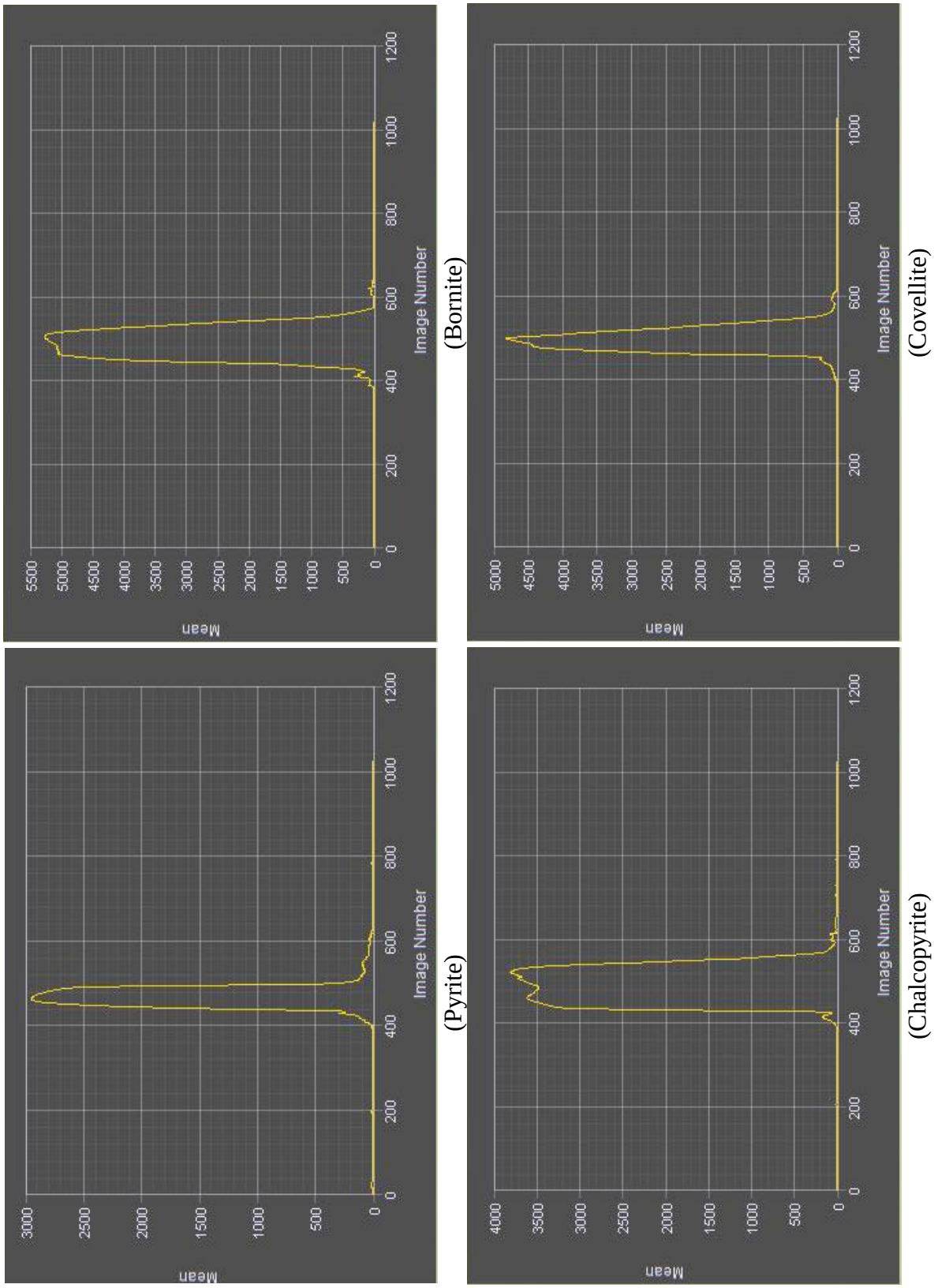

Figure 3.38 – The CT number distribution of all four minerals

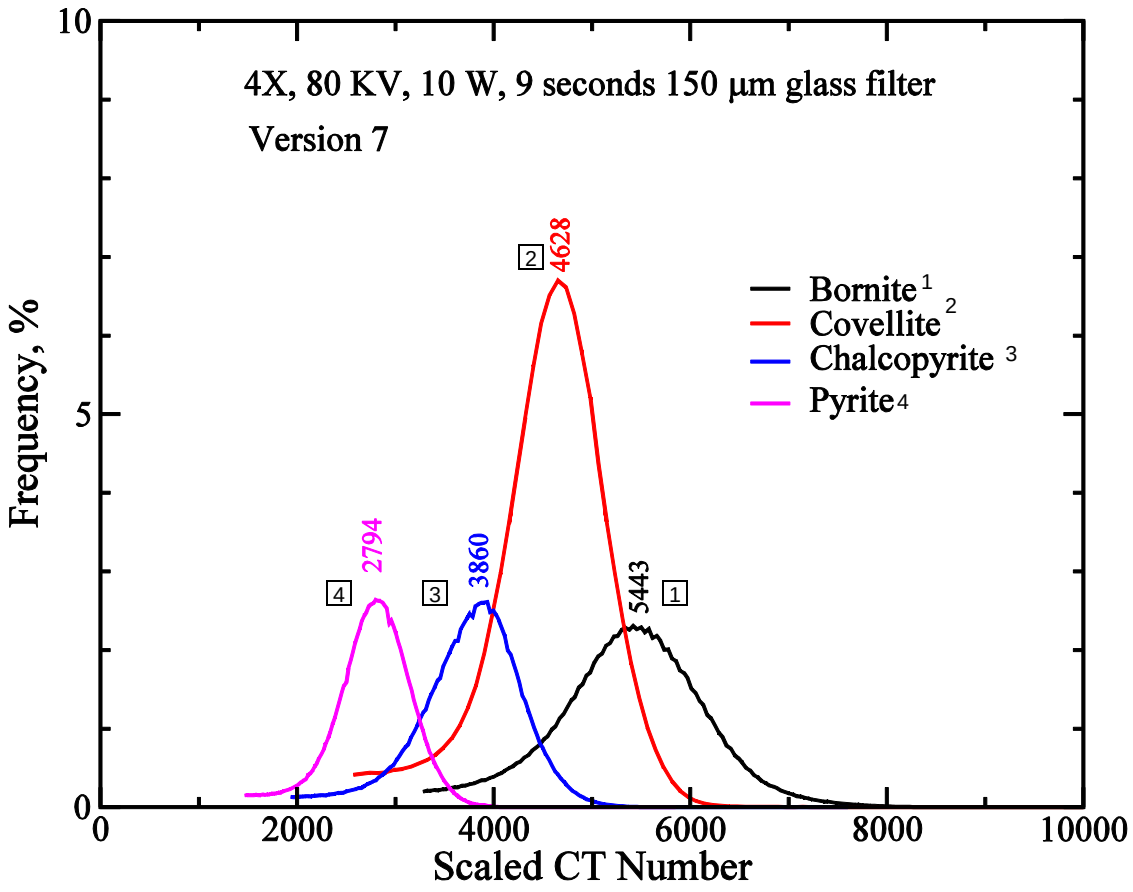

Figure 3.39 – The CT number distribution map of each mineral in the scan.

Although CT scaling can be applied on any scan following the same conditions as the standard scan, several weaknesses of CT scaling must be discussed in order to prevent any misinterpretation before reconstruction. First, sample composition has to be known with primarily the same minerals as included in the CT standard. Mineral characterization for materials not in the standard scan will be more likely to use the interpolation method for attenuation coefficient calculation rather than the extrapolation method. Minerals' attenuation coefficients are not predictable at certain levels of energy. For instance, lead and gold will absorb most of the x-ray photons under the bornite standard scan conditions, and are not able to be distinguished because the reading on the detector is relatively low and the contrast is also below 5%.

Second, if the sample contains several mineral phases, choosing a proper mineral for the making of the standard is important. Mineral characterization is based on the differences of attenuation coefficient of mineral phases. One mineral phase can be distinguished from another if the difference is higher than a certain range (sigma of the attenuation coefficient distribution, see Figure 3.39). For example, a standard sample contains few pure minerals including mercury, iron oxides, phosphates and carbonates. In this case, if mercury is selected into the standard, the high attenuation coefficient that mercury has will compress the range of other low attenuation coefficient minerals. In order to prevent such a situation for the attenuation coefficients, iron oxides, phosphate and carbonates can be measured for the attenuation coefficients and densities while the mercury mineral must be excluded in the first standard selection. After the first CT standard has been set, a second standard with the mercury mineral can be set serving specific purposes. On the other hand, it is very difficult to distinguish materials having close attenuation coefficients using HRXMT, even with CT standards. For example, bornite and chalcocite(Cu_2S) are very difficult to be distinguished because of their close mass attenuation coefficients. To distinguish two adjacent mineral phases, the attenuation coefficient reading on the detector has to have at least 3000 counts and 10 % difference according to Section 3.3.3. The HRXMT requires sufficient contrast with the attenuation coefficient of the two mineral phases by increasing exposure time or extending the distance of source and detector, while the reading on the detector is still in the range of 16-bit and the reference image is not overexposed. It is difficult to achieve for high densities, high atomic number materials or a low magnification scan.

3.5.2 Comparison with QEMSCAN

Quantitative Evaluation of Minerals by Scanning electron microscopy (QEMSCAN) is the most frequently used SEM technique for the examination of mineral composition and chemical properties. In the mining industry, most of the SEM imaging of the sample is accomplished by scanning it with a high energy beam of electrons. When the electrons interact with the surface material, signals are produced including secondary electrons, back-scattering electrons (BSE), x-ray characteristics, etc. Based on x-ray characteristics, QEMSCAN provides mineral distribution maps for the sample surface.

By using the SIP (Species Identification Protocol), a database that stocks a great amount of readings for different minerals under different conditions, the mineral properties can be identified based on specific standards, from previous scans of similar materials. In this way, QEMSCAN provides a mineral distribution map and the percentage of each mineral in the sample under interrogation. Advantages of mineral classification such as less scan time, reliable chemical composition and graphical results are attractive to the mineral and metal industries and QEMSCAN is a commonly used analytical procedure.

On the contrary, HRXMT is a 3D multiphase mineral characteristic technique. Mineral identification is based on the x-ray attenuation coefficient which measures the extract of x-ray absorption. The HRXMT analysis can not provide for direct elemental analysis and mineral identification such as is done for QEMSCAN analysis. In this regard, HRXMT analysis can be facilitated by comparison with the 2D information from QEMSCAN and mineral identification will be enhanced. The 3D HRXMT analysis will be complemented by QEMSCAN analysis.

3.5.2.1 Experimental Conditions and Procedures

For comparison, a packed bed of copper ore particles was prepared in a 5mm cylindrical container for HRXMT scan. The sample was mounted in an epoxy resin, cut, and the surface polished for QEMSCAN analysis. Finally, a cross section plane match was located and comparison between HRXMT and QEMSCAN was discussed.

The sample comes from a copper mine in Mexico. The mining company operates a concentrator to collect copper, gold and silver minerals and rejects other minerals to a tailing pond. The mineral recovery process has been studied by Juan Francisco Medina, PhD candidate in Metallurgical Engineering at the University of Utah. Gold resides with quartz minerals and can be consolidated by the quartz flotation process. The goal of the research is to identify gold in the flotation concentration. In this regard, a CT scan was used to classify specific mineral phases. If gold is present in certain particles, it will be easy to locate the position and size in the sample. It is a good opportunity to compare both QEMSCAN results with results from the CT scan.

Table 3.14 shows a list of minerals in copper ore feed identified by chemical analysis. The HRXMT scan conditions will follow the bornite standard in order to emphasize the existence of copper minerals, and not losing the contrast of silicates. Minerals having high attenuation coefficients such as native gold and galena will gain a high CT number close to maximum under these settings. However, due to the fact that the content of these heavy minerals is relatively low (< 5ppm), the scan will focus on the existence of those minerals rather than identification. On the other hand, quartz is expected to be the most abundant mineral in the sample. Thus, good image contrast to identify grain shape and position for comparison with QEMSCAN analysis is necessary.

Table 3.14 – Minerals of the copper ore from Mexico, measured by chemical analysis.

Mineral	Formula	Calculated Density [g/cm³]	Average of Actual Density [g/cm³]
Chalcopyrite	$CuFeS_2$	3.97	4.19
Covellite	CuS	4.13	4.68
Bornite	Cu_5FeS_4	4.70	5.08
Chalcocite	Cu_2S	5.27	5.65
Pyrite	FeS_2	3.06	4.90
Enargite	Cu_3AsS_4	4.00	4.45
Tetrahedrite	$Cu_{12}Sb_4S_{13}$	4.37	4.97
Argentiferous Tetrahedrite	$Cu_{12}Sb_4Ag_3S$	7.84	-
Native Copper	Cu	8.96	8.945
Pyrargyrite	Ag_3SbS_3	5.58	5.82
Native Silver	Ag	10.50	10.60
Native Gold	Au	19.30	17.15
Arsenopyrite	FeAsS	4.50	6.07
Sphalerite	ZnS	3.87	4.00
Molybdenite	MoS	5.04	4.68
Galena	PbS	6.98	7.58
Quartz	SiO_2	1.51	2.66
Electrum	(Au, Ag)	16.50	-
Calaverite	$AuTe_2$	8.85	9.25

A sample was taken from the original tailings with amounts of approximately 20 millions tons, and then statistically divided from 2,000 kilograms to 1 kilogram. The selected 1 kilogram sample was used as feed for bench scale flotation to recover copper minerals. The tailing from the bench scale flotation process was sent to a 2^{nd} flotation process in order to remove quartz. At last, the concentrate from quartz flotation was collected. The final product, 0.7 grams, was divided into 2 sample tubes and named BLP1 and BLP2. Figure 3.40 shows the BLP1 sample tube. Particles are sealed in a 5mm diameter syringe tube as a packed bed. The size of the sample is fitted to the field of view of the 4X magnification lens, which provides a voxel resolution of 5 microns. Under this resolution, high density material is able to be visualized

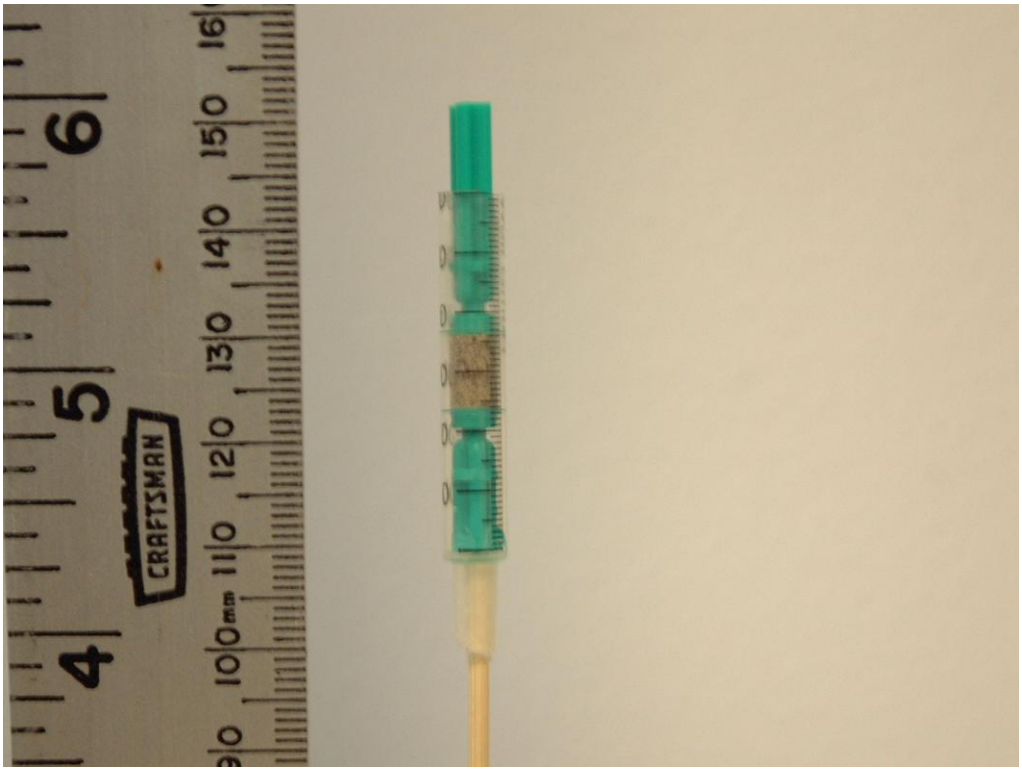

Figure 3.40 – BLP1 sample tube.

3.5.2.2 HRXMT Result

Table 3.15 shows the operating conditions of the BLP1 CT scan. The sample of 0.35 grams was sealed in a syringe tube as a packed particle bed. Both ends of the tube were sealed by hot melt adhesives preventing any particle movement. The sample was put on the stage, a full scan was taken with 1,000 projections and then the data were used to reconstruct with copper mineral standards for calibration. In this way, chalcopyrite and bornite in a specific range of CT number also gives a good contrast to low attenuation coefficient materials such as silicates, which is the most abundant mineral in this sample. Other minerals having higher attenuation coefficients such as molybdenite and silver can be characterized with the CT number. Minerals having high atomic numbers and densities are classified in one group with maximum a CT number of 255.

Table 3.15 – CT operating parameters for the BLP1 scan.

Sample Name	BLP_1_+75µm
Date	February 12th, 2010
Total Scan Time	4 hours
Objective	4X
Source Settings (kV/W)	80kV/10Watts
Pixel size (µm)	4.85 microns
Start and End Angle	-95 degrees to 95 degrees
Number of Views	1000
Time per View (sec)	9 seconds
Source/Detector Positions	-44mm / 20mm
Camera Binning	2
Physical Filter	150 µm glass
Source Drift	-8
Reference Type	Averaged Multireferences
Secondary Filtered Reference Details	None
Software Filtering	None
--	--
Recon Binning	1
Ring Removal	None
Beam Hardening	0.5
CT Scaling or Max/Min counts	Cu Ore Standard

Figure 3.41 shows a cross section image of the BLP1 sample. The image is one along the Z axis (from top to bottom, cut in XY plane). The sample dimension is 992x1013x994 by voxels (voxel size 4.85 micron), and reconstructed in unsigned short format with the copper ore standard. The different grey scale refers to the CT number observed for each particle. Particles with light color (white) have a higher CT number and are denser than the grey particles, which are mostly silicates. Although grain size distribution is wide and particle shape also varies in this tailing sample, the different phases can be identified based on the scaled CT number shown in Table 3.16. A small particle with high CT number reading in the circled area in Figure 3.41 is corresponding to the high density material at the right image in Figure 3.42.

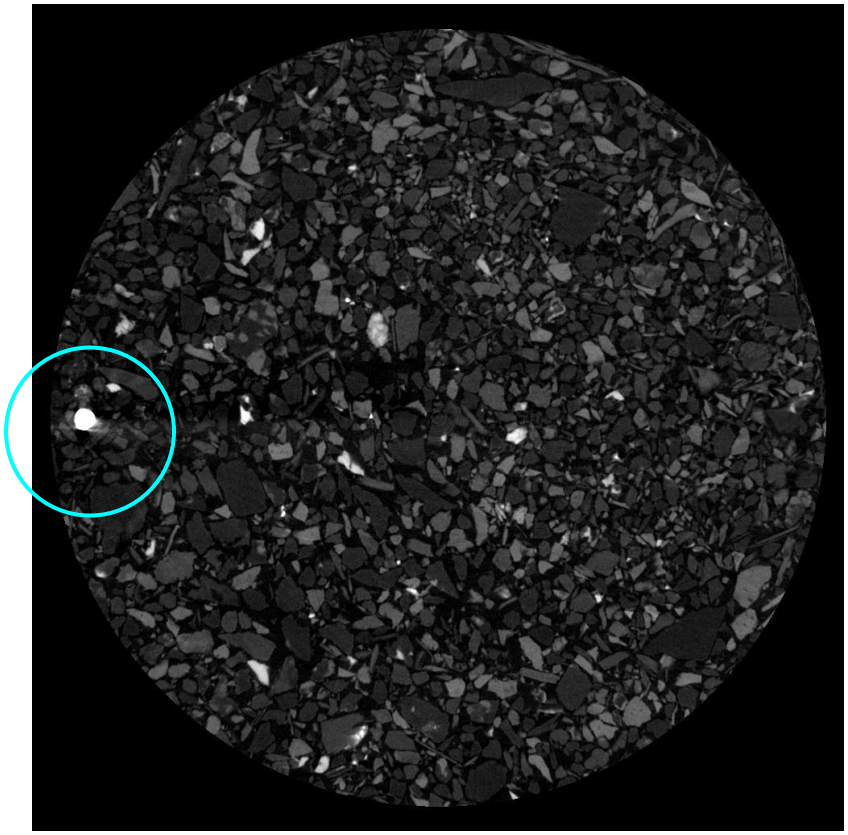

Figure 3.41 – A cross section view of HRXMT result at slice 386.

Table 3.16 – Identical minerals and corresponding CT numbers in the copper standard.

Name	Chemical Formula	CT Number (16bit)	CT Number (8bit)
Pyrite	FeS_2	2794	28
Chalcopyrite	$CuFeS_2$	3860	39
Bornite	Cu_5FeS_4	5443	55
Covellite	CuS	4628	46

The tomography file is converted from 16-bit unsigned short to 8-bit unsigned byte to reduce the file size. The CT number scale is also decreased from 65,535 to 255. Table 3.16 shows a list of CT numbers with corresponding minerals help for mineral characterization and quantification by calculating voxels and CT numbers. The selected minerals are also isolated and the volumetric visualization is presented in Figure 3.42 using Volsuite (Volsuite, 2006).

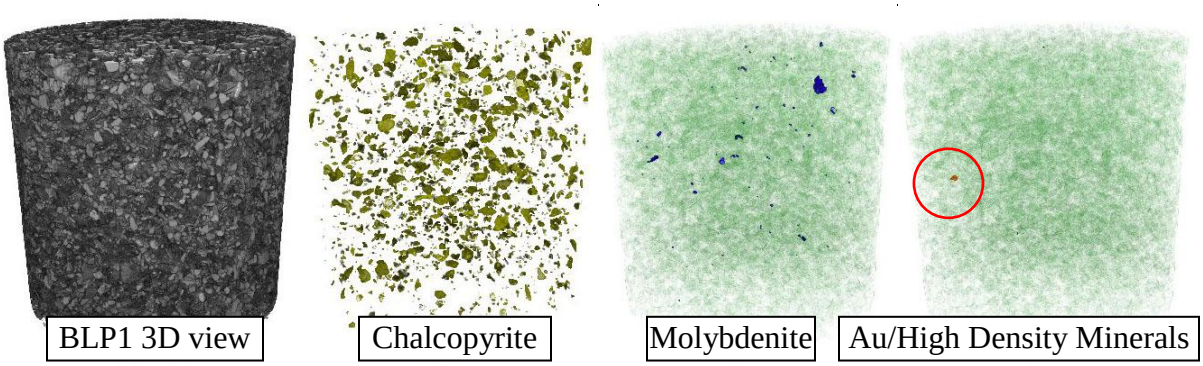

Figure 3.42 – 3D images of BLP1 sample scan using HRXMT.

The left image in Figure 3.42 shows a three-dimension view of the BLP sample and the rest of the images show some selected minerals which can be identified in the copper ore CT standard. Silicates are visualized as light green particles, and chalcopyrite is the dominant copper mineral in this sample. Note that only one high density particle has been identified. Based on the distribution of CT numbers, different mineral phases can be identified.

CT numbers are displayed using ImageJ as shown in Figure 3.43. The CT number distribution curve is shown in normal scale as dark peaks, and rescaled in log scale as grey peaks. The most left peak shows the air/void phases and the rest of the peaks are different mineral phases in this sample. Different mineral phases can be defined by seeking a "valley" of the map, which means the turning point of the distribution curve, and also can be determined by CT number according to specific mineral CT numbers of the copper standard provided in Table 3.16. A brief list of accumulated voxel attenuation coefficient is shown as Table 3.17. CT numbers are shown in an 8-bit scale and ordered by mineral phases. CT numbers and range are also listed using copper standard with percentage by volume.

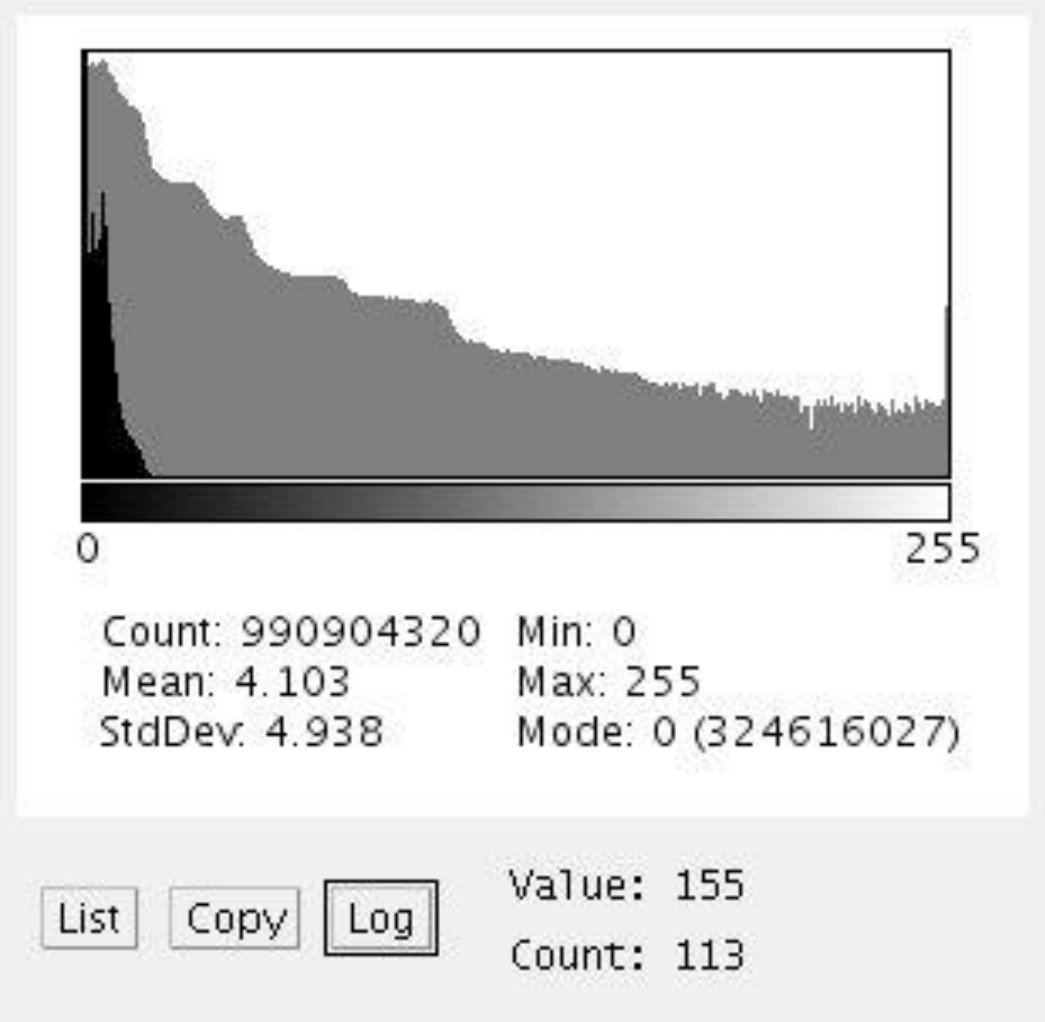

Figure 3.43 – The CT number distribution of HRXMT result plotted using ImageJ.

Table 3.17 – CT number and voxel counts from HRXMT analysis.

	CT Number Range	Counts	Volume Percent (Solid)
Air	0-3	534081867	--
Total Voxels	4-255	456822453	100%
Silicates	4-24	451109699	98.7495%
Copper and Sulfide Minerals (pyrite, chalcopyrite and bornite)	25-70	5575867	1.2206%
Molybdenite	70-120	131016	0.0287%
High Denisty Materials	241-255	2231	0.0005%

3.5.2.3 QEMSCAN Results

The QEMSCAN lab is located at FASB 303, Department of Geology, University of Utah, and is managed by Professor Erich Petersen. Once BLP1 sample was scanned by HRXMT, the sample tube was further prepared for QEMSCAN analysis. Figure 3.44 shows the BLP1 sample before being mounted in the left image; the right image shows the BLP1 sample mounted in resin with a cross section view from the top. The green stick cap of the sample shown in Figure 3.40 was first removed from the tube in a vertical direction. During this procedure, the tube is firmly fixed in the vertical direction, and any disturbance causing particle movement is avoided. The sample was then slowly and carefully filled with resin, and impregnated with epoxy. The particles are thus mounted in epoxy. After the sample is well sealed, the sample container tube and packed bed of particles are fixed. Then the sample surface is scraped out 1-2mm and polished for QEMSCAN. It is noted that the polished surface and orientation may not match the sectioned HRXMT scan image exactly. It is expected several planes may need to be examined for comparison between two techniques. However, a unique mineral particle or particle shape are the keys to identify the identical surface and proceed with a comparison of the result from HRXMT and QEMSCAN.

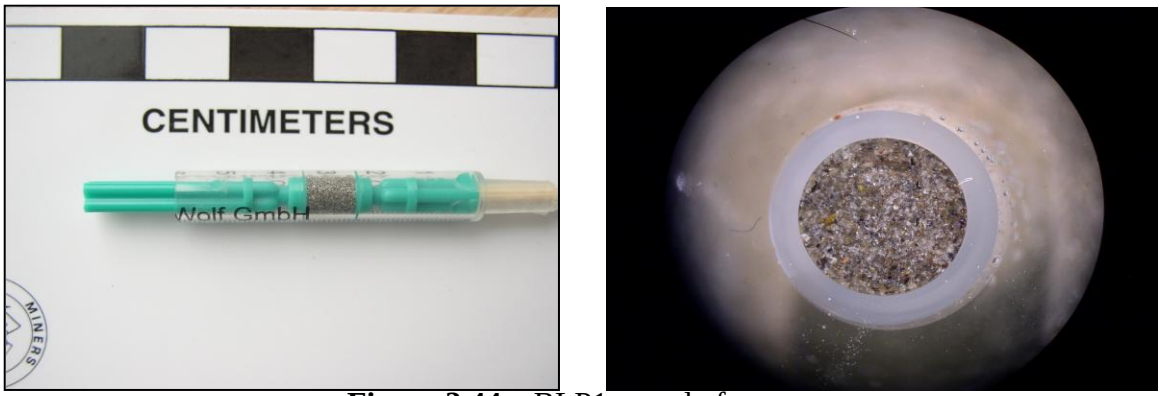

Figure 3.44 – BLP1 sample features

QEMSCAN criteria had been set according to the sample condition. The cross section of the sample surface area is a 5mm diameter circle, which equals 19.64mm². A proper scan area is to impose 1000 by 1000 micron grids (1mmx1mm) to cover the whole cross section in a round shape, which required 20 grids to cover the whole cross section area. The average particle size is about 75 microns, but the gold deposit or other high density minerals may reside in the silicate minerals with a size down to 10 to 20 microns. A moderate scan resolution for QEMSCAN is 10 micron per pixel which meets the resolution of HRXMT scan for comparison result. Hence, a 10 micron resolution scan and a minimum scan time of 10 milliseconds for one mineral spectra at each pixel require a total scan time of 2000 seconds (100 rows x 100 spots x 20 grids x 0.01sec/spectra). Figure 3.45 shows the cross section images converted from a BSE (Back Scatter Electron) image which is originally computerized in a grey scale.

Mineral Name	Percentage
Quartz	20.10
Epidote	19.48
Amphibole	13.72
Feldspar	11.79
Calcite	10.62
Micas	8.63
Plagioclase	5.95
Background	4.00
Chlorite	1.66
Mg(Fe,Mn)silicate	1.26
Pyrite	1.22
Nontronite	1.14
Garnet	0.89
Fe-Ox/CO3	0.46
Chalcopyrite	0.36
Copper minerals	0.03
Other Sulphides	0.03

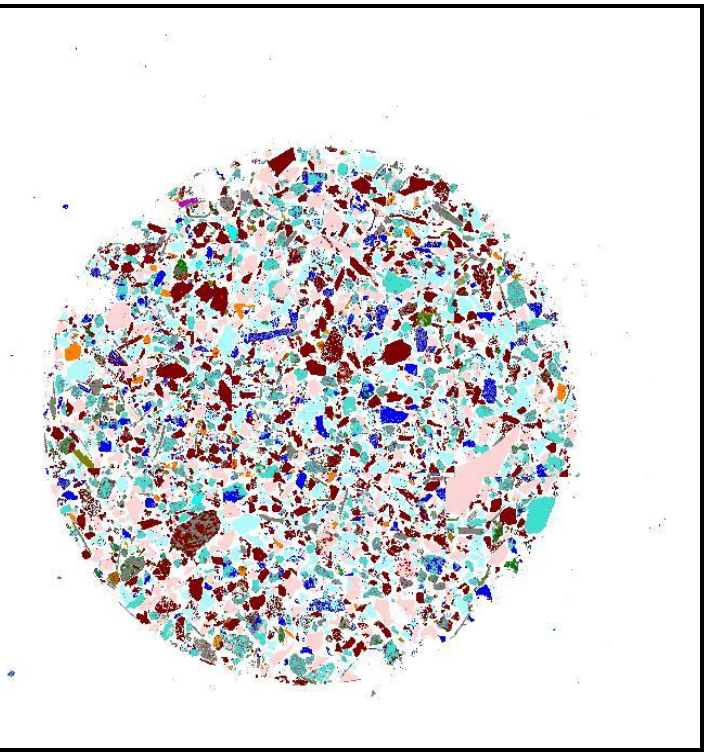

Figure 3.45 – List of mineral composition and the mineral distribution map.

The right image is the surface scanned under a 15X magnification providing 10 microns resolution. Using the computer software iDiscover, the image is visualized by different level of colors representing individual mineral groups. The primary database is set using SIP (Species Identification Protocol) 710A and no secondary database. The left-hand side of Figure 3.45 shows a list of one these general or specific minerals present in the sample. It is obvious that quartz and silicates dominate the sample; meanwhile, a small amount of iron and copper minerals are also present; pyrite and chalcopyrite are at 1.58%. Bornite is under the group of copper minerals and is calculated as 0.03. High density minerals which are assumed as gold or silver are grouped with other sulfides with an amount of 0.03%. Figure 3.46 shows the match plane of QEMSCAN and HRXMT results. To find this match plane, the first thing is to look for an identical high density particle. The upper-left circled area is a bismuth particle which is very obvious to locate in both QEMSCAN and HRXMT results; the other 2 circled areas in Figure 3.46 are two grains similar in shape which also helped to locate this specific match plane.

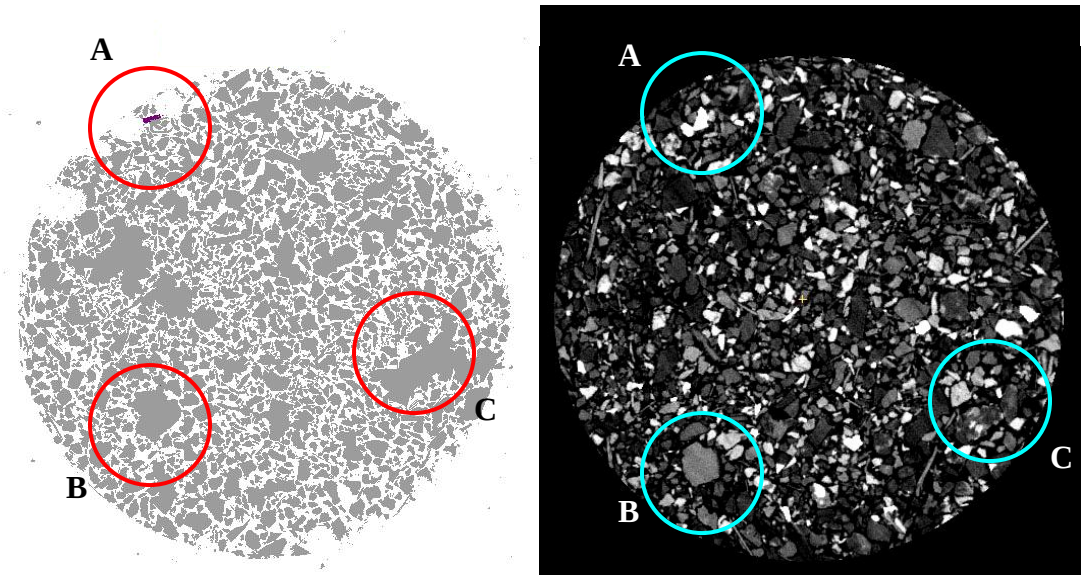

Figure 3.46 – A match plane of QEMSCAN polished surface and HRXMT result.

3.5.2.4 Comparison and Discussion

A very fundamental basis to compare the results is finding the HRXMT corresponding plane which matches the QEMSCAN plane that has been analyzed. The polish surface of the epoxy mounted sample for QEMSCAN is not exactly perpendicular to the HRXMT Z axis. Thus, a useful tool is introduced to help us find the designed HRXMT plane by tilting the slice in every axis for a three-dimensional view of the HRXMT results. Volume Viewer is a plug-in for ImageJ providing camera angle elevation and tilting among three axes X, Y and Z. By using this tool, the grain size, shape and mineral composition can be identified and a 2D HRXMT plane which matches the polished surface from QEMSCAN analysis can be found.

Figure 3.46 shows such a plane similar to the epoxy mounted sample surface examined by QEMSCAN. The left image is from QEMSCAN and the right image is from HRXMT at slice 924. The right image is also tilted using ImageJ. Area B and Area C indicate two significant grains having similar size and shape in both HRXMT and QEMSCAN results; and in area A a particle having a high attenuation coefficient is identified as bismuth in the QEMSCAN analysis. The bismuth particle in Area A in HRXMT has a very high attenuation coefficient which goes to almost 255. Such a particle is very easy to identify and compare with respect to size and shape. In this regard, a high density/attenuation coefficient material is very helpful to determine the specific plane for comparison. Also, the epoxy mounted sample is cut and polished from the top by 0.5 millimeters, which is very close to the distance for slice number 924 (100 slices*4.85microns) from the top for the HRXMT results.

Since a matching plane is found, a comparison of mineral composition is to be considered. Table 3.18 shows a CT number distribution for HRXMT results at slice 924. According to the CT standard (bornite standard), we know that copper minerals are having CT numbers from 25 to 70 with an 8-bit scale. Hence, we can calculate the total voxels having CT number in this range and get the percentage of copper minerals comparing the data of copper minerals in Figure 3.45. Table 3.18 also provides a comparison of the results for the whole volume, the results for slice 924, and the results for QEMSCAN.

Table 3.18 shows the copper concentration at slice 924 is 0.7866%, which is lower than the amount of pyrite and chalcopyrite (1.58%) in QEMSCAN; however, bornite concentration is 0.0990%, which is higher than the measured concentration in QEMSCAN (0.03%); as the high density/attenuation coefficient material, HRXMT can not identify the property due to the limitation of the applied CT standard, but the measured volume amount is 0.0030%, which is ten times lower than the measured amount in QEMSCAN.

Table 3.18 – CT number and voxel counts of HRXMT results at slice 924 and comparison with total volume results and QEMSCAN results.

	CT Number Range	Counts (slice 924)	% (Slice 924)	% (Volume)	%(QEMSCAN)
Total Voxels	0-255	471897	100%	100%	--
Air	0-3	--	--	--	--
Silicates	4-24	--	--	--	--
Copper and Sulfide Minerals (pyrite, chalcopyrite and bornite)	25-70	3712	0.7866%	1.2206%	1.58%
Molybdenite	70-120	33	0.0070%	0.0287%	--
High Denisty Materials	241-255	14	0.0030%	0.0005%	0.03%

In summary, the match plane of the HRXMT is not exact with the QEMSCAN polished surface. Surface polishing for QEMSCAN is not able to be controlled at the micron level, and the difference between the polished section in QEMSCAN and the 2D slice image in HRXMT is inevitable. Second, mineral characterization using HRXMT depends on the mineral composition of the applied CT standard. For the bornite standard which is applied in this scan, the selected minerals are pyrite, chalcopyrite, covellite and bornite. The mineral quantification will be more accurate when measuring these minerals. Molybdenite, which is not in the minerals for the CT standard scan, can be identified by its high attenuation coefficient in a certain range. However, we are not able to differentiate which materials have very high atomic number and density because their attenuation coefficient exceeds the maximum value of the selected calibration standard used. Thus, we can only categorize those minerals as "high density/atomic number materials" in the HRXMT results. On the other hand, QEMSCAN can provide a detailed mineral composition on the surface with the help of the SIP database. In this scan, the particle in area A, the left image of Figure 3.46, is confirmed as bismuth.

With the help of QEMSCAN, mineral composition of the sample is easy to be identified and quantified. On the other hand, HRXMT provides a quick way to characterize a large number of minerals more than a cross section surface. By finding a match plane of both results discussed in this section, it is possible to combine these two methods and achieve mineral characterization with large amount samples. Meanwhile, HRXMT has great advantages of volumetric sample information, and can be compared with QEMSCAN analysis without sterology issue. The sterology problem of mineral characterization will be discussed in Section 4.2.

3.6 Database Query to Establish Operating Conditions

As numerous analyses have been done, and many types of minerals have been studied, it is necessary to build up a database with convenient query functions in order to help users review or decide the scan conditions when a new sample arrives. This database should be able to store full scan conditions and records, and be sorted or listed by different criteria. Data update and edit functions also must be developed including records and sorting options. A query function should also be connected to the database to search specific records or scan conditions by time, magnification, or CT standard and be supported for multiple criteria. At last, the database has to have an easy-accessible graphic user interface (GUI) for the user to operate with daily scan and maintenance.

Considering the requirements above, this database is set and built on Microsoft Access, a simple database solution for small business purposes and managing data records with less than a few hundred thousand entries. The user interface is established on a web browser with IIS, an internet service provided by Microsoft Windows, with the coding language Action Script and SQL. The advantage of using these tools is to offer an intuitive and simple GUI for user based access on the web browser. The user does not have to install specific software or update their system to use this database.

The main menu of the database query using Internet Explorer as the web browser is shown as Figure 3.47. This application provides every scan condition that has to be determined during the scan procedures. Query options in Figure 3.47 will be discussed as follows. First, to create a new record, click on [ADDNEW] hyperlink and a new window will pop out with many columns. Input options are listed in the following paragraph with the function of use.

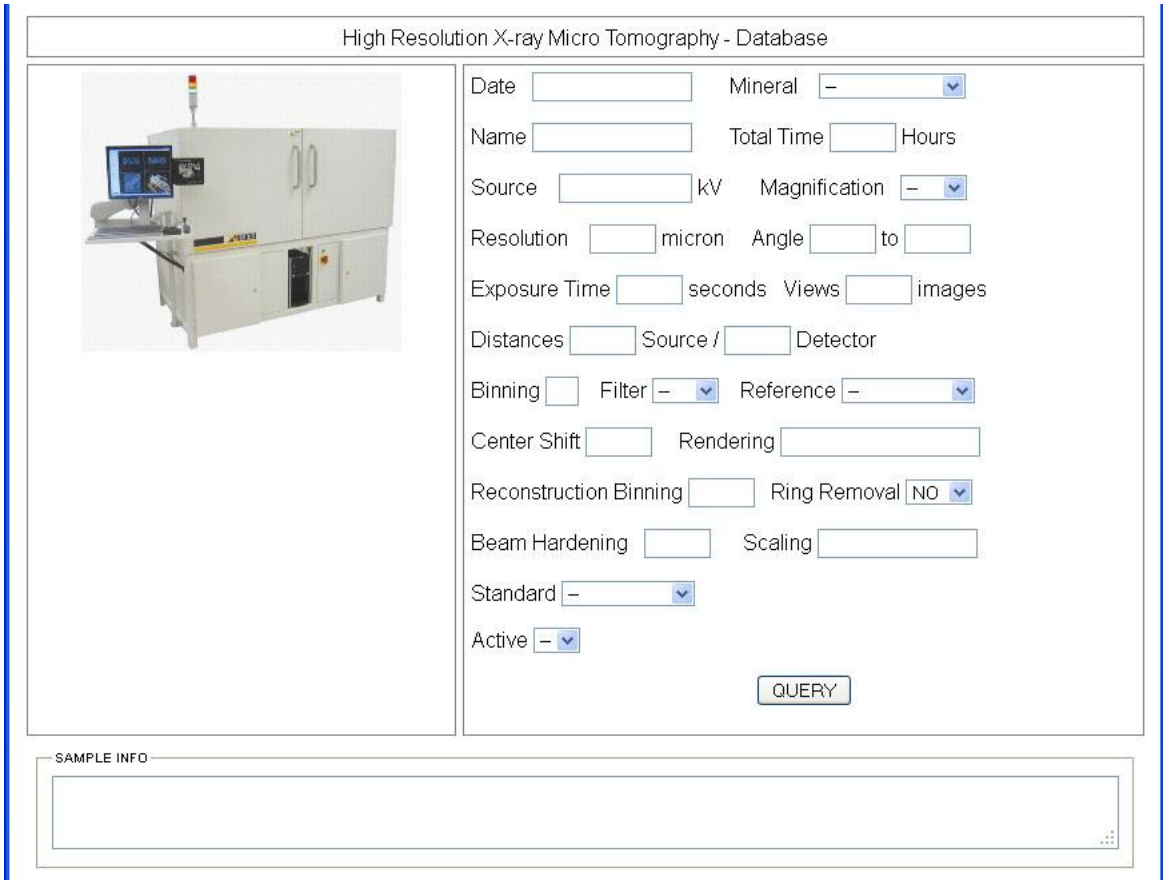

Figure 3.47 – Main menu of the Database Query System.

1. Date: These two columns are empty text boxes, in which you can input the start date in the first column, and end date in the second column. The query will provide all records found between these dates. The format is mm/dd/yy.
2. Mineral Type: A few mineral types had been set for minerals of most common interest. Choice of mineral types will not affect the scan conditions, but help the query and organizing.
3. Name: Sample name or experiment name can be searched by inputting part of the sample name as keywords. It is recommended using company name or ore source as the naming rule.
4. Time: Input the total required time on XMController.

5. Magnification: Based on XCT 400, there are 5 magnifications that can be chosen: 4X, 10X, 20X, 40X and 0.5X. Select the magnification match to your scan.
6. Source: Input the source energy level (kV).
7. Resolution: Input the voxel size of the scan. This information can be found in the single image of the scan (in micrometer).
8. Angle: Scanning angle of the sample. It can be a half circle (from -90 to 90 degrees) or a full rotation (360 degrees).
9. Exposure Time: Input the exposure time for each image frame that has been taken.
10. Views: Input the total images taken during the scan.
11. Distances: Input the source and detector distances (in millimeter).
12. Binning: Input the scan binning number (default value is set at 2).
13. Filter: Choose one physical filter applied on the scan.
14. Reference: Choose one reference type applied on the scan.
15. Center Shift: Input the center shift number in the reconstruction stage.
16. Rendering: Input any software rendering / correction here.
17. Reconstruction Binning: Input the reconstruction binning number (default: 1)
18. Ring Removal: Check this option if ring removal is applied.
19. Beam Hardening: Input the beam hardening number.
20. Scaling: Choose a scaling method if the scan is reconstructed using CT standard (default is set at Global Scaling).
21. Standard: Check this option if the scan is scanned for building CT standards.
22. Active: Check this option if the scan has correctly been done (default: checked).
23. Introduction: A text area for the user to write down comments of the scan.

All those conditions are editable and stored in the database (HRXMT.mdb). After the records are set, select one / few criteria and then click [QUERY] hyperlink, the database will search match results and list below. Users can build up detailed scan conditions and search for similar conditions or scans easily. While users are determining scan conditions, this database is a reliable reference and will save a lot of time and effort. The decided records can also be printed out as a paper copy and saved in the log book.

3.7 Summary

In this chapter, scan conditions have been discussed, from the technique of sample preparation and sampling, to considerations for scanning, including the evaluation and determination of source voltage, magnifications, distance of source and detector, physical filters, field of view, exposure time, image counts and reference states. Theory and results are also discussed and displayed. Users will have a basic concept of running HRXMT scans and know how to adjust these parameters in order to improve the image quality. In the reconstruction stage, beam hardening, CT standard, and file conversion are investigated in detail with the effect and operating procedures. These operations will help users reduce the noise in the scan, and be able to characterize the mineral phases in the sample. Users can set up their own standard for specific mineral scans for different objectives. At the end of this chapter, a database has been established for establishing scan conditions. Common minerals that have been scanned or CT standards that have been established can easily be found and all the scan conditions listed for the user’s scan evaluation.

CHAPTER 4

APPLICATIONS

High Resolution X-ray Micro CT (HRXMT) allows for further advances in the 3D characterization of multiphase systems. Previous studies include liberation/exposure to improve separation efficiency in mineral processing plant optimization (Miller et al., 2009), particle segmentation based on 3D watershed algorithms (Videla, 2006) and breakage and crack pattern analysis of HPGR crushing (Kodali, 2011). HRXMT provides highly reliable, sample-recoverable and scan-repeatable results with high resolution (<5μm), easy-accessible and x-ray attenuation coefficients-based images. HRXMT has the benefit of not requiring the same level of sample preparation needed for SEM techniques. The following section will discuss some applications using HRXMT including: (1) describing the internal structure of an oil shale core drill, (2) searching for precious metals in large particles using rapid scan radiology and (3) evaluating the mineral characterization of ivory materials. Depending on the objectives of the research, scanning conditions are adjusted accordingly. In general, these case studies focus on how to achieve high quality, well contrasted images by adjusting scan conditions, and mineral characterization using CT standards compared with other techniques such as SEM (Scanning Electronic Microscopy) and QEMSCAN (Quantitative Evaluation of Minerals by Scanning Electron Microscopy) . Results are discussed based on the parameters such as sample preparation, image usage and data analysis.

4.1 Oil Shale – Inner Structure and High Resolution Results

Oil shale is a rediscovered source of unconventional fuel, which is currently of interest because of increasing oil prices. Unconventional fuel resources are defined as extra heavy oil and bitumen associated with oil sand deposits and as kerogen associated with oil shale resources. The oil shale sample used in this research had a very hard fine grained laminated structure composed of dolomite, calcite, quartz and clay mineral layers. Those lamellar structures of different mineral ores were distributed in very thin and parallel laminar imbedded in clay minerals and carbonate minerals. To extract kerogen from oil shale, a pyrolysis process is applied which involves heating the oil shale to different temperatures and then collecting vaporized kerogen from injected nitrogen.

The natural crack channels and porous structure become important issues in this process. The fluid mechanics of nitrogen and kerogen decide the efficiency of resource recovery and energy consumption. The first challenge of fluid mechanics analysis is the scale. The clay mineral layers range in thickness from 20 to 30 μm, while the carbonate mineral layers range in thickness from 10 to 20 μm. It is very difficult to acquire a real geometry of the inner structure under such a small scale. Hence, HRXMT has been used to obtain the internal structural images in a three-dimensional view with noninvasive, nondestructive advantages.

Once the CT data have been acquired, the fluid mechanics simulation can be completed as the next step. The scan objectives focus on sample internal structure and voxel resolution. To achieve good image quality, the scan conditions are configured to enhance image contrast of the different mineral phases, such as kerogen to silicate, or void to solid.

Figure 4.1 shows the features of three oil shale core drill samples. These samples are after pyrolysis processing at different heating rates from 1ºC per minute to 100ºC per minute. The final temperature is 400ºC. The procedure for scanning the left sample (MD-11, 1ºC 1”Core) is described in the following paragraph. The sample is first mounted on a styrofoam bowl to keep the sample fixed and stable on the stage while scanning. The sample size is larger than the field of view under 4X magnification. The homogeneous sample material and cylindrical shape help reduce the beam hardening artifact. 4X is the optimal operating magnification when considering pore size and resolution. The source moves away slightly from the sample in the beginning to obtain a larger field of view, also to increase the image contrast.

Initially, to enhance the difference in mineral phase boundaries, the scan conditions will be adjusted to 80kV, a longer exposure time and greater distance ratio of source/detector. A 150 µm glass filter is applied and camera binning is set at 2. Finally, the image acquisition is set at 1000 images and the rotation is also set at -93 degrees to 93 degrees (the scan angle is set at 180 because the scan was taken before the XMController software was updated to a full rotation version). Table 4.1 lists the scanning conditions.

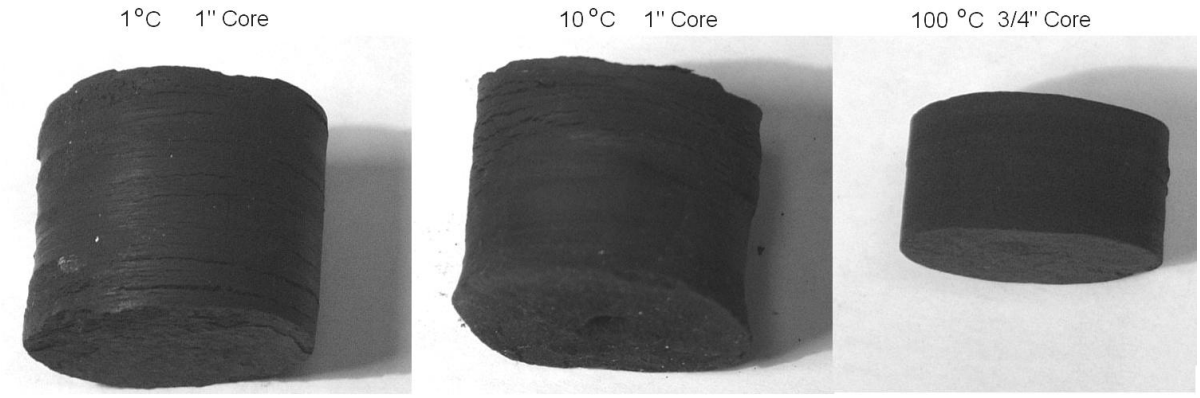

Figure 4.1 – Three cylindrical samples from an oil shale core drill.

Table 4.1 – Conditions of the HRMXT scan of the oil shale sample.

Sample Name	Oil Shale MD-11 1ºC
Date	November 23rd, 2010
Total Scan Time	4 hours
Objective	4X
Source Settings (kV/W)	80kV/10Watts
Pixel size (μm)	4.49 microns
Start and End Angle	-93 degrees to 93 degrees
Number of Views	1000
Time per View (sec)	15 seconds
Source/Detector Positions	-60mm / 30mm
Camera Binning	2
Physical Filter	150 μm glass
Source Drift	2
Reference Type	Averaged Multireferences
Secondary Filtered Reference Details	None
Software Filtering	None
--	--
Recon Binning	1
Ring Removal	None
Beam Hardening	0.5
CT Scaling or Max/Min counts	Global Scale

Figure 4.2 shows the volume rendering images using Volsuite (Volsuite, 2006). The file is saved as .raw format. In Figure 4.2, the top-left image shows a full view. The layered structures are easy to see and the porous structures are also visible. Bright particles represent mineral grains which are more dense than shale (silicate base), and the dark stripes represent porous structures, cracks or voids. In the top-right image, the sample view is cut through the Z axis. Internal structures and porous channels are also visible. Large channels, which can be observed at the bottom part of the same image, are possibly leaking vaporized kerogen with nitrogen gas rather than small channels as in the top part. These channels can be measured by width or volume, providing more information of the gas/fluid flow mechanics.

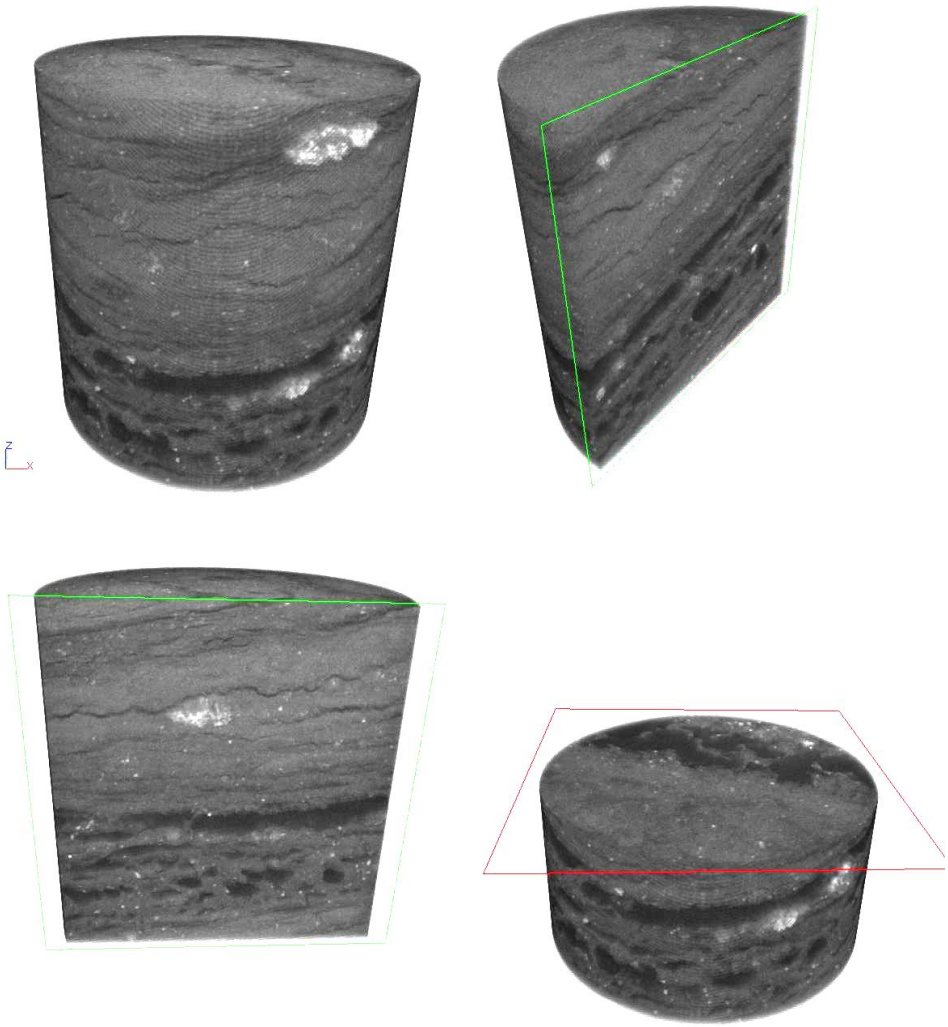

Figure 4.2 – The oil shale MD-11 1ºC sample in 3D view.

The bottom-left image is another sample cross section view through the Z axis at different angle and the bottom-right image is a cross section view cut from the XY plane. It should be noted that the axes of the image are based on Volsuite and not matched to the tomography axes of the image acquisition. These cross-sectional planes can be adjusted by software for any size, angle or color in the visualization process. Making custom cutting planes is available depending on the user's requirement. In Figure 4.3, a cross section view from the XY plane at slice 711 is shown in grey scale. Internal structures such as mineral grain, channel and porous structure are very clear to identify.

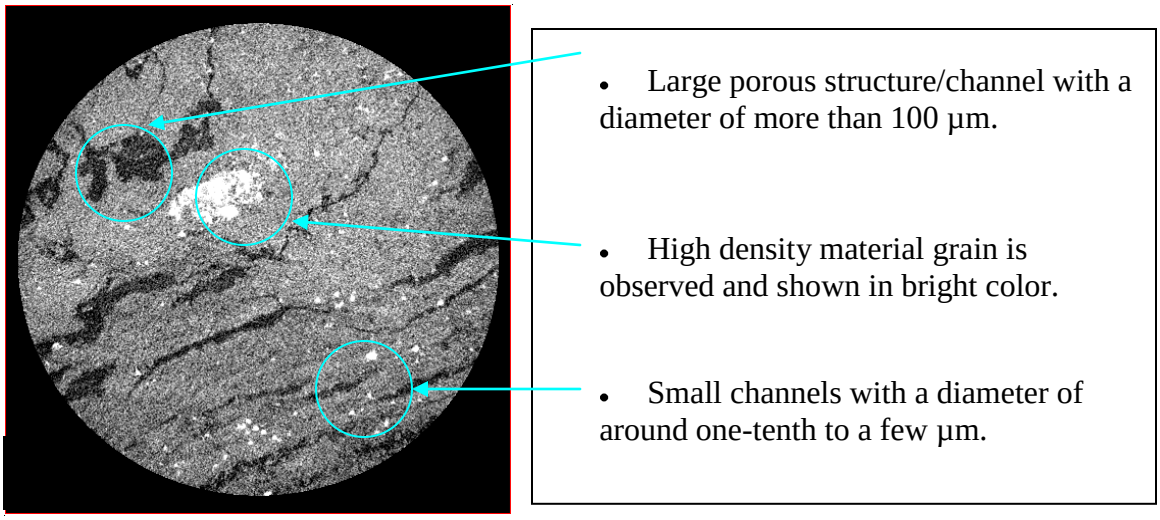

Figure 4.3 – 2D cross section (XZ plane) of MD-11 1ºC sample at slice 711.

These images provide many advantages that other methods can not provide. First, the sample is recoverable. These brittle, small channels can not be processed by surface polishing or probing. Any mounted method for surface polishing would crush or destroy the small channels of less than 10 microns during the polishing process. Second, the sample image after the pyrolysis procedure can be coupled with the sample image from before pyrolysis to characterize and locate the kerogen layer and other beneficial minerals. This information can be compared with the collected amount of kerogen gas after the heating process to evaluate experimental efficiency and accuracy. Third, real sample geometry rather than a built-up model can be put in the mathematical algorithm/model to calculate the gas flow rate and pattern. This high resolution image can provide an accurate visualization of the porous structure compared to assumed porosity numbers. A technique has been applied for the fluid simulation using the Lattice-Boltzmann Method (LBM) to compute fluid dynamics under a micronmeter level. By integrating the HRXMT result and the LBM simulation, the flow rate of the kerogen/nitrogen mixed gas (micro darcy) can be obtained (Lin et al., 2010).

4.2 Rapid Radiograph Scans

Sampling for precious metals is always problematic in mineral processing. The natural concentration of precious metals varies from a few ppm (parts per million) to a few ppb (parts per billion) in mixed compounds. Conventional 2D polished section measurements are biased in favor of the sterology of the cutting surface, as shown in Figure 4.4. When a surface scan technique is applied for mineral characterization, it will examine the polished surface of the top cross section. The mineral concentration is possibly misinterpreted depending on the cutting part of the particle. The rarity of precious metals in the mineral sample results in limited accuracy, thus more scans are required for increased accuracy. HRXMT has many advantages over 2D polished section measurements and has been introduced to examine dedicated precious metals.

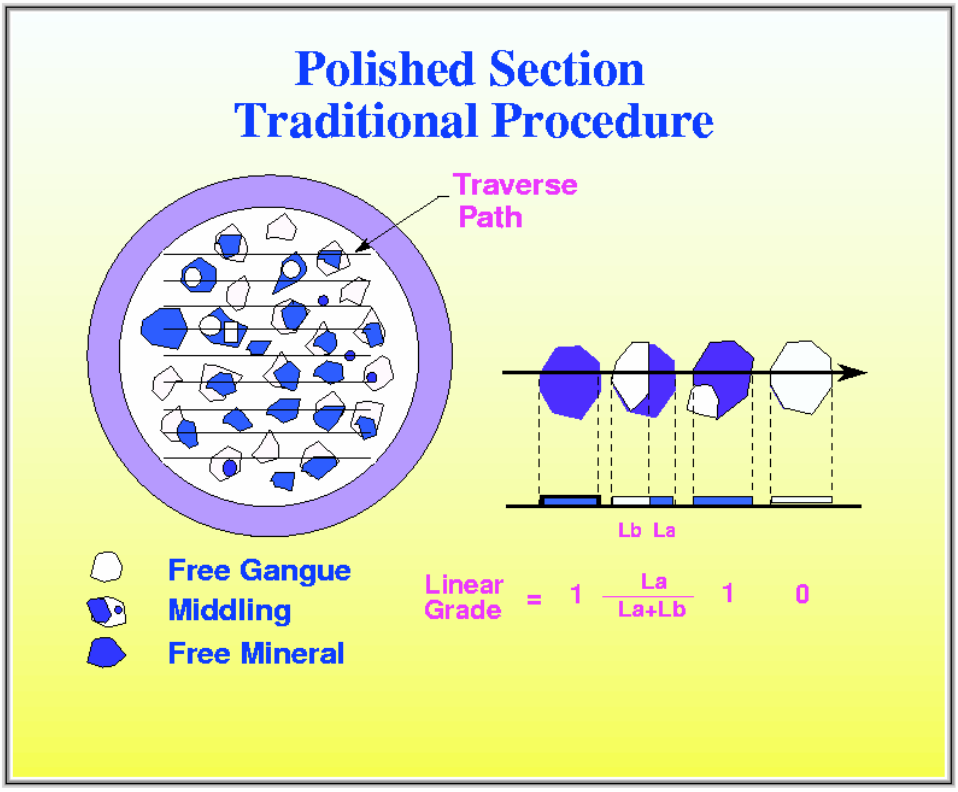

Figure 4.4 – The stereology of a polished section surface.

4.2.1 Concept of Rapid Radiographic Scans on HRXMT

The dimension of an HRXMT scan is 1024 by 1024 by 1024, providing more than one billion voxels in one sample scan for sampling. Based on sampling statistics, huge amounts of voxels dramatically increase the chance of finding precious metals in the amount of a few ppm, even a few ppb. Secondly, the scan is a 3D image of all sample particles, providing the spatial location of a specific region or selected particle. The non-invasive, nondestructive sample preparation and scan procedure allow the precious metal to remain in the sample for further analysis, and there is no stereology issue as with polished sections. Thirdly, the sample preparation and prescan time is easy and short. In this regard, a rapid scan method using radiography can recognize the region of the sample containing the targeted mineral phase first, then a complete 3D HRXMT scan can be implemented to identify the specific mineral phases.

Two ore samples from South America were used to demonstrate the rapid scan method of precious metal acquisition. The ore samples contained small amounts of silver in a silicate base. The goal of the HRXMT scan was to locate the silver minerals. The samples are named “comphead” and “composite2” shown in Figure 4.5.

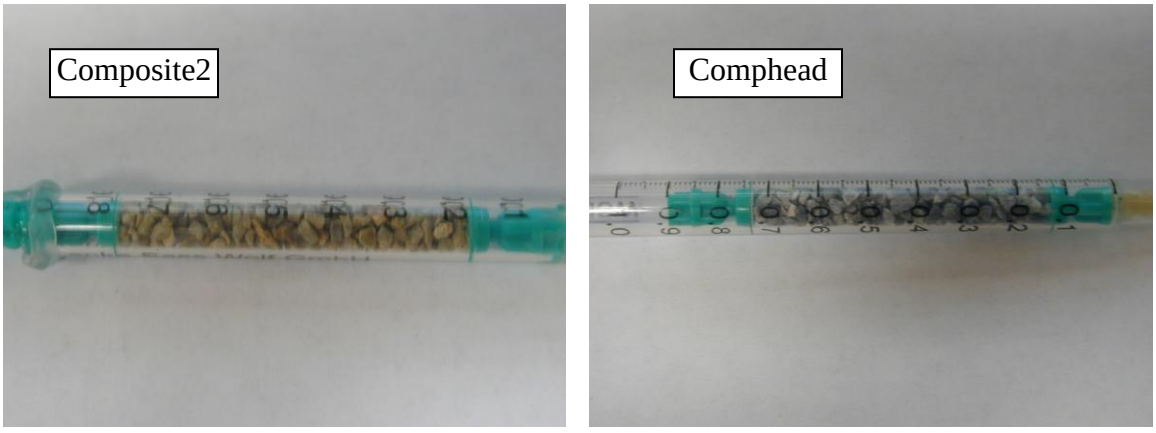

Figure 4.5 – Silver ore samples.

4.2.2 Scanning Procedures and Results

In Figure 4.5, the left image is composite2 and the right image is comphead. Samples came from different locations of the mine field with similar mineral composition. Both samples were of particles with a size fraction of 0.85mm to 1mm sealed in a long tube syringe as a packed bed. In Section 4.2, the CT scan conditions will be discussed to locate and enhance silver minerals using radiography and tomography. An EDAX (energy-dispersive X-ray spectroscopy) scan will be held as the reference. In the end of the section, a few pure silver and gold particles will be scanned using HRXMT to obtain the real CT number compared to the result of the comphead and composite2 scans.

Rapid scan radiography was first used to locate the high density minerals. Under a high source voltage and with short distances between source and detector, low density materials lose contrast with high x-ray intensity counts and are difficult to identify. High density and high atomic number materials have sufficient x-ray intensity and are able to be recognized. Single image acquisition for one radiograph projection can be done in a few seconds, and then the high x-ray intensity part is analyzed through calculation of the maximum reading of region of interest (ROI). In a 4X magnification scan, the field of view is about 5mm in height and 5mm in width. With some overlapping areas for image stitching, a prescan of a sample of a 3.2cm length packed bed can be done in 5 minutes, including the time for image acquisition and sample reallocation. More than one sample tube can be examined in a short period of time to increase the chance of finding precious minerals.

With regard to scan conditions, a CT standard must be used to identify specific mineral phases such as silver. The copper standard in the 4X magnification is the CT

standard applied for this scan, providing a moderate reading of high density, high atomic number materials such as silver, while not losing the contrast of low density materials like silicates. Figure 4.6 shows selected minerals in the comphead and composite2 sample using XMuDat to obtain a linear regression relationship of the mass attenuation coefficient of each mineral phase. Bornite (Cu_4FeS_4), galena (PbS) and pure silver (Ag) are introduced into this simulation. The energy level is set at 80kV which is equal to 40keV according to Figure 3.11. Full scan conditions are listed in Table 4.2.

Figure 4.7 shows a stitched image of different locations at left, a single radiograph at top-right and a 3D view of the complete HRXMT scan at bottom-right. The stitched image was composed by a total of 13 images and stitched with some overlapping parts using Photoshop. Each of the images was acquired under a 4X magnification, binning 2, and the distances of source/detector were 10mm/-40mm, with the voxel resolution at 5.625 micron. The source energy level is 150kV with 5 seconds exposure time, and the images are taken from top to bottom, moving 2600μm downward per image. It is noted that the scan conditions are different with the copper standard because these scan conditions are specific for single radiograph enhancing the existence of high density materials. Two dark parts are clearly scanned in the No.7 image which has mass attenuation coefficients higher than the nearby silicate minerals. In Figure 4.7, the upper-right image shows a single radiograph that reallocates the field of view to the coordinate of the No.7 image. Obviously the two specific mineral grains have higher mass attenuation coefficients than the nearby grains. To identify the selected minerals in the HRXMT scan, we applied the copper standard conditions to complete a full scan on the region of interest which is the same as image No.7.

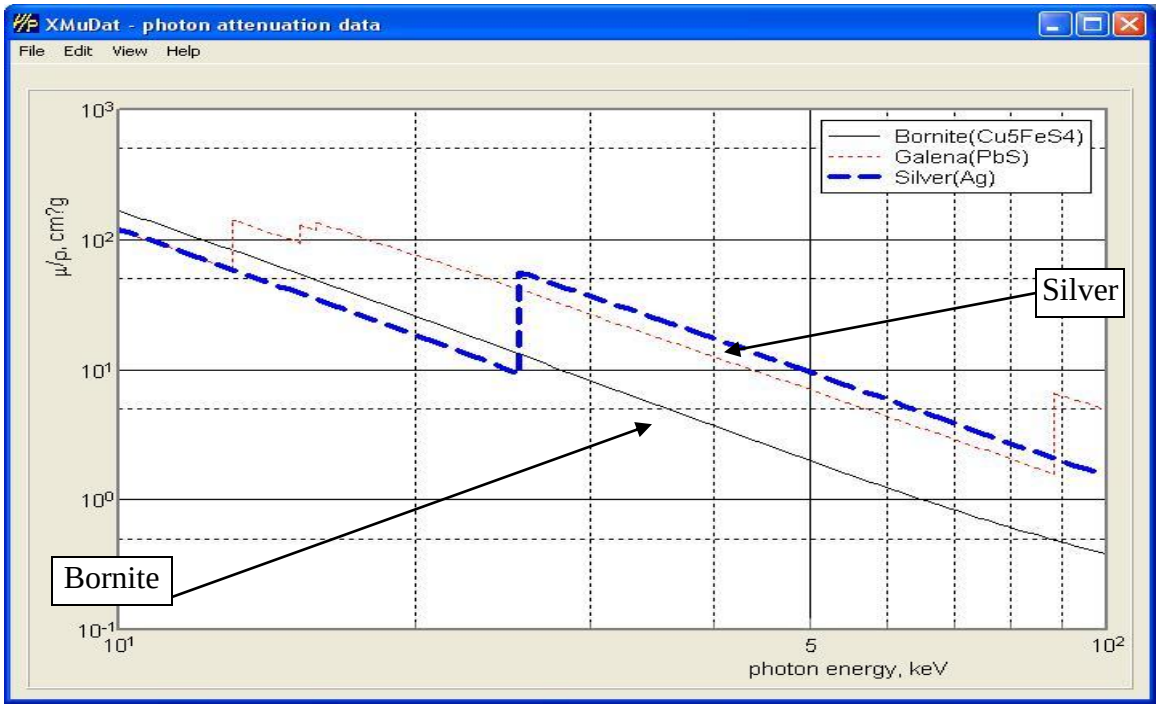

Figure 4.6 – Mass attenuation coefficients of Bornite, Galena and Silver using XMuDat.

Table 4.2 – Conditions of the HRMXT scan on the region of interest at the No.7 image.

Sample Name	Ag Composite2 – 1st tube, No.7
Date	April 20th, 2011
Total Scan Time	4 hours
Objective	4X
Source Settings (kV/W)	80kV/10Watts
Pixel size (μm)	5.05 microns
Start and End Angle	-94 degrees to 94 degrees
Number of Views	1000
Time per View (sec)	9 seconds
Source/Detector Positions	-60mm / 20mm
Camera Binning	2
Physical Filter	150 μm glass
Source Drift	2
Reference Type	Averaged Multireferences
Secondary Filtered Reference Details	None
Software Filtering	None
--	--
Recon Binning	1
Ring Removal	None
Beam Hardening	0.5
CT Scaling or Max/Min counts	Bornite Standard

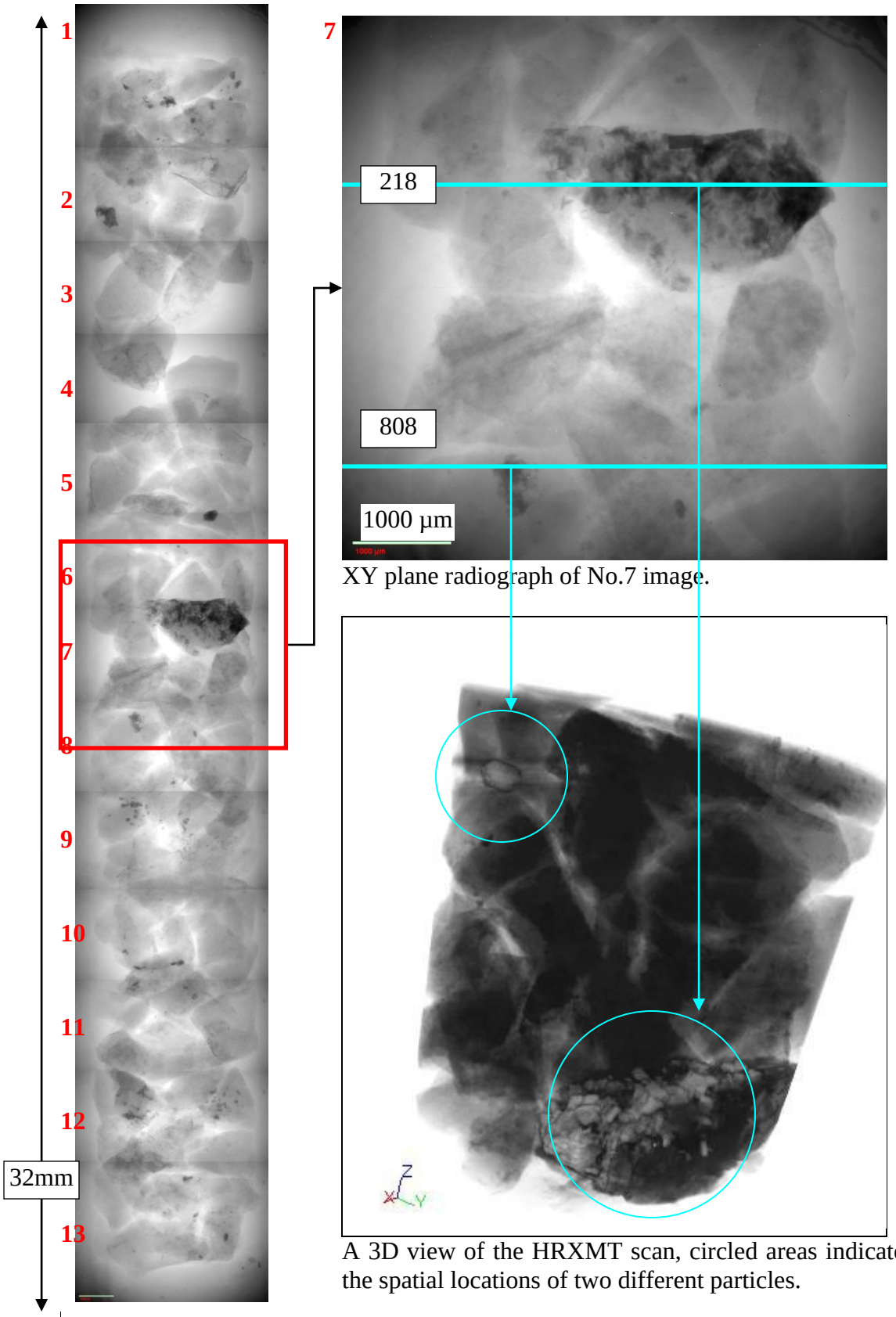

XY plane radiograph of No.7 image.

A 3D view of the HRXMT scan, circled areas indicate the spatial locations of two different particles.

Figure 4.7 – Full view of sample composite2

The copper standard provides CT scaling for tomography in the reconstruction stage. Thus, we can identify the mineral phase according to the x-ray intensity relationship to the bornite mineral in the reconstructed image. Density and atomic number are obtained and referenced according to Section 3.5.1. In the result, two slices from the HRXMT scan were picked to analyze the mineral composition. Figure 4.8 shows the 2D cross sectional view of slice 218 and 825. Mineral phases at the lower-right in slice 218 are brighter than the nearby region because of their higher mass attenuation coefficients.

Figure 4.8 also shows the XZ plane cross section of slice 825 in the right image. The mineral phase to be investigated is located at the upper-right having higher CT number than nearby minerals and higher brightness. These images are reconstructed using the copper standard, which provides a scale for copper minerals with the attenuation coefficient. Circled areas in Figure 4.8 have been marked and the attenuation coefficient counts measured. Table 4.3 shows the measurements.

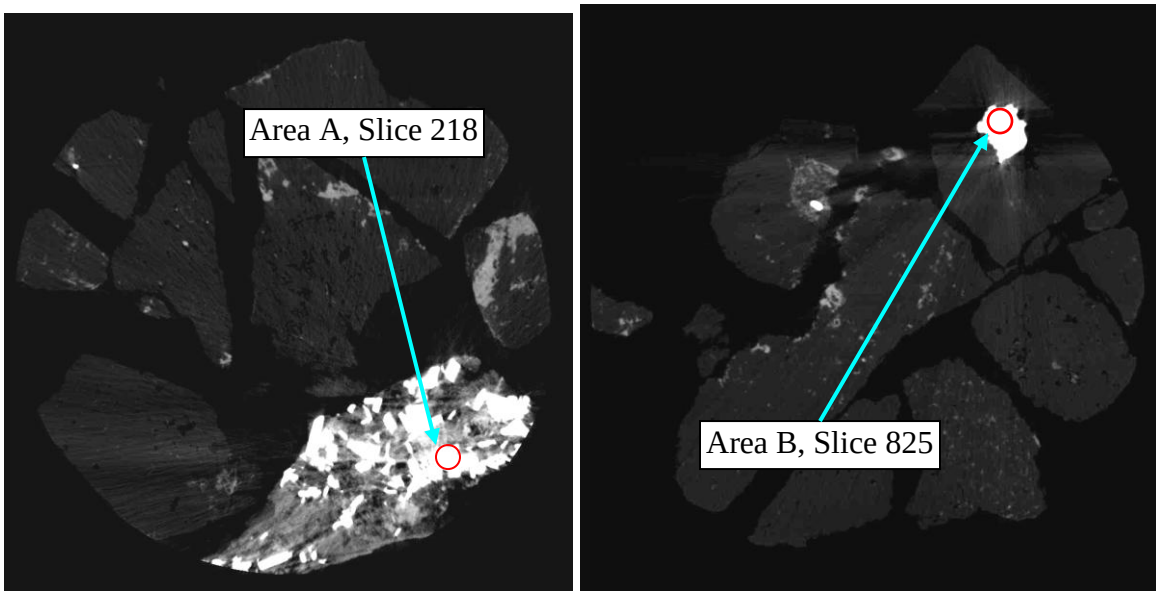

Figure 4.8 – 2D cross section views of HRXMT scan of composite2 sample.

Table 4.3 – CT numbers of slice 218 and slice 825 in the circled sections of composite2.

Slice	Area	Avg	STDDEV	Min	Max
218	A	11888.727	2663.7244	4092	15124
825	B	12407.583	1318.7787	6796	17150

Both regions of interest in slice 218 and slice 825 reveal similar results of about 15,000 and 17,000. According to the bornite standard scale in 16-bit, the reading of bornite is around 5,000. According to Figure 4.6, bornite has a mass attenuation coefficient close to 4 and silver has a reading close to 12. The ratio is 1:3. Compare with the reading of bornite (5,100) and the two regions of interest (15,124 and 17,150), both regions of interest show very similar results, and may possibly be the silver mineral.

The comphead sample scan was scanned based on the same procedures. While the first and second long tube samples contained no high density and no high atomic number materials, the third tube contained a particle having approximately same the x-ray intensity reading as the high density particles in composite2. To make a comparison of the comphead and composite2 results, scan conditions were kept the same and reconstructed in the bornite standard. Figure 4.9 shows a stitched image of all radiographs to see the whole tube at left, a single radiograph at top-right and a 3D view of the complete HRXMT scan. An individual particle can be identified in the third radiograph. The third radiograph also shows the location of a high density particle. A full HRXMT scan was taken and reconstructed for the comparison. In Figure 4.10, a high density mineral grain area which was much brighter in grey scale was located and confirmed as the specific particle observed in the third radiograph at slice 501. The red circled area was later measured for the CT number using ImageJ.

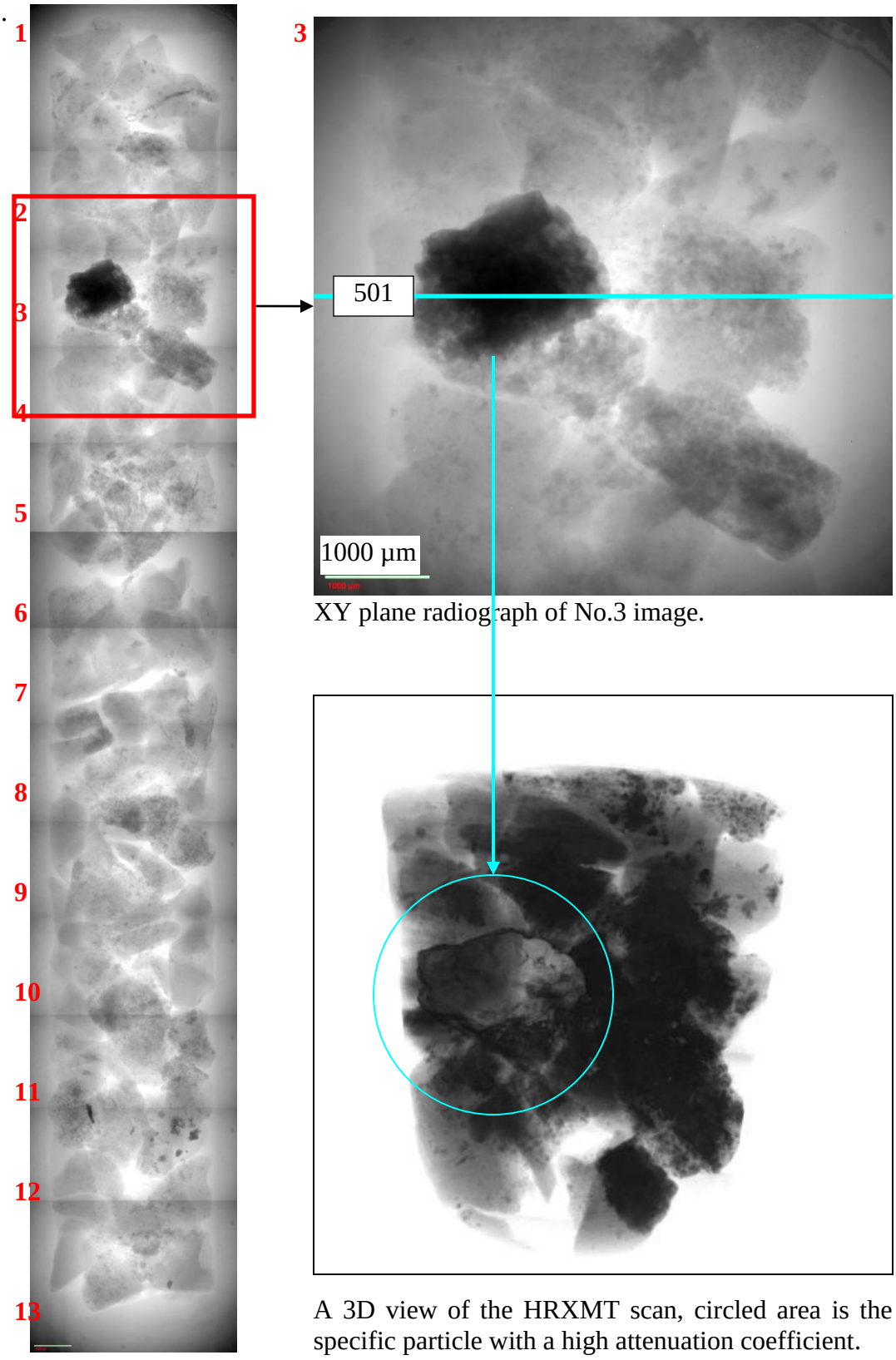

XY plane radiograph of No.3 image.

A 3D view of the HRXMT scan, circled area is the specific particle with a high attenuation coefficient.

Figure 4.9 – Full view of sample comphead

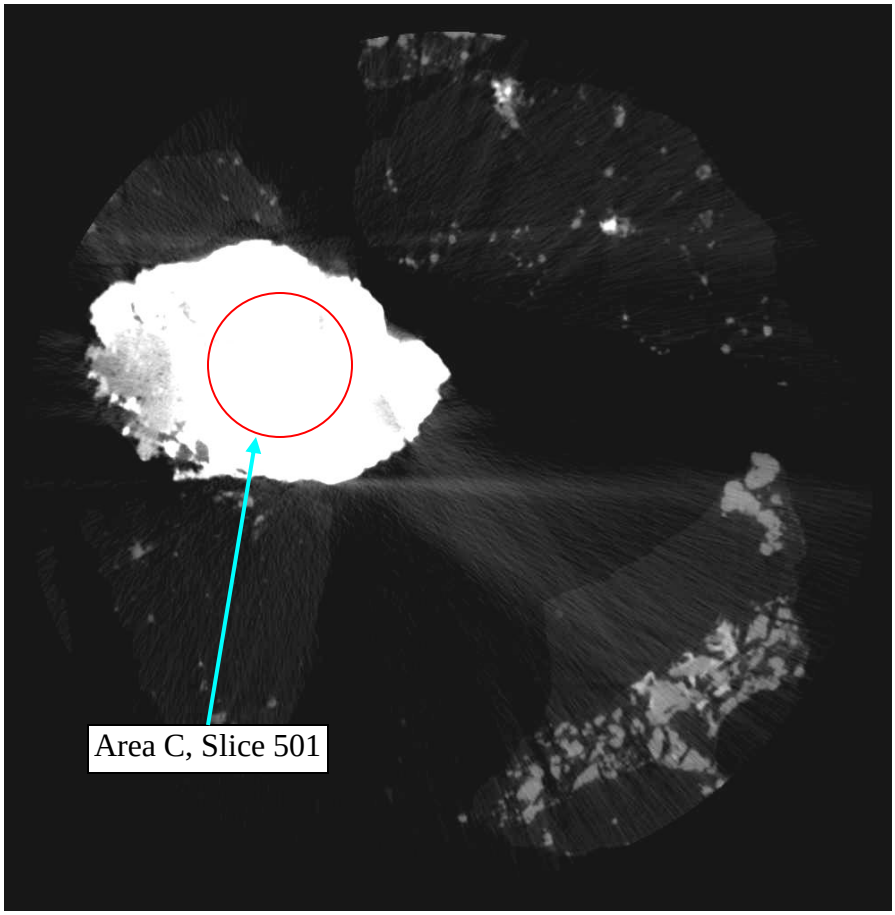

Figure 4.10 – 2D cross section views of HRXMT scan at slice 501 of comphead sample.

Table 4.4 shows the measurements of the circled region of interest of slice 501. Both composite2 and comphead samples have similar counts of mass attenuation coefficient, around 15,000, of the high density material. Since those two samples are from the same source but different location, the high density mineral can be assumed to be the same type of mineral. However, the mineral is still unknown and unidentified even with the attenuation coefficient. It could be molybdenite, galena or silver because these minerals all have high density and high atomic number. To characterize the specific mineral phase, another examination method will be introduced and then compared with the HRXMT result in the following section.

Table 4.4 – CT numbers of slice 501 in the circled section of comphead.

Slice	Area	Avg	STDDEV	Min	Max
501	C	15482.162	485.29852	11737	16590

The CT standard is one way to identify the mineral composition, relatively. The high density material is possibly something else having very close density and mass attenuation coefficient to silver, such as galena. Mineralogy is one method to identify the mineral composition. Note that the high density minerals in both samples performed square-like geometry, which is very similar to the crystal structure of galena. To identify the specific mineral phase, other methods of examination have to be applied to confirm the HRXMT results. Since the spatial location of the individual particle has been located, the specific particle can be isolated to observe the mineral characteristics such as shape or boundary minerals using optical microscopy. The composite2 sample tube was unsealed and the particles poured out, and divided into a few sections to locate the specific particle. The specific particle was picked from the sample tube and identified by SEM/EDAX examination.

EDAX (Energy-Dispersive X-ray Spectroscopy) is an analytical method used to identify elements or characterize chemicals of a sample. By analyzing the x-ray emitted from the material stimulated by source electrons, information from the x-ray provides the element characterization of the sample in a specific area. Element types and concentrations are also listed. Figure 4.11 and Figure 4.12 show the results of EDAX spectroscopy of two random locations on the surface of the larger particle in Figure 4.9, slice 218, composite2 sample tube. The concentration of each individual element is also listed in the figures.

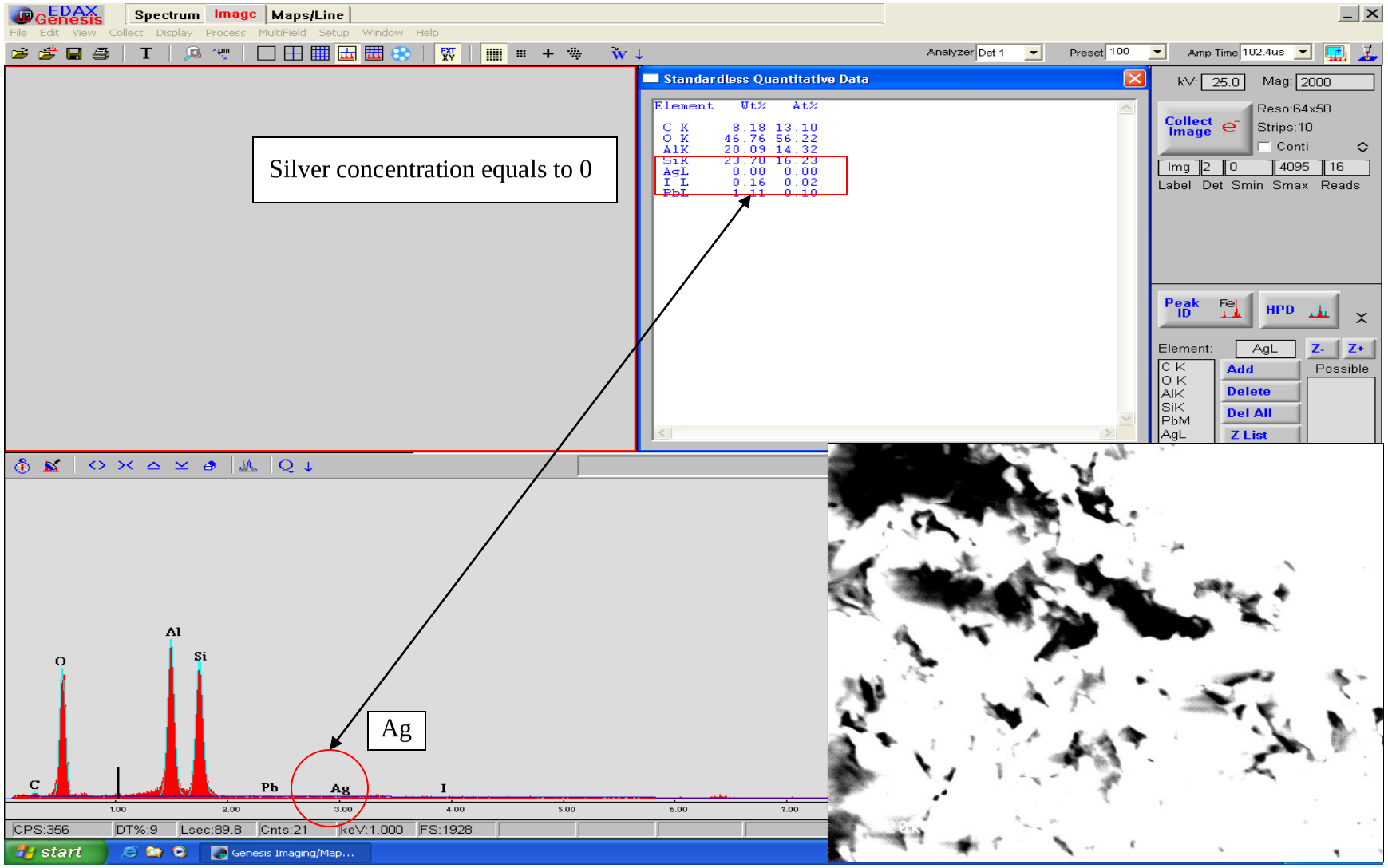

Figure 4.11 – Mineral composition at the first random location is measured by SEM/EDAX. Silver concentration equals to 0. Image is shown as example of option and menu location.

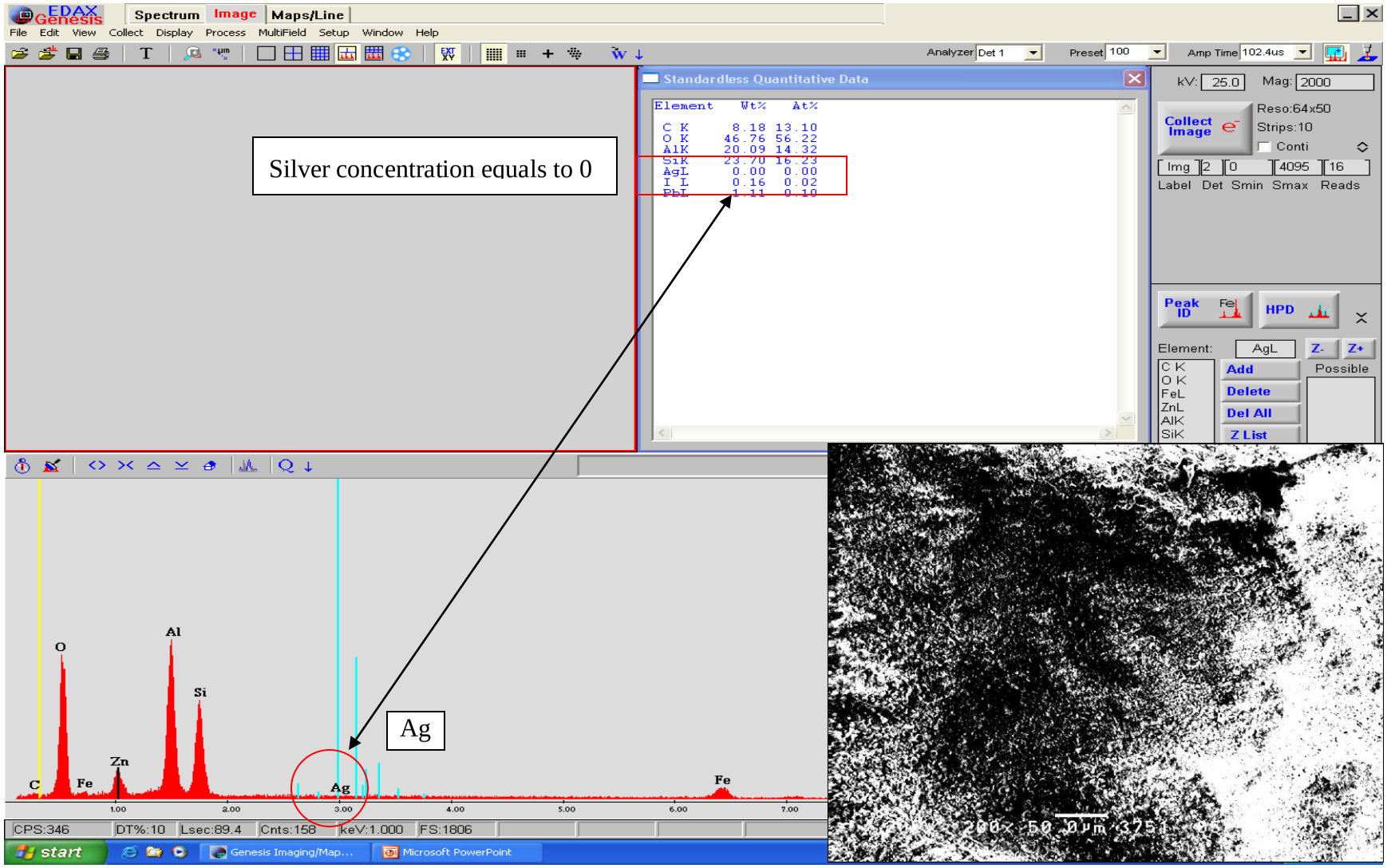

Figure 4.12 – Mineral composition at the second random location is measured by SEM/EDAX. Silver concentration also equals to 0. Image is shown as example of option and menu location.

Figure 4.11 shows the mineral composition measurements of the specific particle (slice 218) from composite2 sample at the first random location on the surface using EDAX with magnification 200X. Image at bottom-right shows the surface state. At the top-right is the concentration list of different elements in the specific area. The image at the lower right is the specific surface area photograph at 20X magnification. The spectrum map shows carbon, oxygen, aluminum and silicate. A small amount (0.1%) of lead was detected, and no silver element was found. Gangue minerals (SiO_2 and Al_2O_3) were confirmed. Galena (PbS) was also confirmed in the mineral composition. Another surface scan was taken and the results are listed in Figure 4.12.

Figure 4.12 shows the mineral composition measurements of the specific particle (slice 218) from composite2 sample at the second random location on the surface using EDAX with magnification 200X. The image at bottom-right shows the surface state. The element composition shows very similar results to the previous scan. A few additional elements such as zinc and iron were found, but no silver.

To confirm the results from the SEM/EDAX scan and CT scans, another scan was initiated. One selected silver particle and a few gold particles (around 50 microns) were marked and poured into a long syringe tube with composite2 sample particles. The silver particle was marked in red color with a few gold particles sealed in a Styrofoam ball. Those specific particles were first located and scanned in the HRXMT to acquire CT numbers, and then analyzed by SEM/EDAX to get a reference spectrum. A reference sample scan was operated under the same conditions as the copper standard to compare the results for comphead and composite2 samples.

Two objectives were considered in the reference scan: first was the attenuation coefficient for the silver mineral in the HRXMT scan using bornite as the standard. The reading for silver was then compared to the readings acquired from scans of the previous comphead and composite2 samples. If the reading for the silver particle in the reference scan is similar to the reading of the high attenuation coefficient material in the comphead and composite2 scans (around 15,000), it will be confirmed as silver. If the reading for the silver particle is lower or higher than 15,000, the high density material in the previous scans will be considered as gold (higher than silver) or galena (lower than silver).

After the sample was well prepared, the radiographic images and the HRXMT scan were taken from top to bottom. To acquire similar CT numbers for the comparison, the HRXMT scan for composite2 particles with a silver/gold reference sample used the same scan conditions as used for composite2 and comphead samples. Figure 4.13 shows a stitched image at left, totally 21 images of a 7cm length sample tube. A single radiograph of the gold particles is shown at top-right and a single radiograph of the silver particle is shown at bottom-right. This radiograph helped us to identify the two specific minerals with their size and location.

The HRXMT scan focused the field of view on these two minerals in one scan which took 4 hours to complete. Figure 4.14 shows some fine gold particles (~50μm) and a large pure silver particle in the scan result. These images were generated by VolSuite and the particles were visualized in different colors. The left image shows the spatial location of a silver particle at bottom-left and small gold particles at upper-right. The right image is a cross sectional view from the XZ plane. Silver and gold particles are marked in the circled areas.

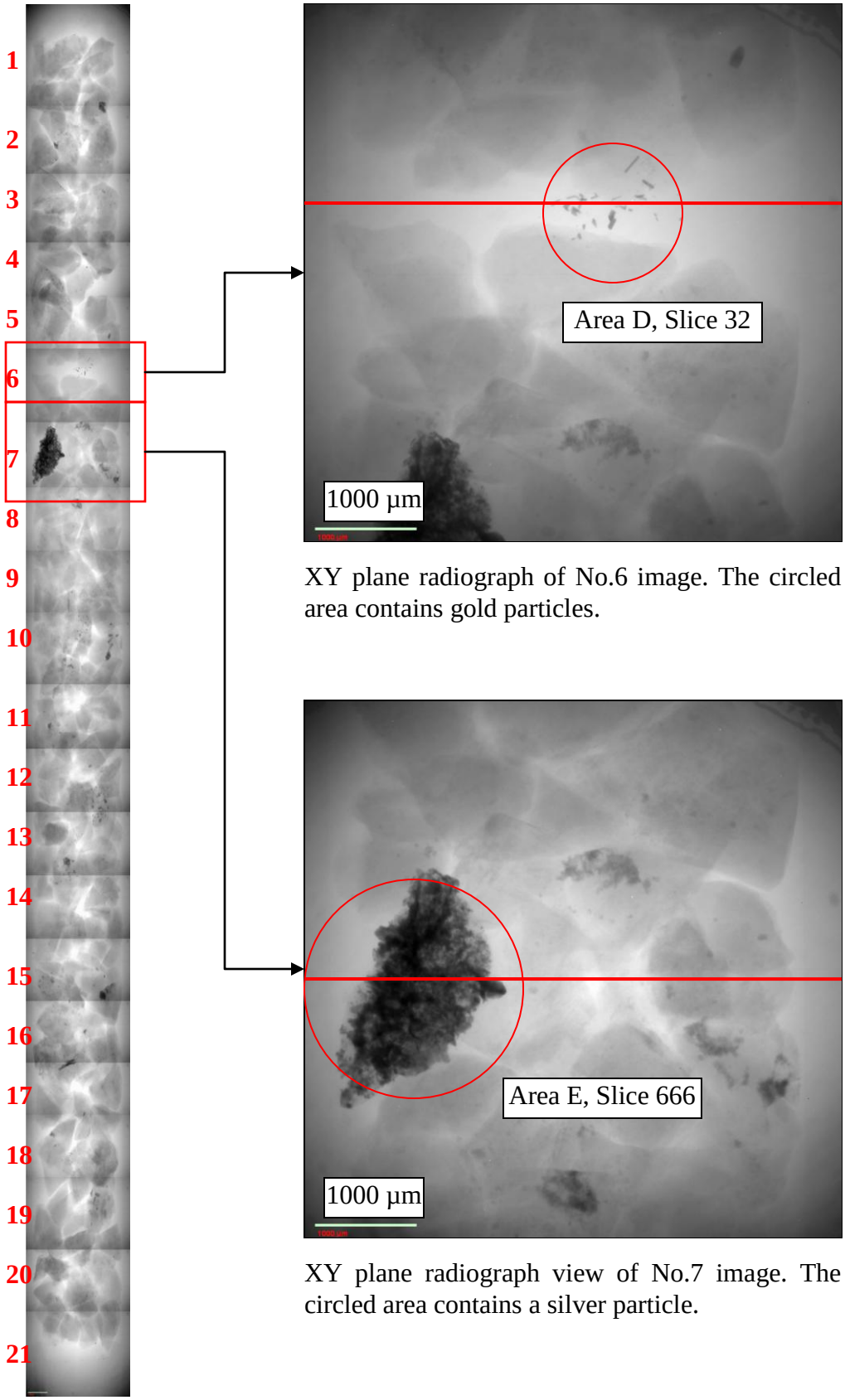

XY plane radiograph of No.6 image. The circled area contains gold particles.

XY plane radiograph view of No.7 image. The circled area contains a silver particle.

Figure 4.13 – Full view of the reference sample.

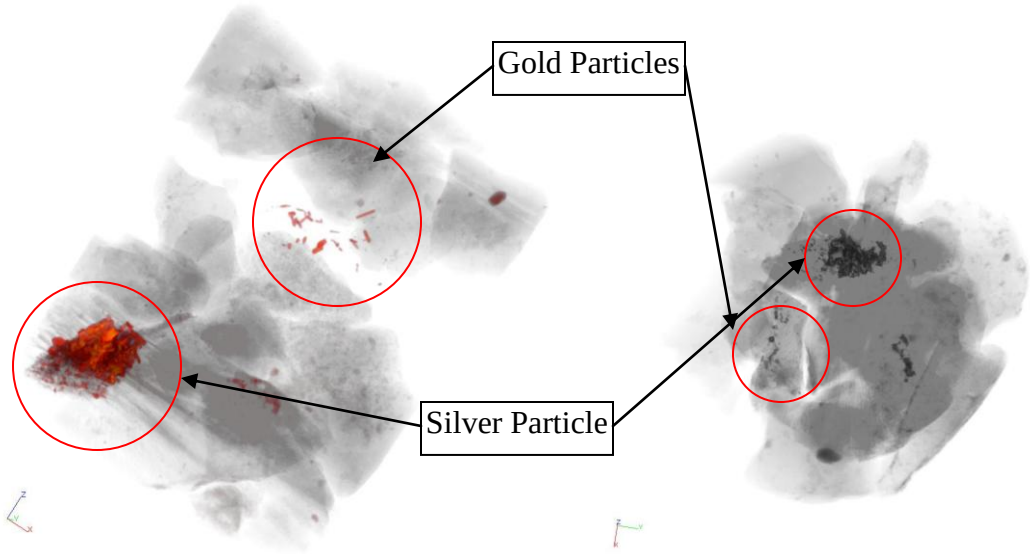

Figure 4.14 –The spatial location of a silver particle and small gold particles.

CT numbers measurements at slice 32 (silver particle) and slice 666 (gold particles) in the circled sections of the reference sample are listed in Table 4.5. The CT number of the silver particle (40,680) was obviously higher than the high density material in the previous scan (15,000). The gold particle reading (26,479) was lower than silver due to the smaller particle size, yet higher than 15,000 which the high density material had in the composite2 and comphead samples. Thus, it was confirmed that the high density materials in the composite2 and comphead samples were neither silver nor gold minerals. The next step was to confirm silver and gold in the HRXMT scan using the SEM/EDAX method. The measurements are listed and shown in Figure 4.15 (silver particle) and Figure 4.16 (gold particles).

Table 4.5 – CT numbers of silver and gold particles from the reference sample.

Slice	Area	Avg	STDDEV	Min	Max
32	D	40680.754	4423.5557	22768	46423
666	E	26479.762	2692.3699	19423	29707

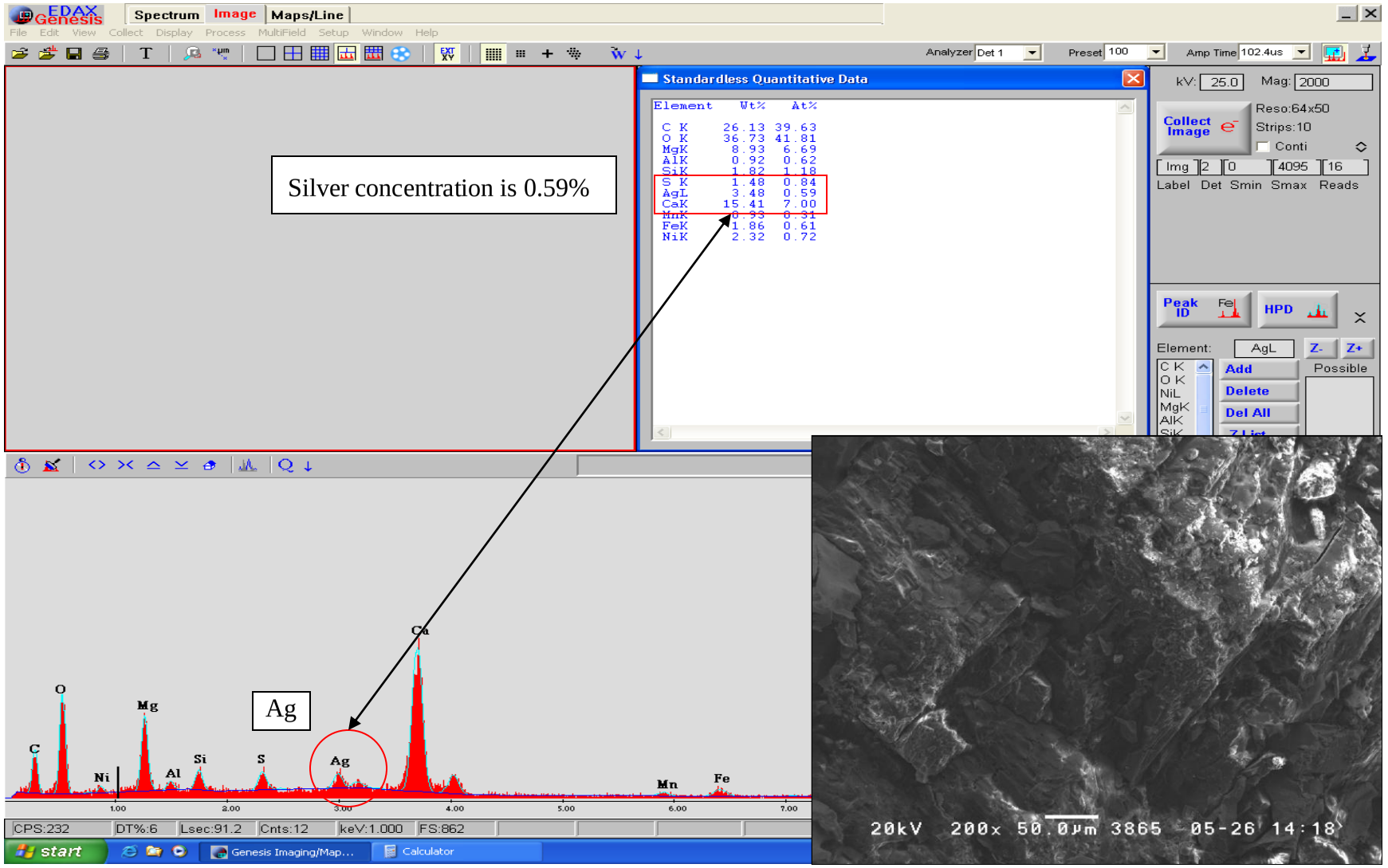

Figure 4.15 – Mineral composition of the specific silver particle is measured by SEM/EDAX. Silver concentration is 0.59%. Image is shown as example of option and menu location.

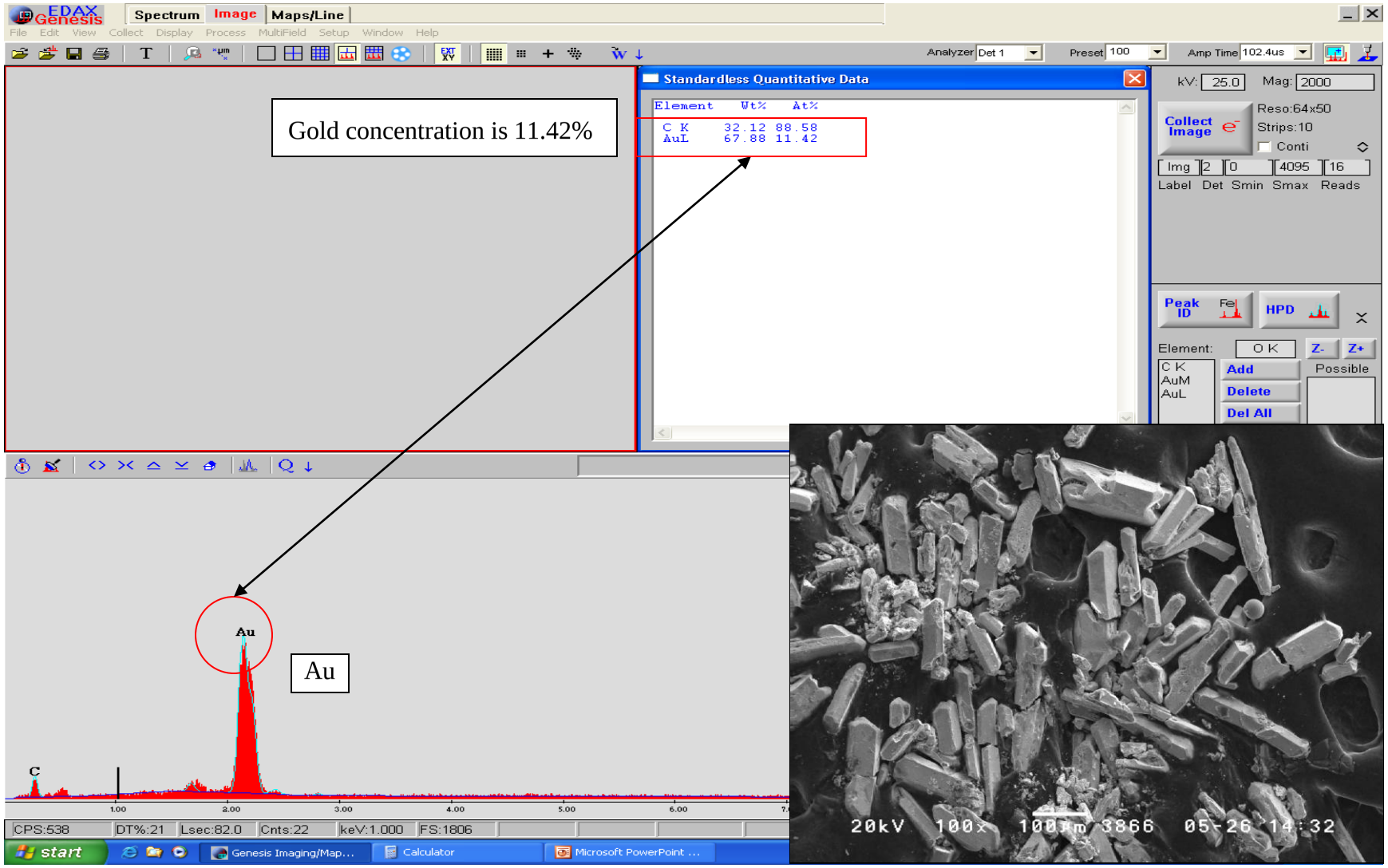

Figure 4.16 – Mineral composition of gold particles is measured by SEM/EDAX. Gold concentration is 11.42%. Image is shown as example of option and menu location.

Figure 4.15 shows the mineral composition measurements of the specific silver particle from the reference sample at a random location on the surface using EDAX with a magnification of 200X. The image at bottom-right shows the surface state. The histogram of element distribution showed that the Ag (silver) concentration was about 0.59%. It was proven that the existence of silver mineral in the sample can be detected and distinguished by both SEM/EDAX and HRXMT. The next step was to identify the gold particle using SEM/EDAX as shown in Figure 4.16; a few gold particles were isolated, located and scanned.

Figure 4.16 shows the mineral composition measurements of the gold particles from the reference sample at a random location on the surface using EDAX with a magnification of 100X. The image at bottom right shows the surface state. Gold particles were identified by SEM/EDAX. It was noted that pure gold (Au) with high concentration (11.42%) was observed. It is confirmed that gold and silver can be identified by both SEM/EDAX and HRXMT. Once the silver and gold particles are able to be identified in both HRXMT and SEM/EDAX results, the high density material in the comphead and composite2 samples is irrelevant, and will not be identified using SEM/EDAX.

4.2.3 Discussions

In summary, it is obvious that the x-ray attenuation coefficients are different in the radiographic image and in the tomography image. The reason for this difference is due to the thickness and shape of the gold particles. According to equation 2.4, the x-ray intensity relates to μ, the mass attenuation coefficient, ρ the density, Z the atomic number, E the energy level, and the key factor here, *x*, the distance over which the x-ray photons are transmitted. Gold and silver have high μ, ρ, and Z values under a fixed E factor in the

scan. In the tomography image, the CT number is assigned by reconstructed images from many different projections. The radiographic image is obtained from one projection, and is biased due to the lack of transmission distance. Since the silver particle is much larger than the gold particles, it definitely absorbs more x-ray photons but with less x-ray intensity than gold in the radiographic image. The radiographic image is not able to differentiate elements, but gives the location of mineral grains having high linear attenuation coefficients.

Another way to characterize the mineral phase by using a few radiographic images is the dual energy method. Interested minerals can be located using this rapid radiograph method in a very short time. A series of radiographic images will be taken in both a high energy level and a low energy level. The mineral atomic number can be calculated by the mass attenuation coefficients regardless the sample thickness. This method is still developing and will be applied on HRXMT scans.

As discussed above, in order to obtain the quick and accurate evaluation by radiographic analysis, mineralogy, binary mineral phases and mono-size particle distribution must be organized for sample preparation. Those considerations not only help identify specific mineral phases in a quick radiograph evaluation, but reduce misinterpretation caused by the transmission distance, similar minerals or particle size. If the attenuation coefficient of objective mineral is much higher than that of the host minerals, it will be easier to identify and locate the specific mineral. To enhance the image contrast, the distance of source/detector, exposure time and physical filters should also be considered to establish a high quality radiograph.

4.3 Mineral Structure of Teeth

HRXMT not only can be used for minerals but also for soft or solid organic tissues. In this regard, biomaterials such as bones, metallic installments in soft tissue, or teeth structures are discussed in the following section.

4.3.1 Scanning Considerations and Sample Preparation

Figure 4.17 shows an animal tooth sample (ivory_m53.95) which contains both dentin and enamel. It is noted that the enamel becomes calcified during tooth growth. The aged part is at the end of the tooth, which is the thicker part in Figure 4.17, and should have the most calcified enamel. In other words, the tooth is less dense at the root, which is the thinner part in Figure 4.17. The interface between dentin and enamel can be seen in the circled area distinguished by different colors. The objective of this study was to identify the growth and maturity of the enamel in different parts of the tooth. Furthermore, an ivory enamel sample was introduced as the CT standard to differentiate and quantify the enamel from dentin. Figure 4.18 shows the standard enamel sample and the standard dentin sample. The left image is MGL_93, a sample of high purity enamel; the right image is R37, a sample of high purity dentin.

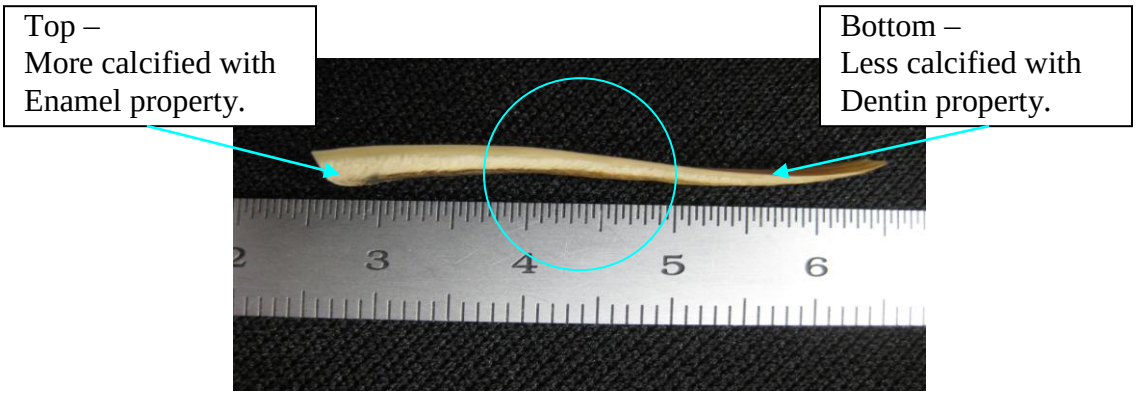

Figure 4.17 – Photograph of an ivory sample containing dentin and enamel parts.

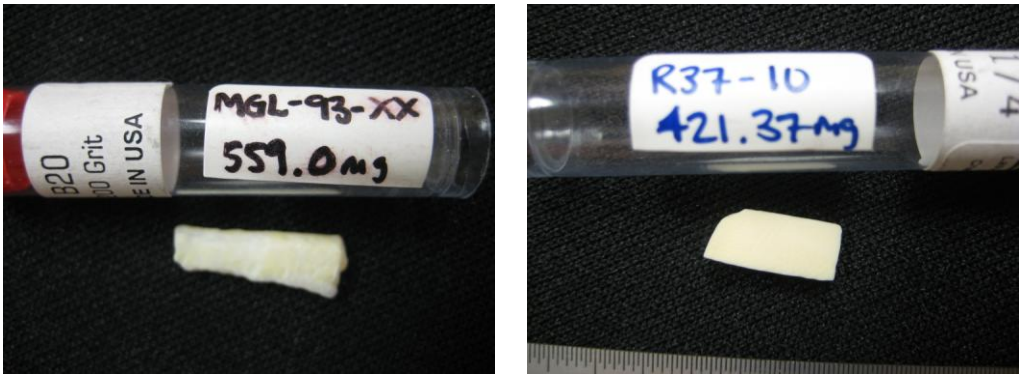

Figure 4.18 – Sample materials for tooth CT standards.

At first, the scan condition had to be set. The tooth sample was composed of enamel and dentin. In this case, the x-ray source voltage was set at 60kV/10watts for calcified tooth. The lens magnification was set at 4X to obtain a voxel resolution of around 5 microns for a detailed examination of the inner structure and material distribution of enamel and dentin. The source/detector distances were set at -60mm and 15mm for a 5mm by 5mm field of view and sufficient x-ray intensity. The exposure time is set at 10 seconds per image for the purpose of clear image contrast of the 3mm-5mm thick sample. A total number of 1000 views were obtained, enough for sampling inner structure and for image quality. The reconstruction conditions were the same as the bornite standard except for the beam hardening. The beam hardening number was set at 0.5 in order to avoid a cupping effect at the boundary area. The process was separated into 2 full scans, the top part and the bottom part. Total scanning time was about 8 hours for each sample. Table 4.6 shows the scan conditions details and Figure 4.19 shows the results of scans displayed in 3D images and 2D cross section images. In Figure 4.19, the left images are the top part of the scan in 3D and a cross sectional view in 2D; the right images are the bottom part of the scan in 3D and a cross sectional view in 2D.

Table 4.6 – Scan conditions of the m53.95 tooth sample.

Sample Name	Ivory_m53.95_01_Top_Bottom
Date	January 12th, 2011
Total Scan Time	4 hours and 4 hours
Objective	4X
Source Settings (kV/W)	60kV/10Watts
Pixel size (μm)	5.05 microns
Start and End Angle	-94 degrees to 94 degrees
Number of Views	1000
Time per View (sec)	10 seconds
Source/Detector Positions	-60mm / 20mm
Camera Binning	2
Physical Filter	150 μm glass
Source Drift	0
Reference Type	Averaged Multireferences
Secondary Filtered Reference Details	None
Software Filtering	None
Recon Binning	1
Ring Removal	None
Beam Hardening	0.5
CT Scaling or Max/Min counts	Global Scaling

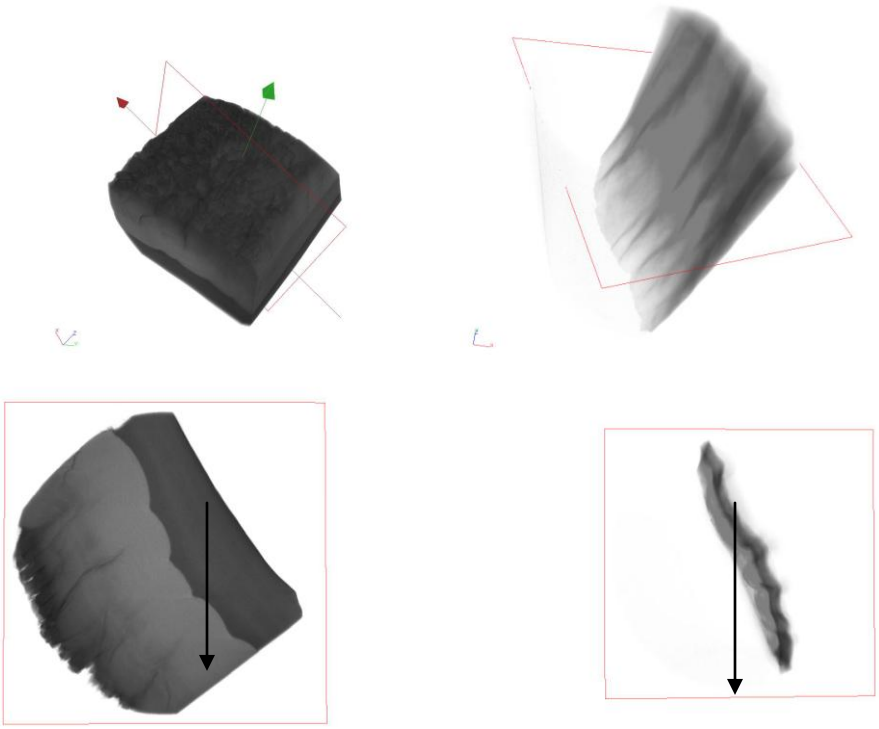

Figure 4.19 – The m53.95 sample scan image in 2D and 3D, generated by Volsuite.

4.3.2 Calibration Using Enamel and Dentin Standard

The standard ivory enamel was used for the calibration of the CT number. The ivory enamel standard sample was a homogeneous piece of elephant tooth containing 96% hydroxlapatite ($Ca_{10}(PO_4)_6(OH)_2$), and 4% organic tissue and water (Hilson, 1986), the same mineral composition as the enamel part in the tooth scan. The bulk density of enamel has been measured as 3.35 g/cm^3. The scan conditions were the same as the previous tooth scan in order to obtain the same attenuation coefficient of enamel. Also, conditions were the same as the previous scan in the reconstruction to create the standard. 189 images were taken (from +94 degrees to -94 degrees plus 1 center image) during the scan. The ivory enamel standard sample scan conditions are listed in Table 4.7.

Table 4.7 – Scan conditions of the ivory enamel standard sample MGL_93 and R37.

Sample Name	Ivory_MGL_93 and R37
Date	January 14th, 2011
Total Scan Time	1hour + 1hour
Objective	4X
Source Settings (kV/W)	60kV / 10Watts
Pixel size (μm)	5.05 microns
Start and End Angle	-94 degrees to 94 degrees
Number of Views	189
Time per View (sec)	10 seconds
Source/Detector Positions	-60mm / 20mm
Camera Binning	2
Physical Filter	150
Source Drift	150 μm glass
Reference Type	Averaged Multireference
Secondary Filtered Reference Details	None
Software Filtering	None
--	--
Recon Binning	1
Ring Removal	None
Beam Hardening	0.5
CT Scaling or Max/Min counts	Global / Tooth Standard

The ivory enamel standard sample was scanned and reconstructed in a global scale. To set up a CT scale for the enamel standard, the region of interest (ROI) function was applied with the same operating procedures as in Section 3.5.1. The selected ROI included the enamel part and the void (air) part. Every voxel attenuation coefficient in the ROI was calculated in each slice, where we needed the total amount of the sample. The voxel attenuation coefficients at the peak and bottom were recorded as 46000 and 22000 and identified as the attenuation coefficient of enamel and air.

Since the density had been measured, the enamel density was introduced in the CT scaling function. Note that only two phases were set because the standard enamel sample contained only air and enamel. The scale had been set by the densities and attenuation coefficients of air and enamel, where air has the density of 0.00 g/cm³ with an attenuation coefficient of 22000, and the enamel had the density of 3.35g/cm³ with an attenuation coefficient of 46000. CT scale was saved and named as tooth standard. The standard enamel scan was reconstructed again with the new CT Standard.

The ivory standard for the dentin sample, which contains 75% hydroxlapatite ($Ca_{10}(PO_4)_6(OH)_2$), and 25% organic material such as collagen, protein and water (Hilson, 1986), has been scanned, too. The bulk density of the dentin sample measured 1.74 g/cm³. The sample was mounted on the stage and scanned under the same conditions as the enamel standard. This scan is also reconstructed using the tooth CT standard

Scans of the standard enamel and dentin samples were converted into raw files and put in the ImageJ. The attenuation coefficients of air were the same in both scans under the same scan conditions. Thus, the attenuation coefficients of enamel and dentin can be obtained. The histogram function of ImageJ calculates the voxel attenuation

coefficient distribution where enamel has the CT number 3010.7 and dentin has the CT number 1085.2. The linear regression has been plotted using XMGrace in Figure 4.20.

The left axis is the scale of the CT number, which means the correlating material attenuation coefficient under the tooth CT standard; the right axis is the density range of the two different phases, enamel and dentin. A is the point corresponding to enamel's density and CT number, and B is the point corresponding to dentin's density and CT number. The linear regression shows a relationship between enamel and dentin. It is capable of predicting similar material densities according to the CT number using the same CT standard. Through interpolation, the linear regression of A and B can provide a prediction of material having a density between them. For materials with densities are higher than enamel or lower than dentin, one can use extrapolation but the accuracy is not guaranteed.

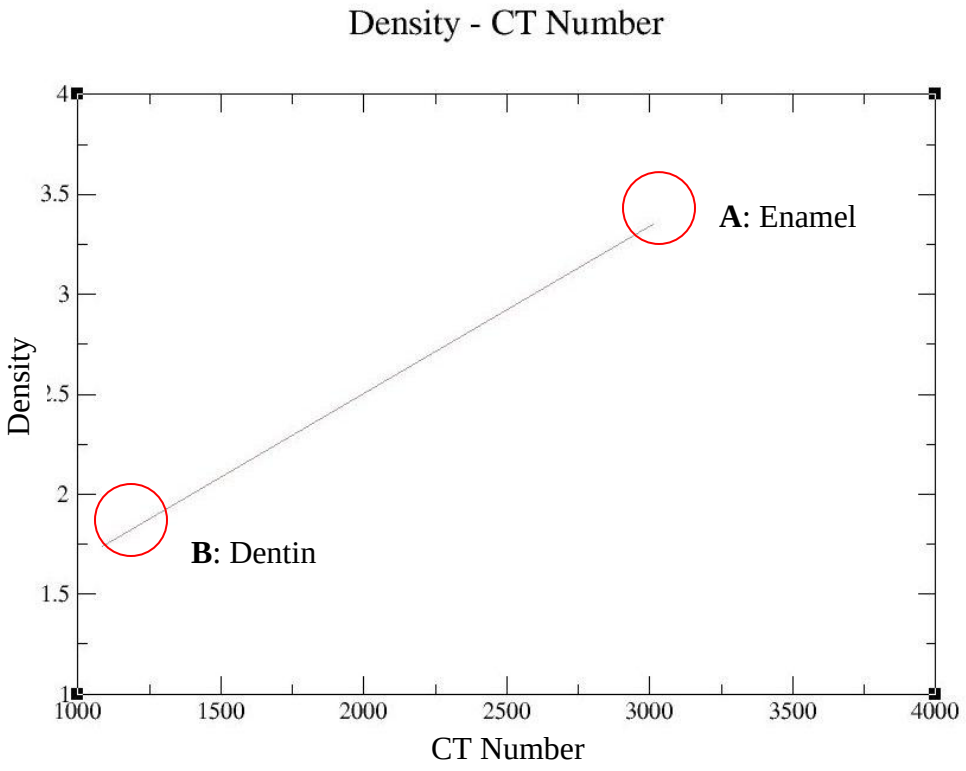

Figure 4.20 – Linear relationship of enamel and dentin with CT number and density.

4.3.3 Results and Discussions

Once the CT number of enamel and dentin were obtained, the next step was to reconstruct the m53.95 sample scans using the tooth standard. Both of the top and bottom scans were reconstructed and rescaled from 16-bit to 8-bit for a new range 0 to 3300. Pure enamel material will came very close to 255 in the 8-bit scale. Figure 4.21 shows the top part scan and the bottom parts of the scans. The CT number distribution across the line was plotted using MIPAV. The image on the top is the 2D cross sectional view at slice 496 of the m53.95 sample (top part of the scan). The CT number distribution along with the line is displayed at right; the image at the bottom is the 2D cross sectional view at slice 496 of the m53.95 sample (bottom part of the scan). CT number distribution along with the line is displayed at the left. The boundaries of enamel and dentin are significant and can be identified easily. Some observations about the results follow. The CT number of the dentin part at the top part of the scan was around 120 to 140, and the reading of the enamel part was above 200; in the bottom part of the scan, the reading of the dentin part was similar to the reading at the top part; however, the reading of the enamel part was lower than that in the top part. As is known, the top part was the end of the tooth which has the most calcified materials. The scan result confirmed that the top part is more calcified and denser than the root part. Secondly, the enamel part in the top part had a slowly decreasing CT number distribution along the line. At the right side of the scan, porous structures were observed as organic tissues and nerves, which secrete and construct calcium for the enamel properties. The decrease shows a growth process by its densities. This exciting discovery should help researchers to understand the growth progress of a tooth and provide more information for the investigation of teeth.

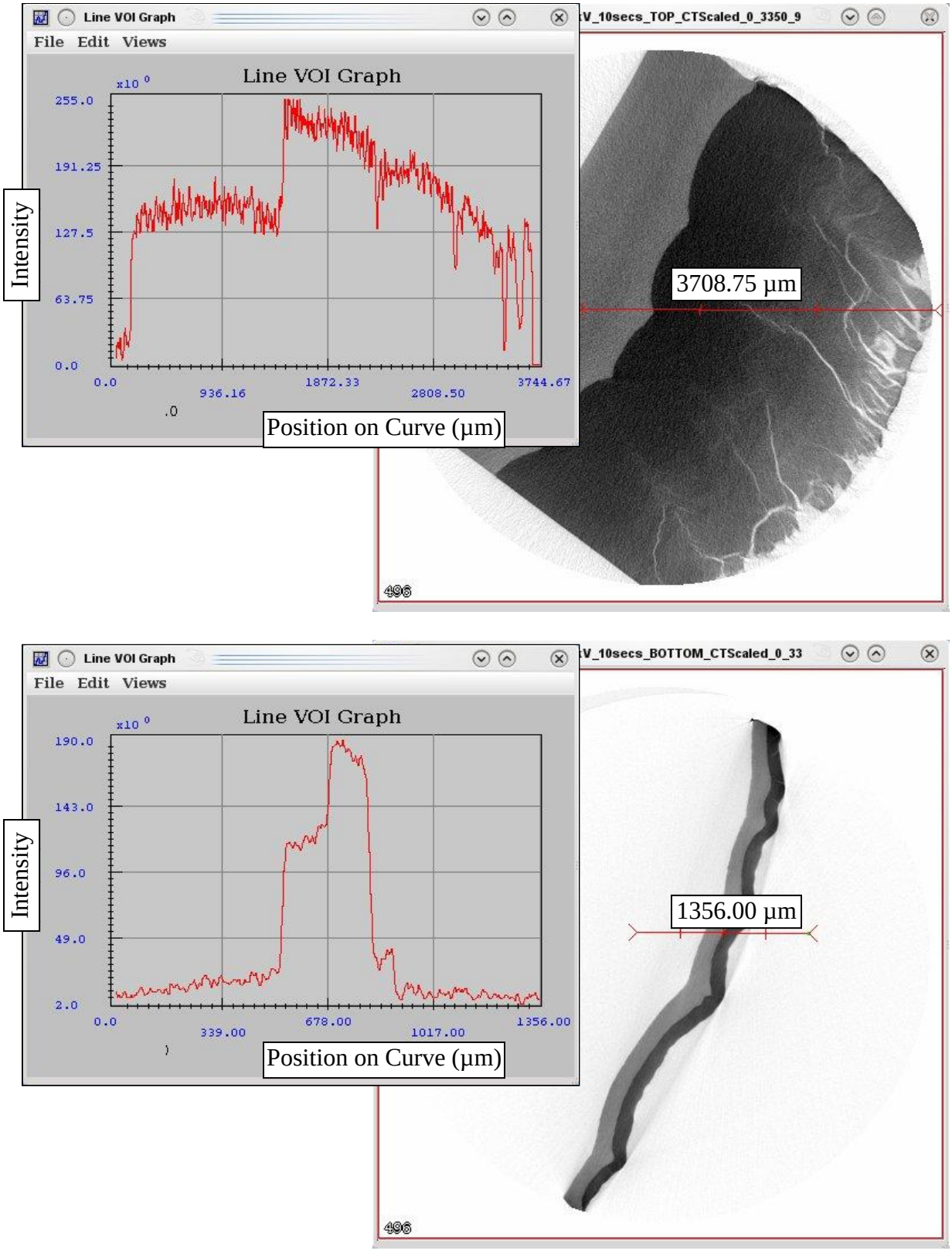

Figure 4.21 – 2D cross sectional views at slice 496 of the m53.95 sample.

CHAPTER 5

SUMMARY AND CONCLUSIONS

In this thesis, High Resolution X-ray Micro Tomography (HRXMT) has been discussed with respect to 3D imaging and data analysis of multiphase mineral samples including a brief history, starting from the conventional cone beam CT instruments, to the more recent systems with advanced optics designs, such as XRadia's Micro XCT 400. The theory of x-ray attenuation coefficient has been identified according to Beer's law, including material density, source energy level and effective atomic number. In order to optimize the use of HRXMT for different mineral phases and purposes, the XMuDat software was introduced to determine the source energy level. Sample preparation methods have been discussed in addition to sampling statistics and packing methods. Scan conditions were studied including considerations of source energy level, lens magnification on the detector, distance specification, filters, field of view, exposure time, projection counts and references. Reconstruction of HRXMT results was determined by certain parameters, including beam hardening, CT standard and file format. For the purpose of mineral identification, the making of a CT standard and comparison of results with QEMSCAN were also developed. At the end of this section, a database was prepared for recording and analyzing scan conditions of all HRXMT results. In this way, the user can organize and develop HRXMT scans to identify specific minerals more easily.

HRXMT can be used for a variety of applications. The observation of internal structure was discussed using oil shale sample scans. High density, high atomic number mineral characterization can be allocated and identified by a rapid scan method. Finally, for other samples, such as elephant teeth, an ivory scan coupled with CT standards was introduced using HRXMT scans.

Following these procedures and instructions, the user can gain a general idea to evaluate and estimate HRXMT conditions for specific mineral scans. The standard operating procedures can be established from sample preparation to data analysis. HRXMT can be developed not only for sample visualization in 3D, but also for mineral characterization, spatial organization of a specific mineral phase and porous structure analysis. The geometry of internal structure at the micron level can be visualized and digitalized for further simulation such as flow through porous media and stress or deformation simulation.

APPENDIX A

XMUDAT SETTINGS

XMuDat is free software developed by the International Atomic Energy Agency for x-ray attenuation coefficient evaluation. In Section 2.2, the consideration of mass attenuation coefficient has been discussed. The operational procedures for building a mineral list with a mass attenuation coefficient graph using XMuDat will be performed

1. The software can be downloaded from http://www-nds.iaea.org/reports/nds-195.htm. Open XMuDat as in Figure A.1.

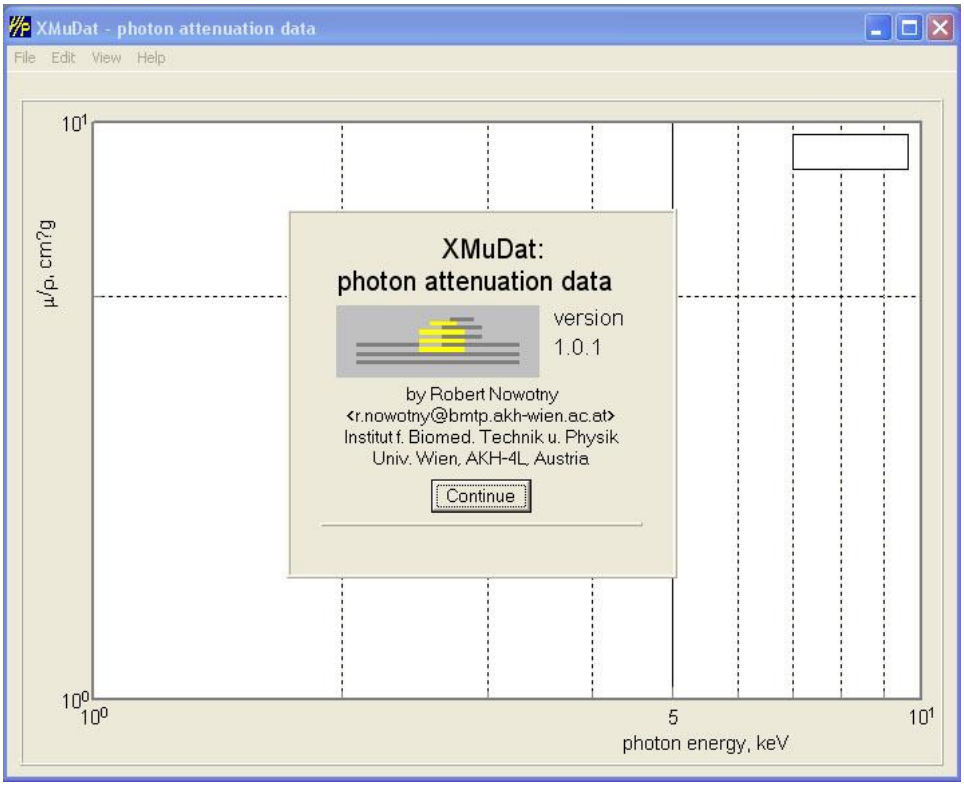

Figure A.1 – A general view of the main menu of XMuDat.

2. Go to File ->New to create a new dataset. Go to File-> Data Setup and a new window will pop up as in Figure A.2.

A total of 6 minerals can be chosen to be included in one mass coefficient attenuation graph. The effective Z, density, electrons and calc.electrons in Figure A.2 will be calculated by the software automatically. Note that in equation 2.3, the power term we applied is 3.8 as the parameter for the photo effect. In XMuDat, it is unknown which term has been applied. However, this parameter does not affect the Effective Z dramatically. The attenuation coefficient type is set at attenuation-total. The data source is set at default "J M Boone, A E Chavez; Med Phys 23(1996)1997" shown in Figure A.2. The plotting line color, width, pattern and legend can be set at the user's convenience.

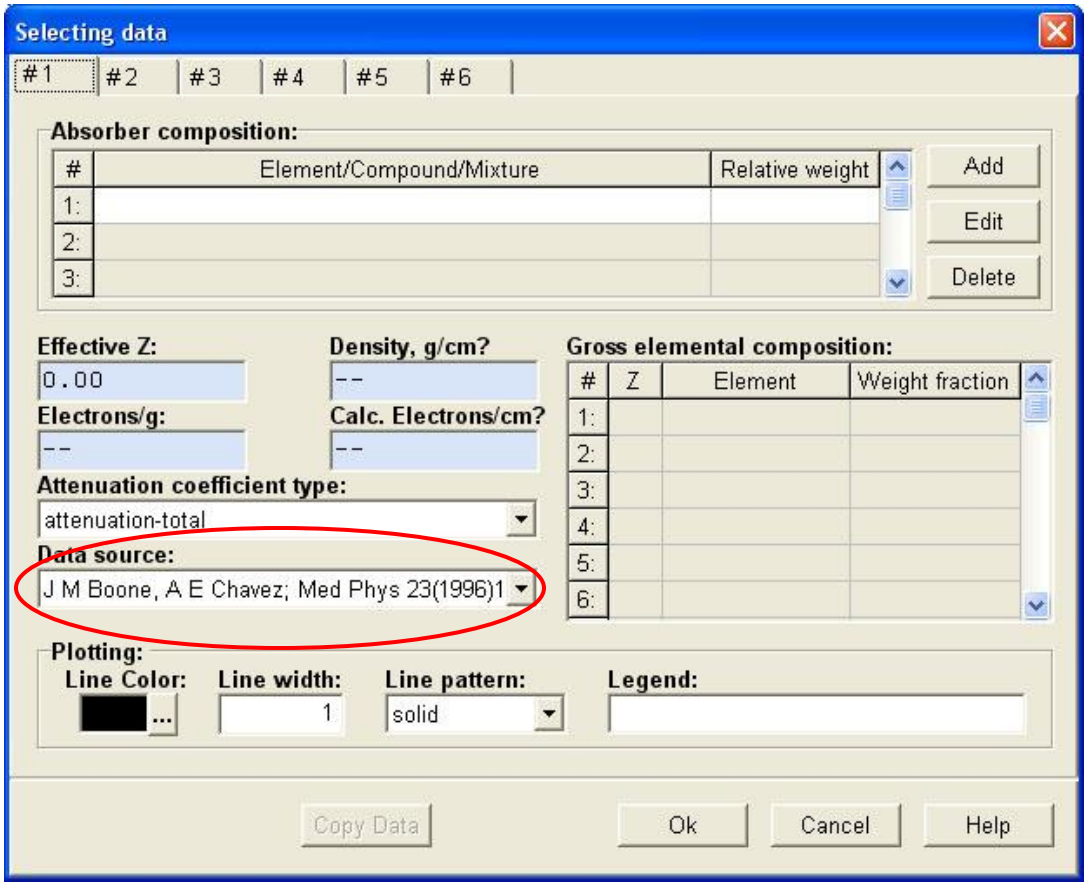

Figure A.2 – Data Setup window of XMuDat.

3. Click on Add; a new window will pop up for selecting elements, compounds or mixtures as in Figure A.3 in order to choose a specific mineral type.

The user can select one of the preset minerals in the list, or choose the element for a mineral compound which is not on the list. The relative weight has to be calculated if the user customizes a mineral compound. For example, carbon dioxide is composed of 1 carbon and 2 oxygen atoms. The atomic weight of carbon is 12.011 and 15.999 for oxygen. The relative weight of carbon and oxygen are calculated as below:

Relative weight of carbon: $\frac{12.011}{12.011+2\times15.999}=0.2729$

Relative weight of oxygen: $\frac{2\times15.999}{12.011+2\times15.999}=0.7271$

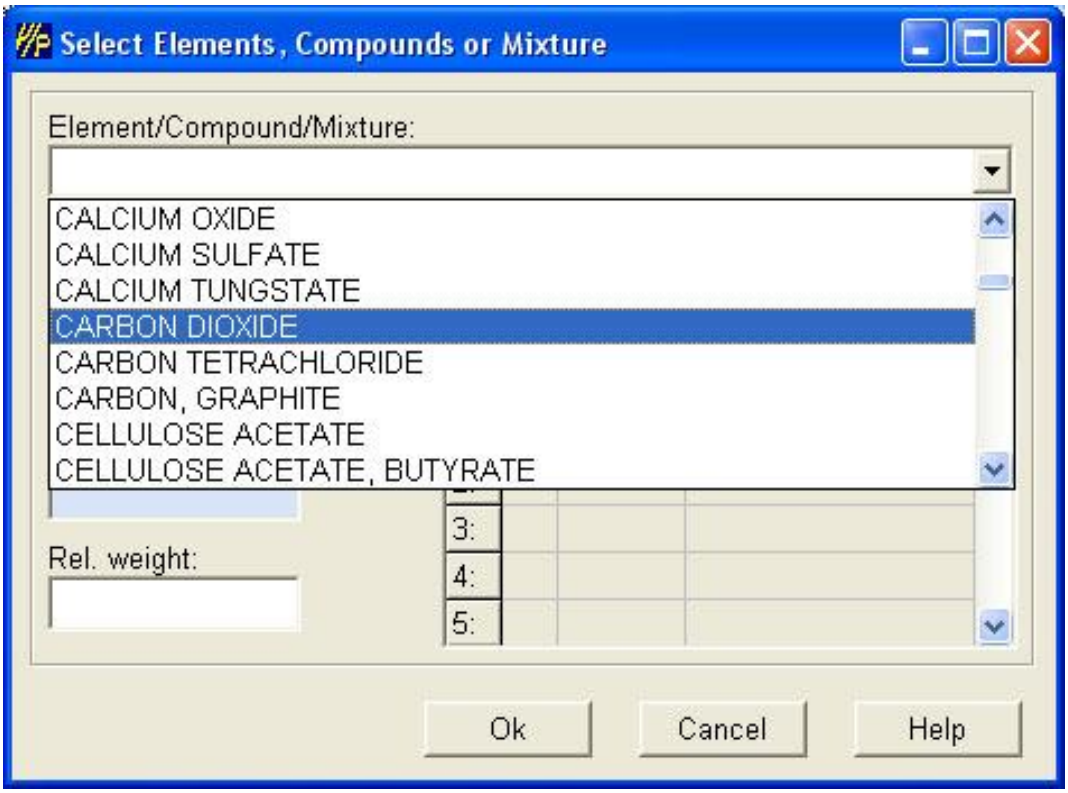

Figure A.3 – Preset mineral types are listed by clicking on drop box.

4. After all five mineral compounds (CO_2, FeS_2, $CuFeS_2$, CuS and $Cu5FeS_4$) are set, press ok and the mass attenuation coefficient – energy graph will be shown as in Figure A.4. Note the unit on the Y axis is the mass attenuation coefficient without the thickness or travelling distance of the material; the unit on the X axis is keV (kilo-electronic volts) which can be transformed into kV by equation 3.5.

5. The source energy level of MicroXCT-400 is from 40 kV to 150kV, which is equal to 26.12 keV to 66.743 keV according to equation 3.5. To enhance the mass attenuation coefficient in this range, the function in Edit -> Plot Range can be set as Figure A.4. The new range is now 1 to 200 with enhanced features of different materials.

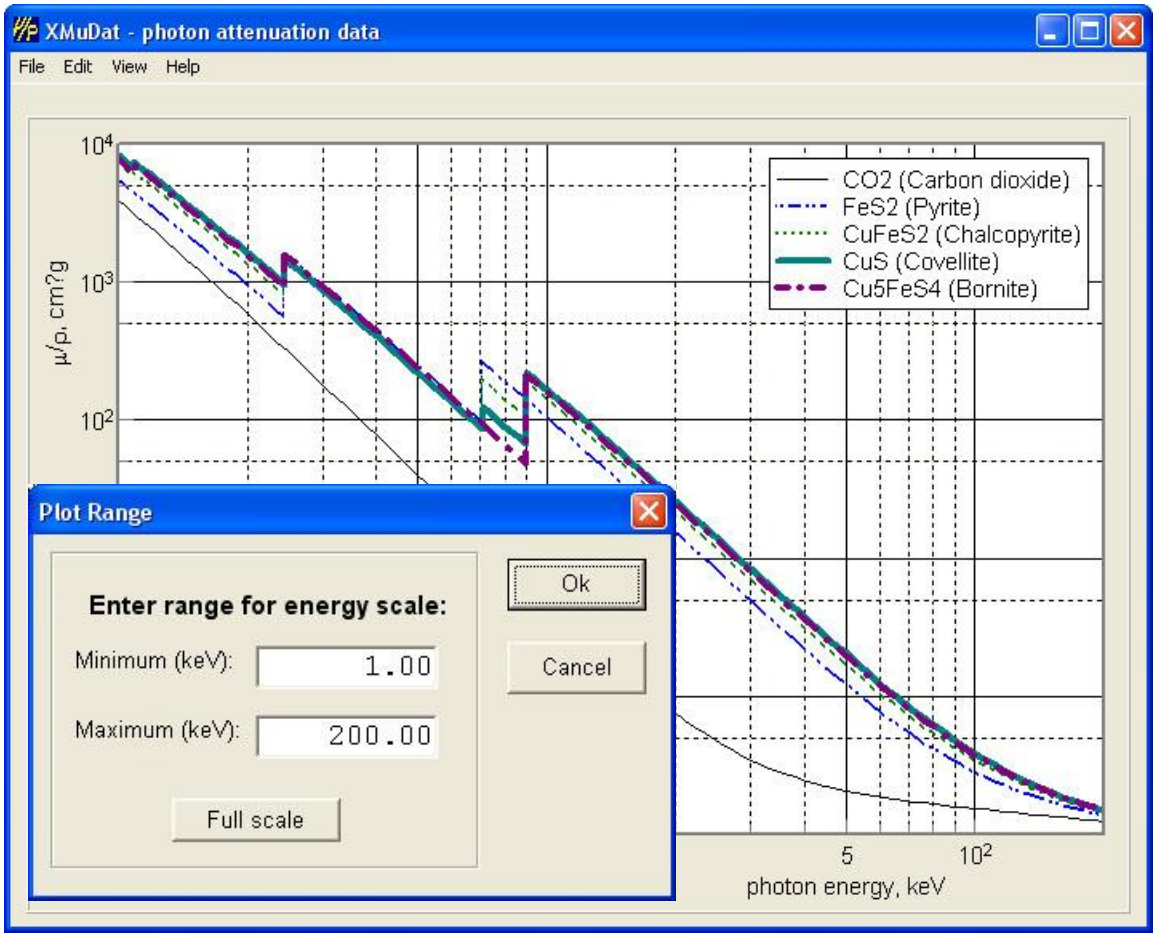

Figure A.4 – The rescaled attenuation coefficient data.

APPENDIX B

SCANNING OPERATING PROCEDURES

The XRadia Micro XCT 400 is the main operating device of the experiments in this thesis. In this section, standard operating procedures will be discussed step by step in order to convey a general idea of the HRXMT scan operation.

1. Warm up the machine by opening the XRay Source dialog box as shown in Figure B.1 and click ON. The orange light on the top of the machine will turn on while the x-ray source is powered. Voltage and power can be adjusted for the user's requirements. Clicking ON or Apply will switch the machine to standby mode (fully warmed up) or warming up mode. The warming up process will take 15 minutes (see Section 3.1).

2. During the warming up process, the sample material is being prepared and fastened on to the sample holder (see Section 3.2).

3. The orange light on the top of the machine will shut off after the equipment is fully warmed up. Open the chamber and put the sample with holder on the stage. Seal the chamber and check if the green light is on.

4. Go to the XRay Source dialog box and click on the "XRay On" button again. This time the machine reaches a specific power level in only a few seconds after being fully warmed up. Set up voltage and power to selected level and click "Apply". The machine will raise the energy the selected level in a few seconds.

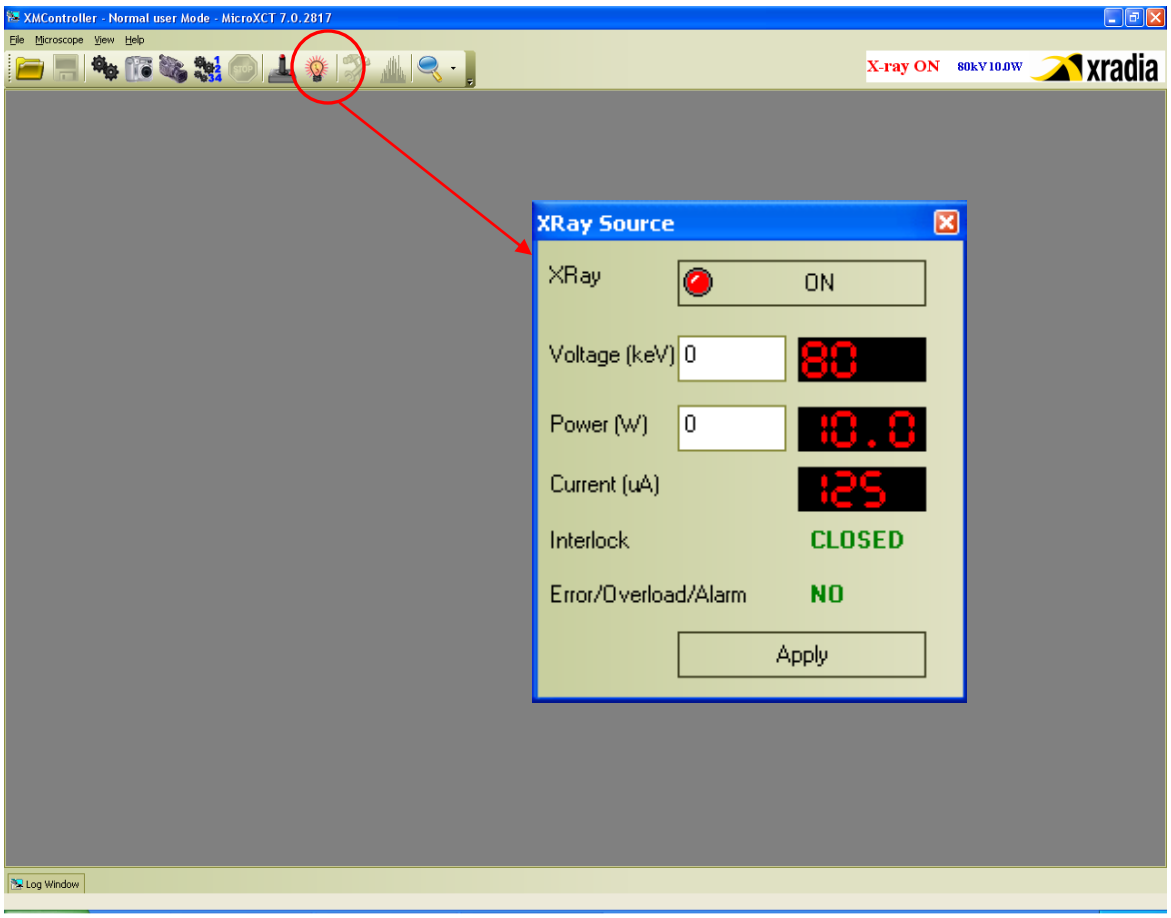

Figure B.1 – The XRay Source dialog icon and window in the XMController.

5. When the power is raised to the selected level, turn on the internal light and the surveillance camera. Go to the "Acquisition Setting" dialog box and select continuous scan with 1 second exposure time, binning 4 shown in Figure B.2. Keep the rest of the settings unchanged and press "Start Acquisition". This step will acquire consecutive projections for field of view calibration. The sample image will be acquired and refreshed every second (depending on the exposure time). Binning 4 helps reducing the file size and the image acquisition time, however, losing the voxel resolution and increasing x-ray intensity on the detector. To acquire a single radiography satisfied the scan requirements, see step 9.

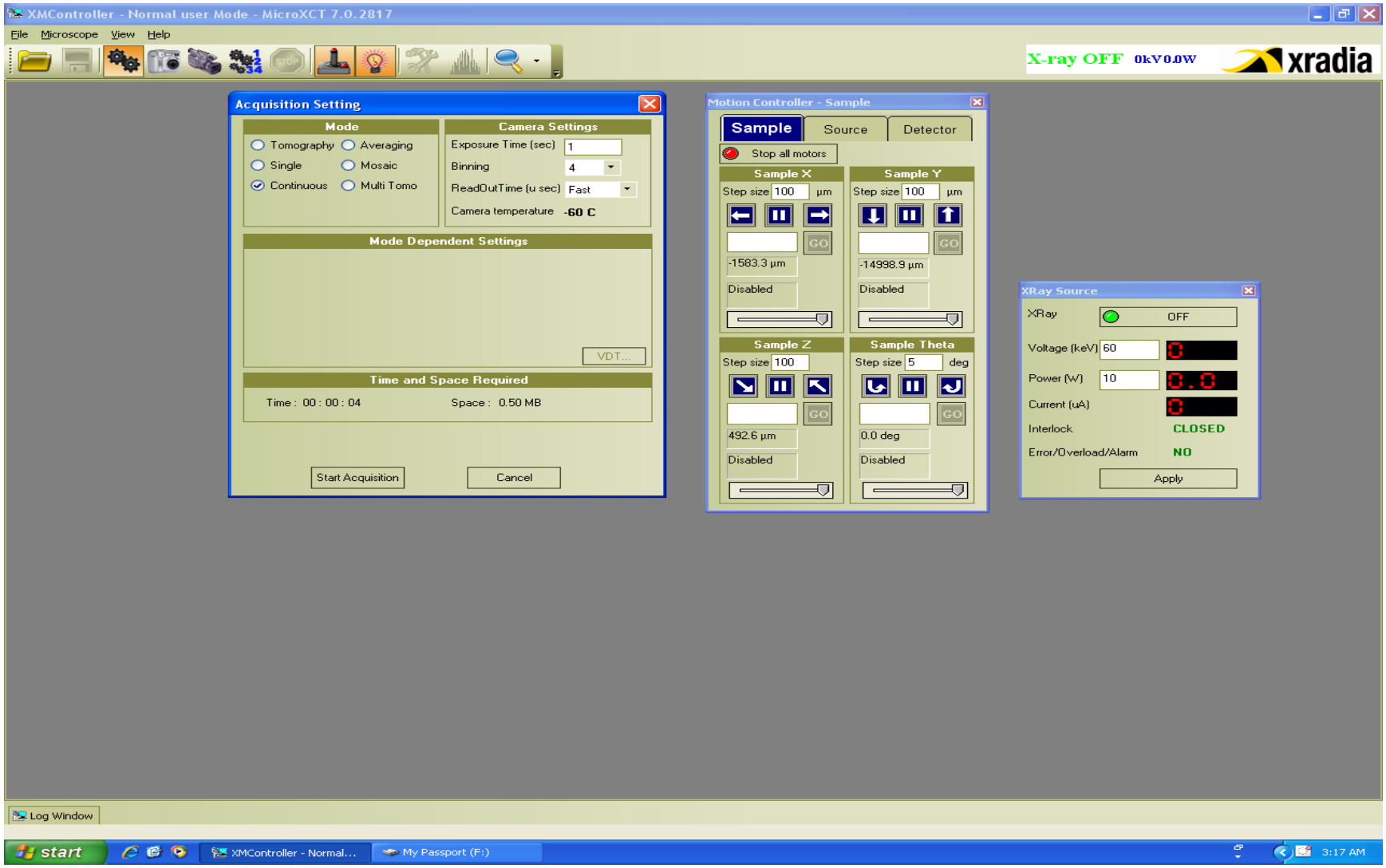

Figure B.2 – A general view of acquisition setting window, motion controller window and the xray source window. Image is shown as example of option and menu location.

The sample or the region of interest has to be kept in the field of view while the stage is rotating during the scan process. Open the “Motion Controller” window as shown in Figure B.2; move the field of view to the region of interest by double clicking the left mouse key on the acquired image shown in Figure B.3. The field of view will be reallocated to a new central point on which the cursor clicks. Go to View and click “Highlight Center of FOV”; a central cross line will show up and indicate the center of the radiographic image. The field of view can be also adjusted by pushing forward or pulling back the joystick on the control panel or by inputting a new coordinate in the motion controller.

6. If the field of view is calibrated, rotate the sample to -90 degrees using the rotation button on the control panel or input the new Theta degree in the controller.

7. Repeat step 6 at -90 degrees. If the sample is well calibrated, then press “STOP” in the icon bar. Move back the sample to 0 degree.

8. Go to the “Acquisition Setting” dialog box again and select single this time. The exposure time is set according to the applied CT standard for the scan. If the scan does not follow any CT standard, the exposure time can be set according to the user’s purpose and image quality. See Chapter 3 for an evaluation of scanning conditions. The binning is set at 2 for a regular scan. Keep the rest of the settings unchanged and press “Start Acquisition”. This step will provide a single radiographic image.

9. Check the single radiographic image for quality and x-ray intensity. See Chapter 3 for additional considerations of the acquired image. If the image quality and scan conditions are satisfactory for the scan requirement, go to File and save this image and name this image as “Single_Shot.”

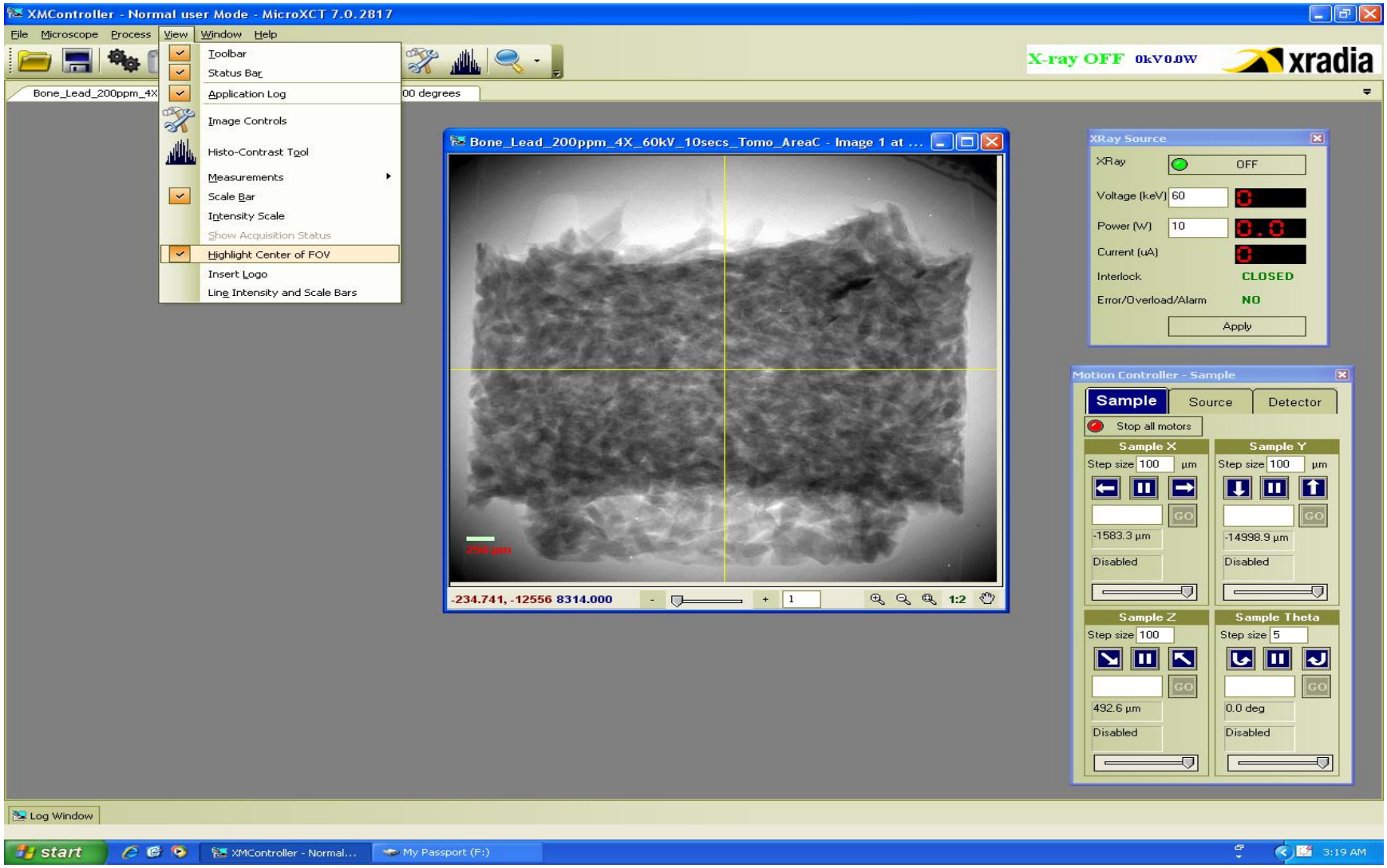

Figure B.3 – Features of the acquired image with the Highlighted Center of FOV are shown. Image is shown as example of option and menu location.

10. Go to View and click “Highlight Center of FOV” again for the central cross line. Go to the “Image Controls” and choose the “Tomography Point Tool” shown in Figure B.4. Move the cursor to the central point and left click. The Tomography Location Set window will pop up as shown in Figure B.4. In this case, only one tomography coordinate is required. Click on “Clean Existing Tomo Location and Registration Point” and choose “Add the point to tomographic location set”, then press ok to acquire the central coordinate. The coordinate can also be obtained from the motion controller with the reading of sample X, Y and Z.

11. Once the coordinate has been acquired, go to “Microscope” and choose “Recipe”. The recipe window will pop up as shown in Figure B.5. Fulfill all the scan conditions. The tomography location can be applied by the function “Add the tomography locations from the current image,” or input the coordinates manually.

12. After the scan conditions are all set, choose “Save as a recipe file…” to save the recipe. The file base name should be included also. The naming rule here is followed by “Sample name,” “Magnification,” “Voltage,” and “Exposure Time.” Click “Run the current recipe...” to start the scan.

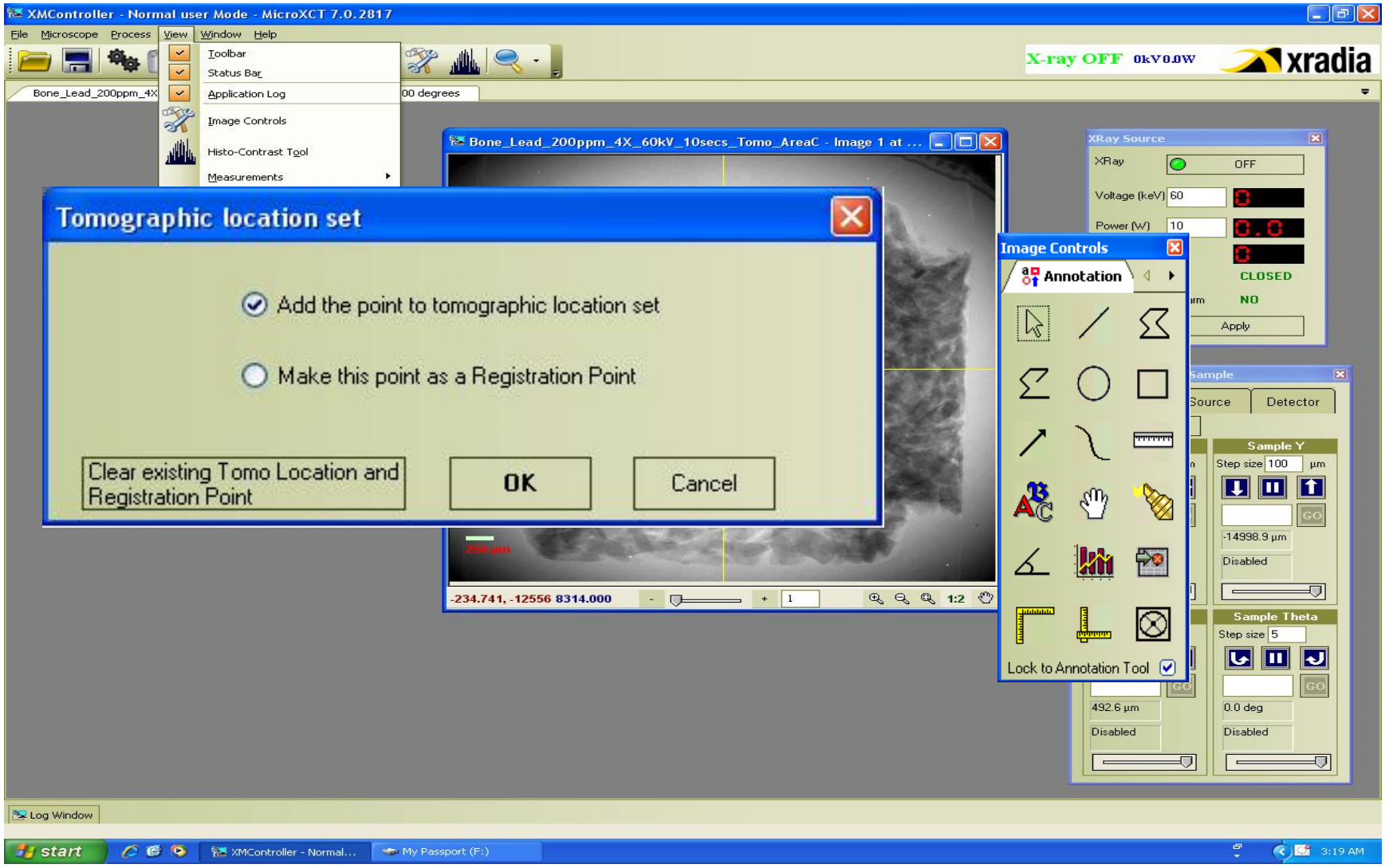

Figure B.4 – The Tomography Point Tool and the Tomography Location Set window. Image is shown as example of option and menu location.

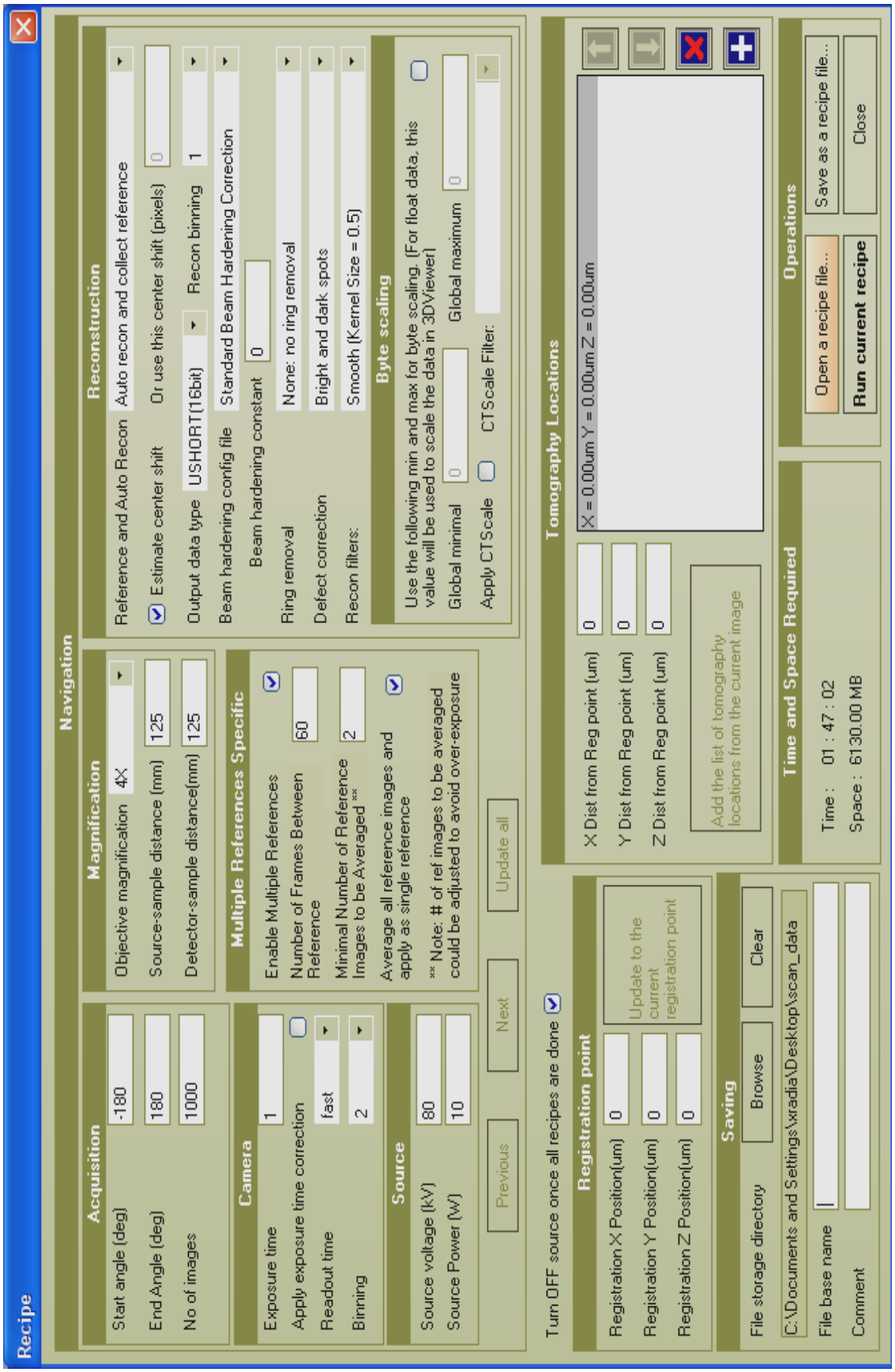

Figure B.5 – The recipe window

REFERENCES

ARACOR, *KONOSCOPE 130/40 Operation and Maintenance Manual*, 2000, pp.11-12.

Metscher, Brian D., "MicroCT for comparative morphology: simple staining methods allow high-contrast 3D imaging of diverse non-mineralized animal tissues", *BMC Physiology*, 2009, pp. **9:**11

Casteele, Elke Van de., "Model-based approach for Beam Hardening Correction and Resolution Measurements in Microtomography", PhD Dissertation, University of Antwerpen, 2004, pp. 4-5.

Favretto, Stephano., "Applications of X-ray Computed Microtomography to Material Science: Devices and Perspectives.", PhD Dissertation, Universita of Degli Studi de Trieste, 2009, pp. 20-21.

Gy, P.M., "The Sampling of Broken Ores: A Review of Principle and Practice," *Proceedings*, Institution of Mining and Metallurgy Symposium, London, 1963, pp.16-27

Herbst, J.A. and Sepulveda, J.L., "Characterization of Test Samples: Particle Size Analysis", *SME Mineral Processing Book*, Vol 2, American Institute of Mining, Metallurgical, and Petroleum Engineers, Inc., 1985, pp. 30-29.

Herman, Gabor.T., *Image Reconstruction From Projections: The Fundamentals of Computerized Tomography*, Academic Press, 1980, pp. 7:180.

Hillson, Simon., *Teeth*, University of London Institute of Archaeology, University College London, 1986, pp.184.

ImageJ, "Image Processing and Analysis in Java", National Institutes of Health, http://rsbweb.nih.gov/ij/, 2011.

Impact Scan, "ImPACT Course: Beam hardening", ImPACT, http://www.impactscan.org/slides/impactcourse/artefacts/img5.html, 2005.

International Atomic Energy Agency, "XMuDat: Photon attenuation data on PC", International Atomic Energy Agency, http://www-nds.iaea.org/reports/nds-195.htm, 1998.

Jason Bryan, "Volsuite: A portable scientific application framework", Ohio Supercomputer Center, http://www.osc.edu/archive/VolSuite/, 2006.

Kodali, Phanindra., Dhawan, Nikhil., Depci, Tolga., Lin, C.L. and Miller, J.D., "Particle damage and exposure analysis in HPGR crushing of selected copper ores for column leaching", *Minerals Engineering 24 (2011)*, 2011, pp. 1478–1487

Lin, C.L., Miller, J.D, Hsieh, C.H., Tiwari, P. and Deo, M.D., 2010, "Pore Scale Analysis of Oil Shale Pyrolysis by X-ray CT and LB Simulation", 6th World Congress on Industrial Process Tomography, Beijing, China, September 2010.

McCullough, E.C., "Photon attenuation in computed tomography", *Medical Physics*, 1975, Vol.2, pp.307.

Miller, J.D. and Lin, C.L., "High Resolution X-ray Micro CT (HRXMT) – Advances in 3D Particle Characterization for Mineral Processing Operations", Mineral Processing Plant Design 2009 – Sept.30 – Oct.3, 3009 Loews Ventana Canyon Resort, Tucson, Arizona, 2009.

Miller, J.D., Lin, C.L., Videla, Alvaro and Medina, Juan., "Three Dimensional Liberation Analysis of Feed and Products from Copper Flotation Circuits Using High Resolution X-ray Micro CT (HRXMT)", VI International Mineral Processing Seminar – PROCESMAN2009, 2-4 December, Santiago, Chile, 2009.

MIPAV, "Medical Image Processing, Analysis and Visualization", National Institutes of Health, http://mipav.cit.nih.gov/, 2007.

Ralph, Jolyon. and Chau, Ida., http://www.mindat.org/, 1993.

Videla, A.R., "Development of Three-dimensional Image Computer Tools for X-ray Computed Tomography Analysis of Multiphase Particulate Systems", Master's Thesis, University of Utah, 2006.

Wellington S.L., Vinegar H.J., "X-Ray Computerized Tomography", *Journal of Petroleum Technology*, August, 1987, pp. 885-886.

XRadia, *MicroXCT-200 and MicroXCT-400 User's Guide*, XRadia, 2010, pp.87, 155, 175, and 283-284.

XRadia: Product > MicroXCT 400, http://www.xradia.com/products/microxct-400.php, 2010.